Lifshitz Spacetime as a Window into Condensed Matter Physics

by

Gino Knodel

A dissertation submitted in partial fulfillment
of the requirements for the degree of
Doctor of Philosophy
(Physics)
in the University of Michigan
2016

Doctoral Committee:

Professor James T. Liu, Chair
Professor Kayhan Gültekin
Professor Finn Larsen
Professor Lu Li
Professor Kai Sun

Acknowledgments

I would like to thank my advisor Jim Liu for his invaluable guidance and support throughout my graduate career. Through my countless interactions with him, I have learned a great deal about physics and how to conduct conscientious research. I would also like to thank my collaborators Cynthia Keeler, Pedro Lisbão, Leopoldo Pando-Zayas and Kai Sun for very fruitful discussions and collaborations. I am grateful to Henriette Elvang and Finn Larsen, who went above and beyond in teaching me and others theoretical physics, and never hesitated to provide encouragement and advice, both academic and personal. I thank all the members of the High Energy Theory group at the University of Michigan for providing a pleasant and friendly, yet always focused environment in which I felt comfortable and encouraged to perform at my best as a graduate student and researcher. Special thanks go to Arash Arabi Ardehali, Anthony Charles, Sebastian Ellis, Pedro Lisbão, Timothy Olson and Samuel Roland for providing feedback on various drafts and presentations throughout my graduate studies.

Contents

List of Tables

List of Figures

List of Appendices

Abstract

We study applications of the AdS/CFT correspondence to strongly coupled condensed matter theories. Specifically, we focus on Lifshitz spacetime, which was proposed as a gravity dual to field theories with Lifshitz scaling symmetry. We first show that higher derivative corrections, such as those arising from string theory, can resolve the apparent tidal singularity of pure Lifshitz spacetime in the deep infrared. We do so by explicitly constructing a toy-model of 4-derivative gravity coupled to Maxwell-dilaton theory to show that the singular horizon can be resolved into a nonsingular $AdS_2 \times \mathbb{R}^2$ geometry. Next, we demonstrate that the non-relativistic Lifshitz symmetry leads to an effective tunneling barrier for matter fields propagating in Lifshitz spacetime. In particular, the tunneling barrier causes scalar modes to either grow or decay exponentially near the boundary. We investigate two consequences of this behavior: First, we show that the boundary-to-bulk correlator, or smearing function, is not well-defined in Lifshitz spacetime, due to a divergence at large momenta and small frequencies. Second, we show that the boundary retarded Green's function for scalar operators is insensitive to small changes in the near-horizon geometry. This insensitivity manifests itself in an exponentially small spectral function at low energies and large momenta. We show that this exponential behavior of the spectral weight is robust with respect to higher derivative corrections in the bulk, and is therefore a concrete prediction of AdS/CFT for condensed matter systems. We conclude by giving a field theory interpretation of the exponential behavior in terms of a non-perturbative resummation of Feynman diagrams.

Chapter 1

Introduction

1.1 The AdS/CFT Correspondence

One of the most remarkable recent advances in string theory is the insight that strongly coupled field theories can be mathematically dual to weakly coupled gravitational systems. This duality is known as the AdS/CFT correspondence, or sometimes more broadly as gauge/gravity duality. The original AdS/CFT conjecture is motivated by constructing a supergravity solution of a stack of N D3-branes, and taking the low-energy (or near-horizon) limit [1, 2, 3]. In its strongest form, the conjecture states that 4-dimensional $\mathcal{N} = 4$ Super Yang-Mills (SYM) with gauge group $SU(N)$ is exactly equivalent to Type IIB string theory on $\mathrm{AdS}_5 \times S^5$. Quantities on the field theory side, in particular the Yang-Mills coupling g_{YM} and the number of colors N are related to quantities on the string theory side via the so-called holographic dictionary (see [1, 4, 5] for reviews). For example, we have

$$g_s = g_{YM}^2 \qquad L^4 = 4\pi g_s N \alpha'^2, \tag{1.1}$$

where g_s is the string coupling, L is the radius of AdS_5 (and S^5), and α' is the square of the string length l_s.

Since the full string theory in $\mathrm{AdS}_5 \times S^5$ is not yet fully understood, it is often appropriate

to rely on a weaker form of the conjecture that arises from taking the 't Hooft limit in the field theory [6]. The limit consists of taking $N \to \infty$, while holding the 't Hooft coupling $\lambda = g_{YM}^2 N$ fixed. On the string theory side, the 't Hooft limit corresponds to taking the classical limit $g_s \to 0$ of Type IIB string theory, in which quantum effects arising from string loop diagrams are suppressed by powers of g_s.

An even weaker (or: more robust) version of the AdS/CFT conjecture is obtained by first taking the 't Hooft limit, and subsequently taking $\lambda \to \infty$ as well. Using (1.2), we see that on the string theory side, this corresponds to taking α' to be small (in units of L), so that the theory reduces to classical type IIB supergravity. Corrections to the classical $\alpha' = 0$ theory arise as a tower of higher derivative corrections to the low-energy effective action, with coefficients proportional to powers of α'. The exact numerical values of the coefficients can be calculated by matching Feynman diagrams of the low-energy theory to string scattering amplitudes [7, 8, 9].

In the $\alpha' \to 0$ or $\lambda \to \infty$ limit, a remarkable feature of AdS/CFT becomes apparent, namely the fact that it constitutes a weak-strong duality. In the large N limit, the relevant coupling in the field theory is not g_{YM}, but rather the 't Hooft coupling $\lambda = g_{YM}^2 N$ [6]. If we take $\lambda \to \infty$, the field theory becomes strongly coupled, while the gravity theory becomes weakly coupled, with dynamics governed by Einstein's equations. Since the two theories are equivalent, this opens up a window for making predictions for strongly coupled theories by carrying out relatively simple calculations in a weakly coupled theory.

1.2 Applying AdS/CFT to Condensed Matter Physics

Almost two decades after its initial proposal, the idea of AdS/CFT has matured to the point where it can be extended to include a large set of theories that go well beyond the initially conjectured case of $\mathcal{N} = 4$ SYM dual to $\mathrm{AdS}_5 \times S^5$. Examples of such extensions include applications of holography to QCD and heavy ion physics [4, 10], as well as to condensed

matter physics (see e.g. [11] and references therein). These developments have opened up the possibility of applying AdS/CFT, and by extension the ideas of string theory and quantum gravity, to real-world systems.

This thesis focuses on applications of AdS/CFT to strongly coupled condensed matter theories, an idea known as AdS/CMT. The goal of this program is to identify gravitational backgrounds that are dual to interesting condensed matter systems, and to extract predictions about strongly coupled condensed matter theories using only the weakly coupled dual gravitational description. While there has been some remarkable recent progress in this direction, one of the most important open questions is whether or not AdS/CMT can make universal predictions that hold for a broad class of condensed matter systems, independent of the specific microscopic details. This is akin to the approach often taken in condensed matter theory itself, where one studies universality classes of theories, where models within each class share common features such as symmetries, but may differ in some of their microscopic dynamics.

In the known case of $\mathcal{N} = 4$ SYM, which posseses a (relativistic) conformal symmetry, one approach to making such universal predictions has been the study of transport coefficients, which has led, for example, to a holographic bound on the ratio of shear viscosity to entropy density in strongly interacting relativistic quantum field theories [10]. Following a similar approach in AdS/CMT is a promising path to making predictions for condensed matter physics. However, it turns out that not all the known concepts of AdS/CFT carry over to the non-relativistic case without difficulty, and a number of challenges arise when trying to apply holography to condensed matter systems. One main challenge is due to the fact that in contrast to relativistic AdS/CFT, where explicit constructions in terms of D-branes often give a precise microscopic description of the duality system, such a "top-down" picture is often lacking, or at the very least incomplete, in the non-relativistic case. Instead, one usually employs a "bottom-up" approach to constructing holographic duals, by matching spacetime isometries to symmetries of the field theory and postulating the duality to hold. The validity

of this assumption is later checked by comparing observables on both the field theory and gravity side, and by trying to connect to some of the existing top-down constructions [12, 13, 14, 15, 16, 17, 18, 19]. Once sufficient evidence for the duality is established, one can make new predictions using the techniques of AdS/CFT.

One example of employing the bottom-up approach mentioned above is the application of AdS/CFT to theories with Lifshitz scaling symmetry [20, 21, 22]. Under this non-relativistic symmetry, space and time scale differently, according to

$$\vec{x} \to \Lambda \vec{x}, \qquad t \to \Lambda^z t, \tag{1.2}$$

where $z > 1$ is called the dynamical (or critical) exponent. An example of a field theory that exhibits the scaling (1.2) is the quantum Lifshitz model in 2+1 dimensions [23], given by the action

$$S = \int d^2x dt \left[\frac{1}{2} \left(\partial_t \phi \right)^2 - \frac{\kappa}{2}^2 \left(\nabla^2 \phi \right)^2 \right]. \tag{1.3}$$

This theory may be considered as the non-relativistic analog of a free scalar field theory. Lorentz invariance is broken by the replacement $\nabla \to \nabla^2$, and the system is Lifshitz scale invariant with $z = 2$. The quantum Lifshitz model represents a line of fixed points characterized by κ that arise, for example, in the description of (smectic) liquid crystals [23, 24].

In the context of the AdS/CFT correspondence, strongly coupled field theories with Lifshitz scaling are conjectured to be dual to Lifshitz spacetime [20], with metric

$$ds^2_{d+2} = -\left(\frac{L}{r} \right)^{2z} dt^2 + \left(\frac{L}{r} \right)^2 \left[d\vec{x}_d^2 + dr^2 \right]. \tag{1.4}$$

The Lifshitz scaling symmetry (1.2), supplemented by a rescaling $r \to \Lambda r$ is realized as an isometry of the background metric (1.4).

Throughout this thesis, we will make use of suitable coordinate transformations to bring

(1.4) into more convenient forms. Letting $\rho = \frac{L}{z}\left(\frac{r}{L}\right)^z$, we can write the Lifshitz metric as:

$$ds^2_{d+2} = \left(\frac{L}{z\rho}\right)^2 \left(-dt^2 + d\rho^2\right) + \left(\frac{L}{z\rho}\right)^{2/z} d\vec{x}_d^2. \tag{1.5}$$

Finally, we may also write (1.4) as

$$ds^2_{d+2} = -e^{2z\hat{r}/L}dt^2 + e^{2\hat{r}/L}d\vec{x}_d + d\hat{r}^2, \tag{1.6}$$

where $\hat{r}$ is defined by $r = Le^{-\hat{r}/L}$. Physical quantities in Lifshitz spacetime can be connected to interesting observables in field theories with Lifshitz scaling by using the holographic dictionary. For example, the behavior of matter fields near the conformal boundary of Lifshitz spacetime can be used to calculate retarded Green's functions of the field theory [25].

Although there exist explicit brane constructions that provide evidence for the conjecture that Lifshitz spacetimes are holographically dual to Lifshitz field theories [12, 16, 17, 18, 19, 26], many aspects of the holographic dictionary are not as well understood as in the relativistic case. This issue carries over to other examples within AdS/CMT, such as Schrödinger spacetimes [21, 22, 27], which are dual to field theories with non-relativistic conformal symmetry.

In this thesis, we study Lifshitz spacetime as a concrete example of a non-relativistic geometry within AdS/CMT, and analyze some of the unique features that arise due to its non-relativistic isometry group. We show how some puzzles, such as the apparent tidal-singularity at the horizon, can be resolved, and demonstrate how to extract universal predictions for condensed matter physics using holographic techniques. In doing so, we provide a small step towards completing the holographic dictionary for AdS/CMT, thus connecting the ideas of string theory to the real world.

1.3 Outline

- In chapter 2, we begin our discussion of Lifshitz spacetime by studying a complication that arises in the near-horizon region of the geometry. An observer falling towards the horizon will experience infinitely strong tidal forces, indicating a physical singularity in pure Lifshitz spacetime. We propose a resolution of this singularity by considering the effect of higher derivative corrections on the geometry. In particular, we explore the effect of curvature-square corrections on Lifshitz solutions to the Einstein-Maxwell-dilaton system. After exhibiting the renormalized Lifshitz scaling solution to the system with parametrized R^2 corrections, we turn to a toy model with coupling $g(\phi)\times\text{Weyl}^2$ and demonstrate that such a term can both stabilize the dilaton and resolve the Lifshitz horizon to a non-singular $\text{AdS}_2 \times \mathbb{R}^2$ geometry. As an example, we construct numerical flows from AdS_4 to an intermediate Lifshitz region, and then to $\text{AdS}_2 \times \mathbb{R}^2$ in the deep IR.

  - Chapter 2 is based on previous work published in
    G. Knodel and J. T. Liu, *"Higher derivative corrections to Lifshitz backgrounds"*, JHEP **1310**, 002 (2013) doi:10.1007/JHEP10(2013)002, [arXiv:1305.3279 [hep-th]], [28].

- In chapter 3, we study boundary-to-bulk correlators in Lifshitz and related non-relativistic spacetimes. We show that the spectrum of scalar modes contains "trapped modes" whose boundary imprint is exponentially supprssed. We use these modes to show that no smearing function exists for pure Lifshitz spacetime, nor for any flow which includes a Lifshitz region. Indeed, for any (planar) spacetime which breaks transverse Lorentz invariance at any radius, we show that one cannot reconstruct the complete local bulk data only from local boundary data. The inability to perform this reconstruction can be interpreted as a restriction on locality in the transverse direction in non-relativistic spacetimes.

  - Chapter 3 is based on previous work published in

    C. Keeler, G. Knodel and J. T. Liu, *"What do non-relativistic CFTs tell us about Lifshitz spacetimes?"*, JHEP **1401**, 062 (2014) doi:10.1007/JHEP01(2014)062, [arXiv:1308.5689 [hep-th]], [29].

- In chapter 4, we investigate the effects of trapped modes in Lifshitz spacetime on holographic two-point functions. We find that the boundary Green's function is generically insensitive to horizon features on small transverse length scales. We explicity demonstrate this insensitivity for Lifshitz with $z = 2$, and then use the WKB approximation to generalize our findings to Lifshitz with $z > 1$, and RG flows with a Lifshitz-like region. Finally, we explore a physical consequence of this insensitivity, namely the fact that the imaginary part of the retarded Green's function (i.e. the spectral function) of scalar operators is exponentially suppressed in a window of frequencies near zero. This behavior is universal in all Lifshitz theories without additional constraining symmetries. On the gravity side, we show that this result is robust against higher derivative corrections, while on the field theory side we present a concrete example where the exponential suppression arises from summing the perturbative expansion to infinite order.

  - Section 4.2 is based on previous work published in

    C. Keeler, G. Knodel and J. T. Liu, *"Hidden horizons in non-relativistic AdS/CFT"*, JHEP **1408**, 024 (2014) doi:10.1007/JHEP08(2014)024, [arXiv:1404.4877 [hep-th]], [30].

  - Sections 4.1, 4.3 and 4.4 are based on previous work published in

    C. Keeler, G. Knodel, J. T. Liu and K. Sun, *"Universal features of Lifshitz Green's functions from holography"*, JHEP **1508**, 057 (2015) doi:10.1007/JHEP08(2015)057, [arXiv:1505.07830 [hep-th]], [31].

Chapter 2

Higher Derivative Corrections

Of course, simply knowing the form of the Lifshitz metric (1.4) is not enough to perform holographic calculations. In particular, (1.4) is not a solution to the vacuum Einstein equations. To find a consistent framework in which to do non-relativistic holography, we first need to identify a matter content that supports Lifshitz spacetime.

Exact Lifshitz geometries were constructed in [32] based on a simple model of a massive vector field coupled to Einstein gravity. Turning on the time component of the vector breaks $d+1$-dimensional Lorentz symmetry in the t and $\vec{x}$ directions, and gives rise to a family of backgrounds with $z \geq 1$. Alternatively, Lifshitz backgrounds may be obtained in the near horizon region of dilatonic branes. A simple realization is to take an Einstein-Maxwell-dilaton system of the form [33, 34, 35, 36, 37, 38]

$$e^{-1}\mathcal{L} = R - \frac{1}{2}(\partial\phi)^2 - f(\phi)F_{\mu\nu}F^{\mu\nu} - V(\phi). \tag{2.1}$$

Lifshitz scaling is obtained by taking a single exponential for the gauge kinetic function along with a constant potential[1]

$$f(\phi) = e^{\lambda_1\phi}, \qquad V(\phi) = -\Lambda. \tag{2.2}$$

[1]Backgrounds dual to systems exhibiting hyperscaling violation may be obtained by instead taking an exponential potential.

The scaling solution has a running dilaton and a dynamical exponent given by the relation

$$\lambda_1^2 = \frac{2d}{z-1}. \tag{2.3}$$

In addition, full solutions that interpolate between AdS_{d+2} in the UV and Lifshitz in the IR may be constructed. As a consequence of the running dilaton, the Lifshitz solution runs into strong coupling either in the UV for the electrically charged solution or in the IR for the magnetic solution (in the case $d = 2$). For the magnetic case, the possibility of quantum corrections was investigated in [39] by constructing a toy model where the gauge kinetic function picks up an expansion in the effective coupling $g \equiv e^{-\frac{1}{2}\lambda_1\phi}$

$$f(\phi) = \frac{1}{g^2} + \xi_1 + \xi_2 g^2 + ... \tag{2.4}$$

Under appropriate conditions, these loop corrections will stabilize the dilaton and lead to the emergence of an $\mathrm{AdS}_2 \times \mathbb{R}^2$ geometry in the deep IR. The emergence of this $\mathrm{AdS}_2 \times \mathbb{R}^2$ region also has the benefit of resolving the Lifshitz horizon, which would otherwise lead to tidal singularities[2] [20, 42, 43]. In contrast with the magnetic solution, the electric solution is not expected to pick up quantum corrections in the IR, as the dilaton runs to weak coupling. In this case, the Lifshitz horizon would not get resolved by the same mechanism. However, in a stringy context (or in that of any UV complete theory of gravity), there is another potential type of corrections, namely those arising from higher curvature terms. Although Riemann invariants remain finite at the tidal singularity, this singularity is nevertheless felt by strings [43]. Hence the Lifshitz horizon could be resolved in a consistent manner in a stringy realization.

In this chapter, we provide evidence that higher curvature terms may indeed resolve the Lifshitz horizon into an AdS_2 region in the deep IR. In particular, we add R^2 terms to the

[2]The dilaton can also be stabilized in the dyonic case [33, 38], as well as in models with multiple Maxwell fields [40, 41].

Einstein-Maxwell-dilaton system (2.1) and seek electrically charged brane solutions that flow from AdS_{d+2} in the UV to Lifshitz and then to $\mathrm{AdS}_2 \times \mathbb{R}^d$ in the deep IR. As demonstrated in [44], higher curvature terms do not necessarily destroy the Lifshitz scaling solution, but simply renormalize the dynamical exponent z. Thus we expect that brane solutions with a large intermediate Lifshitz region do exist. However, whether such solutions will flow smoothly into $\mathrm{AdS}_2 \times \mathbb{R}^d$ will depend on the parameters of the model. We investigate the $d = 2$ case in some detail below, and in particular we confirm numerically that smooth flows do exist that interpolate from AdS_4 to Lifshitz to $\mathrm{AdS}_2 \times \mathbb{R}^2$.

2.1 Lifshitz Solutions in Higher Derivative Gravity

Lifshitz solutions in the presence of higher curvature terms were previously investigated in [45, 46, 47, 48, 49, 50, 51, 52]. Here we focus on the Einstein-Maxwell-dilaton system, (2.1), and take the potential to be a constant, $V(\phi) = -\Lambda$, so that Lifshitz scaling may be obtained at the two-derivative level. The first set of corrections occurs at the four-derivative level, and in the gravitational sector may be parameterized by three constants, α_1, α_2 and α_3, where the action is given by

$$S = \int d^{d+2}x\sqrt{-g}\left(R + \Lambda - \tfrac{1}{2}\left(\partial\phi\right)^2 - f(\phi)F_{\mu\nu}F^{\mu\nu} + \alpha_1 R_{\mu\nu\rho\sigma}R^{\mu\nu\rho\sigma} + \alpha_2 R_{\mu\nu}R^{\mu\nu} + \alpha_3 R^2\right). \tag{2.5}$$

Using Bianchi identities, we may write Einstein's equations as:

$$\begin{aligned} T_{\mu\nu} &= R_{\mu\nu} - \frac{1}{2}g_{\mu\nu}R + 2\alpha_1 R_{\mu\rho\lambda\sigma}R_\nu{}^{\rho\lambda\sigma} + (4\alpha_1 + 2\alpha_2)R_{\mu\rho\nu\lambda}R^{\rho\lambda} - 4\alpha_1 R_{\mu\rho}R^\rho_\nu && (2.6)\\ &\quad -(2\alpha_1 + \alpha_2 + 2\alpha_3)\nabla_\mu\nabla_\nu R + (4\alpha_1 + \alpha_2)\Box R_{\mu\nu} + 2\alpha_3 R R_{\mu\nu} && (2.7)\\ &\quad -\frac{1}{2}g_{\mu\nu}\left[\alpha_1 R_{\rho\lambda\sigma\kappa}R^{\rho\lambda\sigma\kappa} + \alpha_2 R_{\mu\nu}R^{\mu\nu} + \alpha_3 R^2 - (\alpha_2 + 4\alpha_3)\Box R\right], && (2.8) \end{aligned}$$

where the energy momentum tensor on the left hand side is given by

$$T_{\mu\nu} = \frac{1}{2}\partial_\mu\phi\partial_\nu\phi + 2f\left(\phi\right)\left(F_\mu{}^\rho F_{\nu\rho} - \frac{1}{4}g_{\mu\nu}F_{\rho\sigma}F^{\rho\sigma}\right) + \frac{1}{2}g_{\mu\nu}(\Lambda - \frac{1}{2}\partial^\rho\phi\partial_\rho\phi). \tag{2.9}$$

These equations need to be supplemented with the equations of motion of $F_{\mu\nu}$ and ϕ:

$$\begin{aligned} \nabla_\mu(f(\phi)F^{\mu\nu}) &= 0, & (2.10)\\ \Box\phi - f'(\phi)F_{\mu\nu}F^{\mu\nu} &= 0. & (2.11) \end{aligned}$$

Our goal is to find a matter field background that supports the Lifshitz metric, (1.6). From here on, we set $L = 1$ without loss of generality. Thus we have

$$ds^2_{d+2} = -e^{2zr}dt^2 + e^{2r}d\vec{x}^2 + dr^2, \tag{2.12}$$

and we want to determine the form of $F_{\mu\nu}$ and ϕ. We first note that Maxwell's equations, (2.10), can be integrated to obtain an electric solution:

$$F = \frac{Q}{f(\phi)}e^{(z-d)r}dr \wedge dt, \tag{2.13}$$

where Q is an integration constant (the electric charge). Allowing ϕ to depend on r only, the components of the energy momentum tensor are given by

$$\begin{aligned} T_{00} &= g_{00}\left(-\frac{Q^2}{f(\phi)}e^{-2dr} - \frac{1}{4}(\phi')^2 + \frac{\Lambda}{2}\right),\\ T_{rr} &= g_{rr}\left(-\frac{Q^2}{f(\phi)}e^{-2dr} + \frac{1}{4}(\phi')^2 + \frac{\Lambda}{2}\right),\\ T_{ij} &= g_{ij}\left(\frac{Q^2}{f(\phi)}e^{-2dr} - \frac{1}{4}(\phi')^2 + \frac{\Lambda}{2}\right). \end{aligned} \tag{2.14}$$

Invariance of $T_{\mu\nu}$ under Lifshitz scaling requires $\phi \propto r$ and $f^{-1} \propto e^{2dr}$. More explicitly, we may rewrite Einstein's equations, (2.8), as:

$$
\begin{aligned}
(\phi')^2 &= 2(e^{-2zr}\mathrm{RHS}_{00} + \mathrm{RHS}_{\mathrm{rr}}), && (2.15)\\
\Lambda &= \mathrm{RHS}_{\mathrm{rr}} + e^{-2r}\mathrm{RHS}_{\mathrm{ii}}, && (2.16)\\
\frac{Q^2}{f(\phi)}e^{-2dr} &= \frac{1}{2}(e^{-2zr}\mathrm{RHS}_{00} + \mathrm{RHS}_{\mathrm{ii}}). && (2.17)
\end{aligned}
$$

The right hand side of each equation is a fourth order polynomial in z and does not depend on r. (The curvatures are computed in appendix A) After integrating out the electric field, the dilaton equation of motion reads

$$\phi''(r) + d\phi'(r) + 2\frac{f'(\phi)}{f(\phi)}\frac{Q^2}{f(\phi)}e^{-2dr} = 0. \tag{2.18}$$

Plugging in $f \propto e^{-2dr}$ and recalling that ϕ is linear in r, we now find that the gauge kinetic function has to be a single exponential $f(\phi) = e^{\lambda_1\phi}$.

Before we write down the final solution, let us change to a more convenient basis of higher derivative terms by writing the corresponding Lagrangian as

$$\mathcal{L}_{\mathrm{hd}} = \alpha_{\mathrm{W}}C_{\mu\nu\rho\sigma}C^{\mu\nu\rho\sigma} + \alpha_{\mathrm{GB}}G + \alpha_{\mathrm{R}}R^2, \tag{2.19}$$

with the Weyl tensor

$$C_{\mu\nu\rho\sigma} = R_{\mu\nu\rho\sigma} - \frac{1}{d}\left(g_{\mu[\rho}R_{\sigma]\nu} - g_{\nu[\rho}R_{\sigma]\mu}\right) + \frac{1}{d\,(d+1)}g_{\mu[\rho}g_{\sigma]\nu}R, \tag{2.20}$$

and the Gauss-Bonnet combination

$$G = R_{\mu\nu\rho\sigma}R^{\mu\nu\rho\sigma} - 4R_{\mu\nu}R^{\mu\nu} + R^2. \tag{2.21}$$

The Gauss-Bonnet term is topological in four dimensions and vanishes in fewer than four

dimensions. Hence we expect the equations of motion to be independent of $\alpha_{\rm GB}$ for $d \leq 2$. The coefficients in (2.19) and (2.5) are related via

$$\begin{aligned}
\alpha_1 &= \alpha_{\rm GB} + \alpha_{\rm W}, \\
\alpha_2 &= -4\alpha_{\rm GB} - \frac{4}{d}\alpha_{\rm W}, \\
\alpha_3 &= \alpha_{\rm GB} + \frac{2}{d(d+1)}\alpha_{\rm W} + \alpha_{\rm R}.
\end{aligned} \tag{2.22}$$

In this new basis, the final solution is given by the Lifshitz metric (2.12), the Maxwell field (2.13), and the dilaton

$$\phi = -\frac{2d}{\lambda_1} r + C, \tag{2.23}$$

where C is a constant of integration. The gauge kinetic function is $f(\phi) = e^{\lambda_1 \phi}$, where

$$\lambda_1^2 = \frac{d(z+d)}{Q^2 e^{-\lambda_1 C}}. \tag{2.24}$$

The electric charge Q and the cosmological constant Λ are given in terms of z according to

$$\begin{aligned}
Q^2 e^{-\lambda_1 C} &= \frac{1}{2}(z-1)(z+d)\left[1 - \frac{4(d-1)}{d+1}\alpha_{\rm W} z(z-d) - 2(d-1)(d-2)\alpha_{\rm GB}\right] \\
&\quad -2\alpha_{\rm R}\left[z^4 + 2(d-\frac{1}{2})z^3 + \frac{3}{2}dz^2 + \frac{1}{2}d(d^2-2d-1)z - \frac{1}{2}d^2(d+1)\right],
\end{aligned} \tag{2.25}$$

$$\begin{aligned}
\Lambda &= (z+d)(z+d-1) - \frac{4(d-1)^2}{d+1}\alpha_{\rm W} z(z-1)\left(z - 2\frac{d}{d-1}\right) \\
&\quad -2(d-1)(d-2)\alpha_{\rm GB}\left[z^2 + 2(d-\frac{1}{2})z + \frac{1}{2}d(d-3)\right] \\
&\quad +4\alpha_{\rm R}\left[z^3 - \frac{3}{2}d(d-\frac{5}{3})z^2 - d(d^2 - \frac{3}{2}d - \frac{1}{3})z - \frac{1}{4}d^2(d+1)(d-3)\right].
\end{aligned} \tag{2.26}$$

As expected, for $d = 1$ and 2, the Gauss-Bonnet combination does not contribute to the equations of motion. Notice also that due to the shift symmetry $\phi \mapsto \phi + C$, $F_{\mu\nu} \mapsto F_{\mu\nu} e^{-\frac{1}{2}\lambda_1 C}$, only the combination $Q^2 e^{-\lambda_1 C}$ is fixed.

We see that the higher derivative action (2.5) admits Lifshitz solutions with an electric background gauge potential and $\phi \propto r$. The "running" of the dilaton has physical consequences: The effective gauge coupling $f^{-\frac{1}{2}}$ runs from weak coupling in the IR ($r \to -\infty$) to strong coupling in the UV ($r \to \infty$)[3].

The above solution is the straightforward generalization of the previously known Einstein-Maxwell-dilaton background to the case of four-derivative gravity. The effect of the higher derivative corrections is to renormalize the cosmological constant and electric charge by inducing corrections of order z^4. We will demonstrate below that this leads to some nontrivial features of the solution.

2.2 Lifshitz Solutions in Einstein-Weyl Gravity

Let us now focus on the special case of Einstein-Weyl gravity. This theory will be of particular interest to us in the following section, where we will construct smooth flows from AdS_4 to Lifshitz to $AdS_2 \times \mathbb{R}^2$. Lifshitz solutions in pure Einstein-Weyl gravity without additional matter fields have also been studied in [52].

Setting $\alpha_{\rm GB} = \alpha_{\rm R} = 0$, the solution (2.25), (2.26) simplifies to

$$Q^2 e^{-\lambda_1 C} = \frac{1}{2}(z-1)(z+d)\left(1 - \frac{4(d-1)}{d+1}\alpha_{\rm W} z(z-d)\right), \tag{2.27}$$

$$\Lambda = (z+d)(z+d-1) - \frac{4(d-1)^2}{d+1}\alpha_{\rm W} z(z-1)\left(z - 2\frac{d}{d-1}\right). \tag{2.28}$$

This solution has some interesting features. For $d = 1$, the Weyl-tensor vanishes identically and so there are no higher derivative corrections. Next, notice that if $Q^2 \to 0$, $\lambda_1 \to \infty$, $\phi \to$ const., the matter fields decouple and we recover a purely gravitational solution. There are two distinct ways to achieve this: The first one is the case $z = 1$, corresponding to

[3] In four dimensions, we can use electric-magnetic duality to obtain a magnetic solution, $\widetilde{F} \equiv f(\phi) * F = Q_m dx \wedge dy$, with magnetic charge Q_m. Since the duality transformation also requires $f \mapsto f^{-1}$, the dilaton now runs towards strong coupling in the IR.

pure AdS_{d+2} without matter fields. Note that because the Weyl tensor vanishes in AdS, the cosmological constant is not renormalized.

As a second possibility, we may choose

$$\alpha_{\mathrm{w}} = \frac{d+1}{4(d-1)z(z-d-2)}. \tag{2.29}$$

In this case we recover purely gravitational Lifshitz solutions, with

$$\begin{aligned} Q^2 e^{-\lambda_1 C} &= 0, \\ \phi &= \text{const.}, \\ \Lambda &= (z+d)(z+d-1) - (d-1)(z-1)\frac{z-2\frac{d}{d-1}}{z-d-2}. \end{aligned} \tag{2.30}$$

It is interesting to consider the limit of conformal gravity, where $\alpha_{\mathrm{w}} \to \infty$. From (2.29), we expect the scaling parameter to take two possible values, $z = 0$, or $z = d+2$. However, in the latter case, Λ blows up for general d. It is only in the case $d = 2$ that the second solution with $z = 4$ is well behaved. Finally, notice also that for any given α and λ_1, there may be multiple solutions for z.

2.3 Smoothing out the Singularity

The Lifshitz solutions of the previous section have a physical singularity in the infrared. For $z \neq 1$, an infalling extended object, such as a string, experiences infinitely strong tidal forces as $r \to -\infty$ [43]. Hence pure Lifshitz solutions are IR incomplete. However, one might argue that this kind of pathological behavior is simply a signal that our solutions should not be trusted in this particular regime, and the singularity would presumably be resolved in a more complete string theory picture. Some compelling evidence supporting this point of view has been presented in [39, 53, 54].

The analysis of the previous section suggests a straightforward way of resolving the

Lifshitz singularity: In general, a nonzero coupling of the dilaton to higher derivative terms will generate corrections to its effective potential. In this section, we will use a simple toy model in four dimensions to show that by choosing such a coupling appropriately, the dilaton can be stabilized at some finite value ϕ_0. As a result, the geometry flows smoothly from Lifshitz to $\mathrm{AdS}_2 \times \mathbb{R}^2$ in the deep IR, which is free of physical singularities.

In order to imitate the effect of generic higher derivative corrections from string theory, we consider the following theory:

$$S = \int d^4x\sqrt{-g}\left(R + \Lambda - \tfrac{1}{2}\left(\partial\phi\right)^2 - f\left(\phi\right)F_{\mu\nu}F^{\mu\nu} + g(\phi)C_{\mu\nu\rho\sigma}C^{\mu\nu\rho\sigma}\right). \tag{2.31}$$

Since the Weyl tensor vanishes in AdS_4, the higher derivative terms do not source the dilaton in the UV. We therefore expect a smooth flow from AdS_4 to Lifshitz, much like the domain-wall solutions found in [33, 37]. As we flow further towards the IR, the Weyl-squared term is expected to become more important, and the dilaton-Weyl coupling, $g(\phi)$, may then stabilize the dilaton. To be concrete, we choose $g(\phi)$ to be

$$g(\phi) = \frac{3}{4}(\alpha + \beta e^{\lambda_2\phi}). \tag{2.32}$$

For $\beta e^{\lambda_2\phi} \ll \alpha$, $g(\phi)$ is approximately constant and we expect to find Lifshitz scaling solutions of the form described in the previous section. With an appropriate choice of parameters, the exponential becomes more and more important as ϕ runs towards weak coupling and it eventually stabilizes the dilaton in the deep IR.

Since we have introduced a Weyl-squared correction, it is convenient to choose the following parametrization of the metric[4]:

$$ds^2 = a^2(r)\left(-dt^2 + dr^2 + b^2(r)(dx^2 + dy^2)\right), \tag{2.33}$$

[4]We will work in units where $L = 1$ in what follows.

With this choice, the Weyl-invariance of the higher derivative Lagrangian is manifest as a rescaling of $a(r)$. In practice, this means that only $b(r)$ will receive higher derivative corrections in the equations of motion. Fixing $\Lambda = 1$, the AdS_4 solution is given by

$$a = \frac{\sqrt{6}}{r}, \qquad b = \text{const.}, \tag{2.34}$$

while the Lifshitz solution takes the form

$$a \propto \frac{1}{r}, \qquad b \propto r^{\tilde{z}}. \tag{2.35}$$

For this metric, the scaling symmetry (1.2) becomes

$$t \to \lambda t, \qquad x \to \lambda^{1-\tilde{z}} x, \qquad r \to \lambda r. \tag{2.36}$$

In changing from the more common form of the metric, (2.12), to the Weyl form, (2.33), we need to make the following identifications:

$$\begin{aligned} z &= \frac{1}{1-\tilde{z}}, \\ L &\to \frac{L}{1-\tilde{z}}, \\ \alpha &\to (1-\tilde{z})^2 \alpha. \end{aligned} \tag{2.37}$$

As before, we choose a background electric charge:

$$F = \frac{Q}{b^2 f(\phi)} dr \wedge dt. \tag{2.38}$$

Einstein's equations are:

$$
\begin{aligned}
T_{00} &= -2\left(\frac{a''}{a}+\frac{b''}{b}\right)+\left(\frac{a'}{a}\right)^2-\left(\frac{b'}{b}\right)^2-4\frac{a'b'}{ab} \\
&\quad -\frac{4}{3}\frac{g(\phi)}{a^2}\left[\frac{b^{(4)}}{b}+\frac{b^{(3)}b'}{b^2}-2\frac{b''\left(b'\right)^2}{b^3}-\frac{1}{2}\left(\frac{b''}{b}\right)^2+\frac{1}{2}\left(\frac{b'}{b}\right)^4+\left(\frac{b''}{b}-\left(\frac{b'}{b}\right)^2\right)\frac{g'}{g}\phi''\right. \\
&\quad \left.+\left(2\frac{b^{(3)}}{b}-\frac{b'b''}{b^2}-\left(\frac{b'}{b}\right)^3\right)\frac{g'}{g}\phi'+\left(\frac{b''}{b}-\left(\frac{b'}{b}\right)^2\right)\frac{g''}{g}\left(\phi'\right)^2\right], \qquad (2.39) \\
T_{rr} &= 3\left(\frac{a'}{a}\right)^2+\left(\frac{b'}{b}\right)^2+4\frac{a'b'}{ab} \\
&\quad +\frac{4}{3}\frac{g\left(\phi\right)}{a^2}\left[-\frac{b^{(3)}b'}{b^2}+\frac{1}{2}\left(\frac{b'}{b}\right)^4+\frac{1}{2}\left(\frac{b''}{b}\right)^2+\left(\left(\frac{b'}{b}\right)^3-\frac{b'b''}{b^2}\right)\frac{g'}{g}\phi'\right], \qquad (2.40) \\
\frac{T_{ii}}{b^2} &= 2\frac{a''}{a}+\frac{b''}{b}-\left(\frac{a'}{a}\right)^2+2\frac{a'b'}{ab} \\
&\quad -\frac{4}{3}\frac{g(\phi)}{a^2}\left[\frac{1}{2}\frac{b^{(4)}}{b}+\frac{1}{2}\left(\frac{b'}{b}\right)^4-\frac{\left(b'\right)^2b''}{b^3}+\frac{1}{2}\left(\frac{b''}{b}-\left(\frac{b'}{b}\right)^2\right)\left(\frac{g'}{g}\phi''+\frac{g''}{g}\left(\phi'\right)^2\right)\right. \\
&\quad \left.+\left(\frac{b^{(3)}}{b}-\frac{b'b''}{b^2}\right)\frac{g'}{g}\phi'\right], \qquad (2.41)
\end{aligned}
$$

with

$$
\begin{aligned}
T_{00} &= \frac{Q^2}{a^2b^4f\left(\phi\right)}+\frac{1}{4}\left(\phi'\right)^2-\frac{a^2\Lambda}{2}, \qquad (2.42) \\
T_{rr} &= -\frac{Q^2}{a^2b^4f\left(\phi\right)}+\frac{1}{4}\left(\phi'\right)^2+\frac{a^2\Lambda}{2}, \qquad (2.43) \\
\frac{T_{ij}}{b^2} &= \delta_{ij}\left(\frac{Q^2}{a^2b^4f\left(\phi\right)}-\frac{1}{4}\left(\phi'\right)^2+\frac{a^2\Lambda}{2}\right). \qquad (2.44)
\end{aligned}
$$

If we demand that ϕ depends only on r, the dilaton equation of motion simplifies to

$$
\phi''+2\left(\frac{a'}{a}+\frac{b'}{b}\right)\phi'+a^2V'_{\text{eff}}(\phi)=0, \qquad (2.45)
$$

where

$$
V'_{\text{eff}}(\phi)\equiv\frac{2Q^2}{a^4b^4}\frac{f'(\phi)}{f^2(\phi)}+\frac{4}{3a^4}\left(\frac{\mathrm{d}^2\log(b)}{\mathrm{d}r^2}\right)^2g'(\phi). \qquad (2.46)
$$

Hence the effect of the higher derivative terms on the dilaton is to generate corrections to its effective potential.

We would like to find out which choices of $g(\phi)$ allow for an emerging $\mathrm{AdS}_2 \times \mathbb{R}^2$ geometry in the deep IR. Corresponding to $\mathrm{AdS}_2 \times \mathbb{R}^2$, we make the ansatz

$$\begin{aligned} a(r) &= \frac{1}{r}, \\ b(r) &= b_0 r, \\ \phi(r) &= \phi_0. \end{aligned} \tag{2.47}$$

Solving (2.39) through (2.41), we find

$$\begin{aligned} \Lambda &= 1, \\ \frac{Q^2}{b_0^4} &= \frac{f(\phi_0)}{2}\left(1 - \frac{4}{3}g(\phi_0)\right). \end{aligned} \tag{2.48}$$

Since only the ratio Q/b_0^2 is fixed, we are free to set $b_0 \equiv 1$ in what follows. Equation (2.45) gives us the condition

$$V'_{\mathrm{eff}}(\phi_0) = \frac{f'(\phi_0)}{f(\phi_0)}\left(1 - \frac{4}{3}g(\phi_0)\right) + \frac{4}{3}g'(\phi_0) = 0. \tag{2.49}$$

Let us now specialize to the case $f(\phi) = e^{\lambda_1 \phi}$. Since the dilaton runs towards weak coupling as $r \to \infty$, this ansatz is valid even in the deep IR. With our choice of $g(\phi)$, the solution to (2.48) and (2.49) is given by

$$\begin{aligned} Q^2 &= \frac{(\alpha - 1)\lambda_2}{\lambda_1 - \lambda_2}, \\ \phi_0 &= \frac{1}{\lambda_2}\log\left(\frac{\lambda_1}{\lambda_1 - \lambda_2}\frac{1 - \alpha}{\beta}\right). \end{aligned} \tag{2.50}$$

Clearly this solution only makes sense for a certain choice of λ_i, α, β. We will discuss the constraints on these parameters at the end of the next section.

2.3.1 Perturbations around $\mathrm{AdS}_2 \times \mathbb{R}^2$

We would like to find numerical solutions that smoothly interpolate between AdS_4 and $\mathrm{AdS}_2 \times \mathbb{R}^2$, with some intermediate Lifshitz regime. This is most easily accomplished numerically by using the "shooting" technique, starting in the deep IR ($r \to \infty$). The initial conditions have to be chosen such that we follow perturbations that are *irrelevant* in the IR. These are perturbations that fall off faster than the background solution as $r \to \infty$. In other words, they allow a smooth flow *away from* $\mathrm{AdS}_2 \times \mathbb{R}^2$ as r decreases. Requiring the existence of such perturbations will introduce nontrivial constraints on the parameters of our model.

We start by perturbing the $\mathrm{AdS}_2 \times \mathbb{R}^2$ solution, (2.47), in the following way

$$a(r) = \frac{1}{r} + \delta a(r), \qquad b(r) = r + \delta b(r), \qquad \phi(r) = \phi_0 + \delta\phi(r). \tag{2.51}$$

Using the conditions (2.48) and (2.49) repeatedly, the linearized equations of motion may be written as

$$\frac{3}{2g_0}\frac{(r^3\delta a')'}{r^2} + \left(r\delta b^{(3)}\right)' - 2\frac{f_0 g_0'}{f_0' g_0}\left(\frac{\delta b'}{r}\right)' - \frac{g_0'}{g_0}\frac{(r\delta\phi')'}{r} + \frac{g_0'}{g_0}\frac{\delta\phi}{r^2} = 0, \tag{2.52}$$

$$\frac{3}{2g_0}\left(r^2\delta a\right)' + r^2\delta b^{(3)} - 2\frac{f_0 g_0'}{f_0' g_0}\delta b' - \frac{g_0'}{g_0}(r\delta\phi)' = 0, \tag{2.53}$$

$$-3\left(r^2\delta a'\right)' + r^2 g_0 \delta b^{(4)} - 2\left(g_0 + \frac{3}{4}\right) r^2\left(\frac{\delta b'}{r^2}\right)' - 6\frac{\delta b}{r^2} - g_0' r\left(\delta\phi'' - 2\frac{\delta\phi}{r^2}\right) = 0, \tag{2.54}$$

$$\delta\phi'' + V_{\text{eff}}''(\phi_0)\frac{\delta\phi}{r^2} - \frac{8}{3}g_0' r\left(\frac{\delta b'}{r^2}\right)' = 0, \tag{2.55}$$

where $f_0 \equiv f(\phi_0)$, etc. The presence of the δb term in the last equation emphasizes the fact that the higher derivative corrections generate a *gravitational* effective potential for the dilaton. This is different from the case of a quantum-corrected $f(\phi)$, and will in general lead to a nontrivial mixing of ϕ perturbations with gravitational perturbations. Since the first three equations are related via a Bianchi identity, it is possible to eliminate the $\delta b^{(4)}$ terms and reduce the system to a third order coupled ODE. Hence there are only seven

independent solutions:

$$\delta a = -r, \qquad \delta b = r^3, \qquad \delta\phi = 0; \tag{2.56}$$

$$\delta a = -\frac{\frac{3}{4} + \log(r)}{r^2}, \qquad \delta b = \log r, \qquad \delta\phi = \frac{\xi}{r}; \tag{2.57}$$

$$\delta a = -\frac{1}{r^2}, \qquad \delta b = 1, \qquad \delta\phi = 0; \tag{2.58}$$

$$\delta a = A_0 r^{\nu-1}, \qquad \delta b = B_0 r^{\nu+1}, \qquad \delta\phi = P_0 r^{\nu}. \tag{2.59}$$

Here

$$\xi = \frac{6\lambda_1\lambda_2\left(1-\alpha\right)}{\lambda_1\lambda_2\left(\lambda_1+\lambda_2\right)\left(\alpha-1\right)+2\left(\lambda_2-\lambda_1\right)}, \tag{2.60}$$

and the constants A_0, B_0 and P_0 in (2.59) are related by

$$A_0 = \frac{2g_0}{3}\left(\frac{g_0'}{g_0}\left(P_0 + 2\frac{f_0}{f_0'}\right) - \nu\left(\nu-1\right)\right)B_0, \tag{2.61}$$

$$P_0 = \frac{8}{3}\frac{g_0'\left(\nu+1\right)\left(\nu-2\right)}{V''\left(\phi_0\right)+\nu\left(\nu-1\right)}B_0. \tag{2.62}$$

There are four solutions for the exponent in (2.59):

$$\begin{aligned}
\nu &\equiv \frac{1}{2} + \widetilde{\nu}, \\
2\widetilde{\nu}^2 &= -\left(V''_{\text{eff}}\left(\phi_0\right) - \frac{1}{4} - \frac{8}{3}\frac{\left(g_0'\right)^2}{g_0} + x\right) \pm \left[\left(V''_{\text{eff}}\left(\phi_0\right) - \frac{1}{4} - \frac{8}{3}\frac{\left(g_0'\right)^2}{g_0} - x\right)^2 - \frac{16}{3}\left(\frac{g_0'}{g_0}\right)^2\right]^{\frac{1}{2}}, \\
x &\equiv \frac{5}{12} - \frac{1}{2g_0} - \frac{4}{3}\frac{f_0 g_0'}{f_0' g_0}.
\end{aligned} \tag{2.63}$$

For our choice of $g\left(\phi\right)$, given by (2.32), we find

$$\begin{aligned}
\widetilde{\nu} = \pm\frac{1}{2}\Bigg[1 - \frac{\left(1-\alpha\right)\lambda_2}{1-\alpha\frac{\lambda_2}{\lambda_1}}\Bigg[2\lambda_1 - \frac{4}{3\lambda_1} + 2\alpha\lambda_2 \\
\pm\frac{2}{\lambda_1}\left(\lambda_1^4 + 2\alpha\lambda_2\lambda_1^3 + \left(\alpha^2\lambda_2^2 - 4\right)\lambda_1^2 + \frac{4}{3}\alpha\lambda_1\lambda_2 + \frac{4}{9}\right)^{\frac{1}{2}}\Bigg]\Bigg]^{\frac{1}{2}}.
\end{aligned} \tag{2.64}$$

Regardless of the form of the effective potential, there always exist two irrelevant perturbations, (2.57) and (2.58). Whether or not the solutions (2.59) are irrelevant depends on the choice of parameters. Although in general there is a mixing of ϕ with a and b due to the dilaton coupling to $C^2_{\mu\nu\rho\sigma}$, one can check that for $g(\phi) \equiv 0$ the ansatz (2.59) reproduces the purely dilatonic perturbations of the two-derivative theory [39]. Although not technically correct, we will therefore still refer to those perturbations as "dilaton perturbations" in what follows.

To find the desired numerical solutions, we impose the following set of conditions:

1. $\lambda_2/\lambda_1 > 0$: This ensures that $g(\phi) \approx$ const. during the Lifshitz scaling stage and in the deep UV. Thus $g'(\phi)$ only becomes important in the IR, where it stabilizes the dilaton. Since (2.31) is invariant under $\phi \mapsto -\phi$, $\lambda_i \mapsto -\lambda_i$, we shall assume without loss of generality that $\lambda_1 > 0$ and $\lambda_2 > 0$.

2. $V'_{\text{eff}}(\phi_0) = 0$ for some ϕ_0 (see (2.49)): The effective potential stabilizes the dilaton and admits an $\text{AdS}_2 \times \mathbb{R}^2$ solution.

3. We focus on the case $g(\phi_0) > 0$. For negative $g(\phi)$, we numerically find either singular solutions or solutions with $\phi' \ll 0$ as we approach AdS_4. It remains unclear whether the sign of higher derivative terms has a physical interpretation in terms of unitarity or causality or a generalized null energy condition.

4. $Q^2 > 0$, i.e. the vector potential is real-valued.

5. Our numerical analysis, as well as the analysis performed in [39, 53] strongly suggest that we need at least one of the dilaton perturbations to be irrelevant in order to "kick" ϕ out of its local minimum in the IR and roll towards large negative values in the UV. We therefore demand that $\nu < 0$ for at least one of the dilaton perturbations. Notice that there can be at most two solutions that satisfy this condition.

6. We require ν to be real-valued; that is, we exclude oscillating perturbations. We

take the existence of complex eigenvalues as an indication of a dynamical instability. However, due to the higher-derivative nature of our theory, a more detailed analysis of the time-dependent perturbations would be needed in order to determine whether the theory is truly unstable for complex exponents.

Let us now find out what these conditions imply for our parameters $\alpha, \beta, \lambda_1, \lambda_2$. Conditions 3 and 4 allow for two possible choices:

$$\begin{aligned} &1) \quad \alpha \geq 1, && \alpha \frac{\lambda_2}{\lambda_1} \leq 1; \\ &2) \quad 0 < \alpha < 1, && \alpha \frac{\lambda_2}{\lambda_1} > 1. \end{aligned} \tag{2.65}$$

In both cases, condition 2 then requires that $\beta < 0$. Recall that in the electric case $\phi \leq \phi_0$, so choosing the sign of $g(\phi)$ in the IR determines the sign everywhere[5]. Finally, we would like the dilaton perturbations to be non-oscillating (condition 5) and demand that at least one of them should be irrelevant (condition 6). The details of the corresponding calculations can be found in Appendix C. Our results are summarized in Figures 1 and 2. In the green region, all of our conditions are satisfied. The gray region is inconsistent with conditions 1-4, while in the red region $g(\phi) < 0$. The yellow region has $g(\phi) > 0$, but has either no irrelevant dilaton perturbations, or oscillating modes.

For $\alpha < 1$, we find either one or no irrelevant dilaton perturbations, while for $\alpha > 1$ we find either two or none. This result seems to be related to the fact that in the $\alpha > 1$ case, $\lambda_1^2(\tilde{z})$ is not injective, i.e. there exist two possible scaling parameters $\tilde{z}_1, \tilde{z}_2$ for any given λ_1 (see Appendix B). We will address this issue further at the end of the following section. Notice also that while for $\alpha < 1$, all values of λ_1 and $\tilde{z}$ are allowed, for $\alpha > 1$ there is a lower bound on λ_1 and an upper bound on $\tilde{z}$. These bounds stem from the condition that $\lambda_1^2 > 0$ and equation (B.5). We conclude that for a given choice of α, there exists a large region in parameter space that is consistent with our conditions and hence satisfies all basic

[5]Although we will not consider the case of negative $g(\phi)$, let us point out that in this case we would also have to take $\beta < 0$ to satisfy condition 2, so this is a universal result.

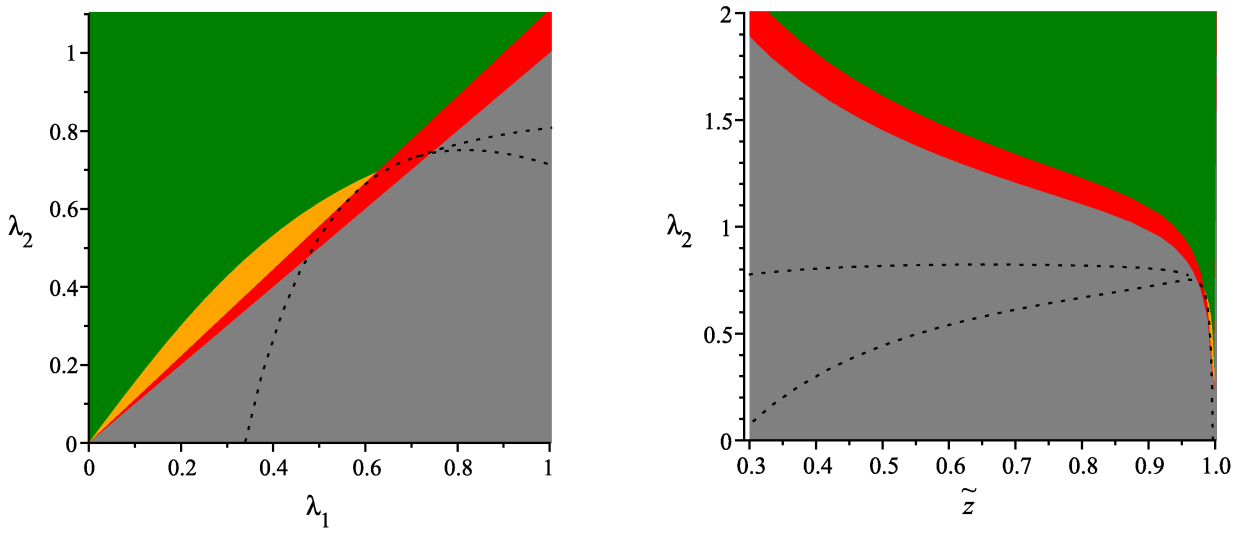

Figure 1: Plot of different regions in parameter space, characterized by the number of irrelevant dilaton perturbations ($\alpha = 0.9$). The regions are bounded by the curves (C.1), (C.2), (2.65) and $\lambda_2 = \lambda_1$. They are colored as follows: $g(\phi) < 0$ (red), $g(\phi) > 0$ but no irrelevant perturbations or oscillating modes (gold), $g(\phi) > 0$ and at least one irrelevant perturbation (green). In the gray area, at least one of the conditions 1-4 is violated.

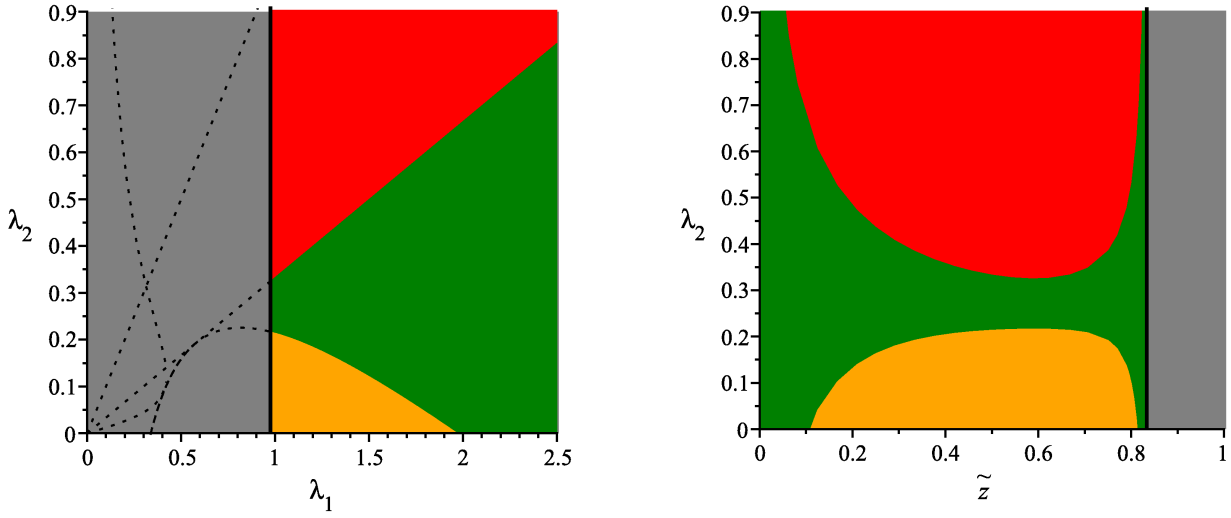

Figure 2: The same plot for $\alpha = 3$. Now the green region has 2 irrelevant perturbations. There is a lower bound on λ_1 and an upper bound on $\tilde{z}$, as indicated by vertical lines.

requirements to admit the desired $\mathrm{AdS}_4 \to \mathrm{Lif}_4^z \to \mathrm{AdS}_2 \times \mathbb{R}^2$ solutions.

2.3.2 Numerical Results

In order to find numerical solutions to our equations, we proceed as follows: We set initial conditions at large r by adding irrelevant perturbations to the exact $\mathrm{AdS}_2 \times \mathbb{R}^2$ solution:

$$\begin{aligned} a(r) &= \frac{1}{r} + \sum_{i=1}^{3(4)} D_i \delta a_i, \\ b(r) &= r + \sum_{i=1}^{3(4)} D_i \delta b_i, \\ \phi(r) &= \phi_0 + \sum_{i=1}^{3(4)} D_i \delta \phi_i. \end{aligned} \tag{2.66}$$

We focus here on the case $\alpha < 1$, for which there are three irrelevant perturbations. The case $\alpha > 1$ is discussed briefly at the end of this section. The amplitudes D_i have to be tuned in order to find a solution that has both an intermediate Lifshitz regime and a smooth flow to AdS_4 in the UV. In practice, it is however easier to choose a different basis for the perturbations in (2.66), which allows us to specify a', b', ϕ' directly. The role of the three initial conditions is then roughly the following: The value of ϕ' determines how long the solution stays approximately $\mathrm{AdS}_2 \times \mathbb{R}^2$. There is a minimum value ϕ'_{min} that is required to "kick" ϕ out of its local minimum and run logarithmically during the Lifshitz stage. The transition stage from $\mathrm{AdS}_2 \times \mathbb{R}^2$ to Lifshitz is shifted towards the IR as we increase ϕ'. The value of a' determines the duration of the scaling stage: We find that in the space of initial conditions, there exists a two-dimensional submanifold $(a'_{\mathrm{crit}}(\phi'), b', \phi')$ with attractor-like behavior. As we approach this critical plane, we observe the emergence of an intermediate Lifshitz stage, which gets wider and wider as a' approaches a'_{crit} from below, while for $a' > a'_{\mathrm{crit}}$ the solution becomes singular. Therefore, by tuning a' we can in principle make the Lifshitz stage arbitrarily long. Finally, the value of b' needs to be tuned in order to achieve a smooth flow to AdS_4 in the UV.

#	1	2
λ_1	1.2	1.1
λ_2	2	0.24
α	0.9	3
β	-1	-1
Q	0.20	4.55
ϕ_0	-0.95	3.91
a'	$-4.9 \cdot 10^{-9}$	$-1.5 \cdot 10^{-7}$
b'	$-5.8 \cdot 10^{-6}$	$2.0 \cdot 10^{-4}$
ϕ'	$8 \cdot 10^{-7}$	10^{-5}
b''	-	10^{-5}
$\tilde{z}$	0.73	0.78
K	0.91	0.82
$\phi_{\rm UV}$	-19.8	-7.6
$b_{\rm UV}$	$1.5 \cdot 10^{-11}$	$2.9 \cdot 10^{-8}$

Table 1: Parameters, initial conditions and fit parameters for numerical solutions.

The parameters and initial conditions of our numerical solutions are summarized in Table 1. Figure 3 shows the evolution of the metric components g_{00} (black) and g_{ii} (blue) for solution #1. (The individual metric functions $a(r)$ and $b(r)$ as well as the dilaton $\phi(r)$ are plotted in Figures 4 and 5.) We chose to plot $d\log g_{\mu\nu}/d\log r$ versus $\log r$ so that power-law relations are clearly visible as horizontal lines. The solution is asymptotically $\mathrm{AdS}_2 \times \mathbb{R}^2$ with $g_{00} \propto r^{-2}$, $g_{ii} \propto r^0$ for large r. At $r \approx 10^{-6}$, the solution approaches an approximate Lifshitz scaling stage with $g_{00} \propto r^{-2}$, $g_{ii} \propto r^{2(\tilde{z}-1)}$, where it remains for several decades. This stage is characterized by an effective scaling parameter $\tilde{z}_{\rm eff} \approx 0.73$ (or $z \approx 3.7$). Notice that $\tilde{z}_{\rm eff}$ decreases slowly towards the UV, as indicated by the slightly positive slope of $d\log g_{ii}/d\log r$. This is due to the fact that $e^{\lambda_2\phi}$ is small but nonzero: Effectively, the coupling constant α is reduced, which in turn increases $\tilde{z}_{\rm eff}$ (see Figure 29). We expect that as we approach the attractor, the solution will take the exact form (2.35) with the predicted value of $\tilde{z} \simeq 0.71$ for $r \to 0$. Finally, it is worth mentioning that both g_{ii} and g_{00} initially overshoot slightly before flowing to Lifshitz.

The dilaton starts out at some large negative value $\phi_{\rm UV}$ for small r and runs towards weak coupling during the scaling stage. In this intermediate regime, $e^{\lambda_2\phi} \ll 1$ and ϕ grows

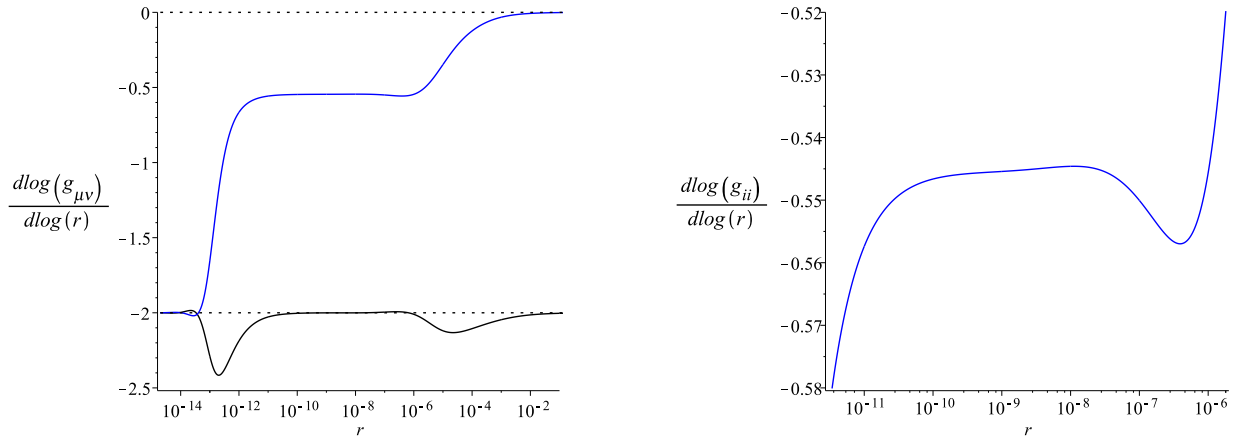

Figure 3: Plot of the metric components g_{00} (black) and g_{ii} (blue) for solution #1 (see Table 1). The figure on the right is a magnified view of the Lifshitz region for g_{ii}. Constant values of $d\log g_{\mu\nu}/d\log r$ indicate a power-law relation. One can clearly see the emergence of an intermediate Lifshitz geometry with $g_{00} \propto r^{-2}$ and $g_{ii} \propto r^{2(\tilde{z}-1)}$. The dotted lines indicate the exact $\mathrm{AdS}_2 \times \mathbb{R}^2$ solution with $g_{ii} \propto r^0$ in the IR and AdS_4 with $g_{ii} \propto r^{-2}$ in the UV.

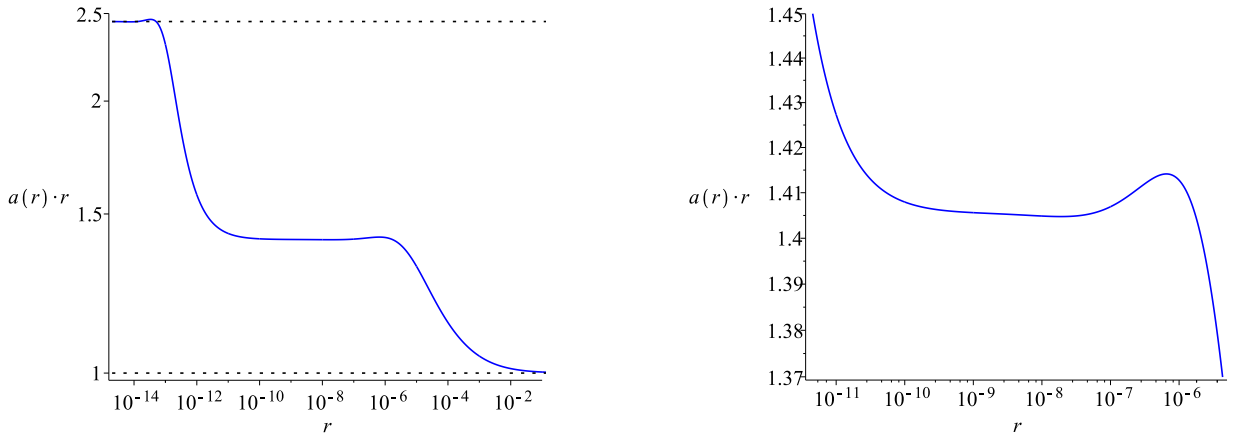

Figure 4: Plot of $a \cdot r$ for solution #1. The figure on the right is a magnified view of the Lifshitz region. The dotted lines represent the exact $\mathrm{AdS}_2 \times \mathbb{R}^2$ solution with $a \cdot r = 1$ in the IR and AdS_4 with $a \cdot r = \sqrt{6}$ in the UV.

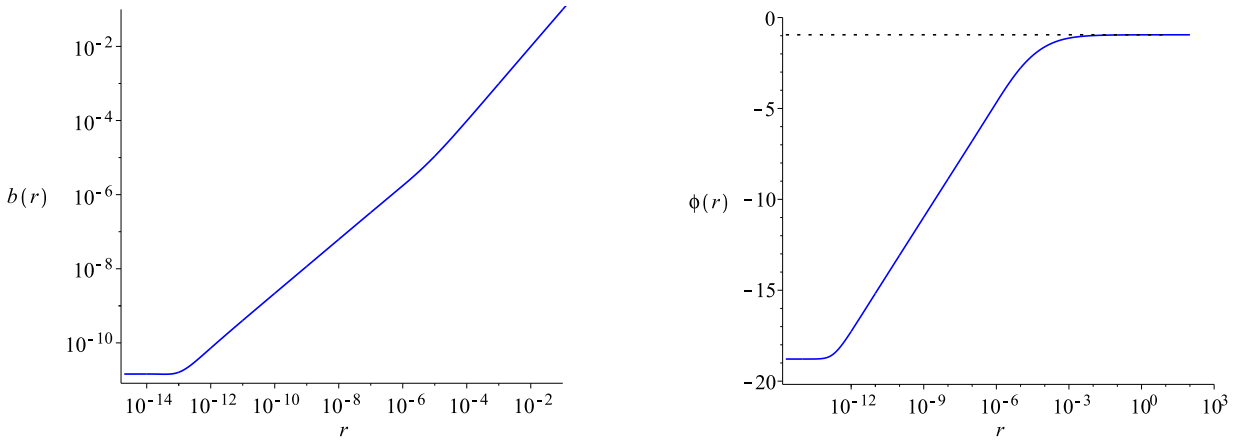

Figure 5: Plot of the metric function b (left) and the dilaton ϕ (right) for solution #1. The dotted line represents the asymptotic value ϕ_0 given by (2.50).

approximately logarithmically, as in (B.2). As ϕ increases, the $e^{\lambda_2\phi}$-term becomes more and more important until at large r, the higher derivative corrections eventually modify the effective potential and stabilize the dilaton at ϕ_0.

In the case of $\alpha \geq 1$, there are two possible dynamical exponents $\tilde{z}_1 < \tilde{z}_2$ (see Appendix B). There is one additional dilaton perturbation, which we can use to fix the value of b'' in the IR. Numerically, we were only able to find flows from $AdS_2 \times \mathbb{R}^2$ to $\text{Lif}_4^{\tilde{z}_2}$, with $\tilde{z}_2 \approx 0.78$ ($z_2 \approx 4.4$). The metric components for this solution are shown in Figure 6. The corresponding values for the exact analytical solution are $\tilde{z}_1 \approx 0.38$ and $\tilde{z}_2 \approx 0.73$. Although a simple counting of dilaton perturbations would suggest that there is one irrelevant deformation leading to each of the two Lifshitz solutions, we were not able to numerically shoot to $\text{Lif}_4^{\tilde{z}_1}$. It therefore remains unclear whether flows to $\text{Lif}_4^{\tilde{z}_1}$ exist.

2.3.3 Flow to AdS_4 in the UV

Our numerical analysis suggests that the solutions exhibit some interesting behavior as they approach asymptotic AdS_4 for $r \to 0$. It is worthwhile to analyze this asymptotic behavior

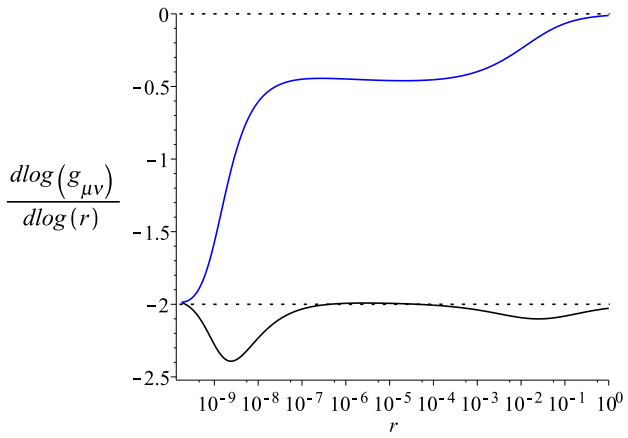

Figure 6: Solution #2 ($\alpha > 1$): Plot of the metric components g_{00} (black) and g_{ii} (blue).

analytically. To lowest order, the solution to the linearized equations of motion is given by

$$\begin{aligned} a(r) &= \frac{\sqrt{6}}{r}\left(1 + a_+ r^{\nu_+} + a_- r^{\nu_-} + a_3 r^3 + a_4 r^4 + \cdots\right), \\ b(r) &= b_{\rm UV} + b_+ r^{\nu_+} + b_- r^{\nu_-} + b_3 r^3 + b_4 r^4 + \cdots, \\ \phi(r) &= \phi_{\rm UV} + \phi_3 r^3 + \phi_4 r^4 + \cdots, \end{aligned} \tag{2.67}$$

where a_3, ϕ_3, $a_\pm$ are free constants and

$$\begin{aligned} a_4 &= \frac{1}{180}\frac{Q^2\left(9 + 2g\left(\phi_{\rm UV}\right)\right)}{b_{\rm UV}^4 f\left(\phi_{\rm UV}\right)\left(1 + 2g\left(\phi_{\rm UV}\right)\right)}, \\ b_3 &= -2 b_{\rm UV} a_3, \\ b_4 &= -\frac{1}{12}\frac{Q^2}{\left(1 + 2g\left(\phi_{\rm UV}\right)\right) f\left(\phi_{\rm UV}\right) b_{\rm UV}^3}, \\ b_\pm &= -\frac{3\left(\nu + 1\right)}{2\nu} b_{\rm UV} a_\pm, \\ \phi_4 &= -\frac{1}{12}\frac{Q^2 f'\left(\phi_{\rm UV}\right)}{b_{\rm UV}^4 f\left(\phi_{\rm UV}\right)^2}, \\ \nu_\pm &= \frac{3}{2} \pm \frac{1}{2}\sqrt{1 - \frac{16}{g\left(\phi_{\rm UV}\right)}}. \end{aligned} \tag{2.68}$$

The leading order perturbations r^ν are purely gravitational. They survive in the limit of pure Einstein-Weyl gravity (i.e. $Q \to 0$) [52]. For $g\left(\phi_{\rm UV}\right) < 16$, ν becomes complex and the

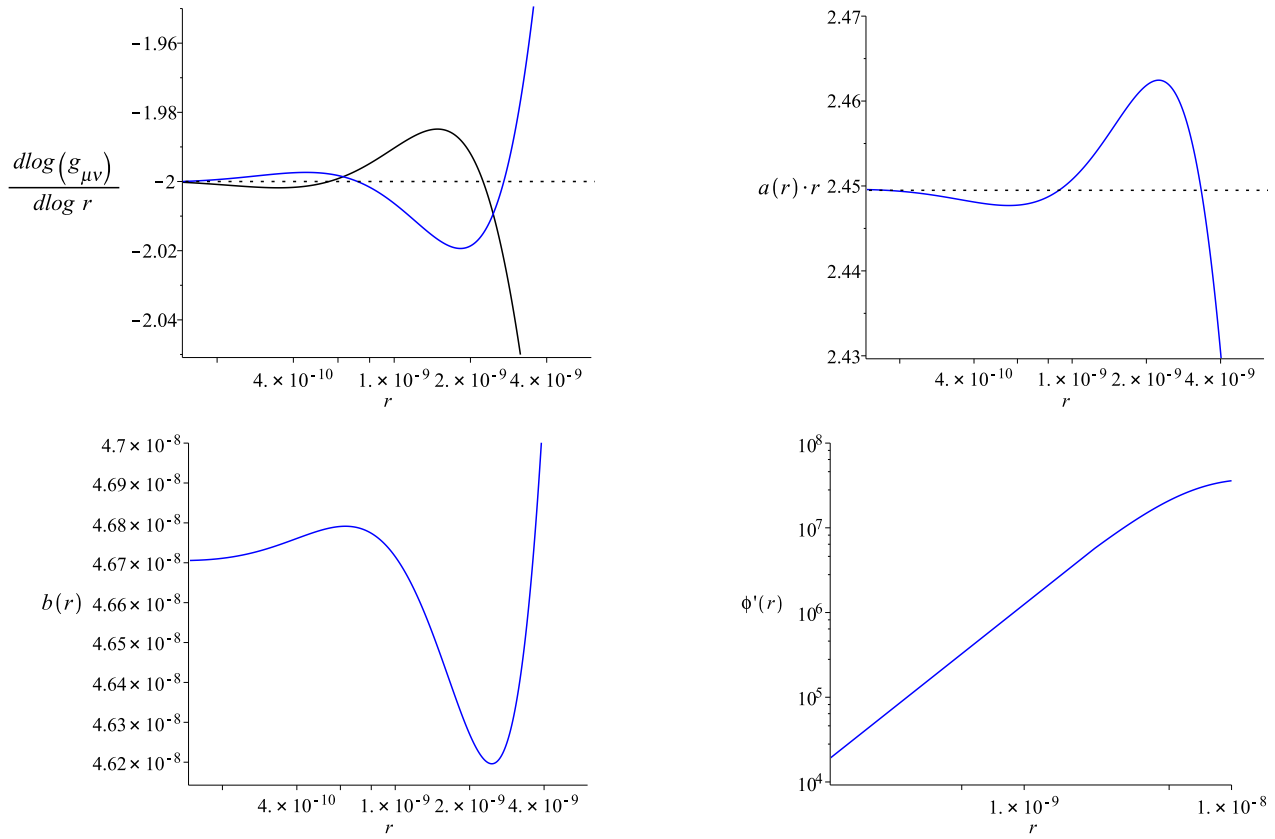

Figure 7: Flow to asymptotic AdS_4 in the deep UV. The first graph shows the metric components g_{00} (black) and g_{ii} (blue). While the metric functions a and b oscillate according to (2.69), the dilaton decreases monotonically.

perturbations oscillate as

$$\begin{aligned} a &\sim r^{\mathrm{Re}(\nu)-1} \cos\left(\mathrm{Im}\left(\nu\right) \log\left(r\right) + \varphi_a\right), \\ b &\sim r^{\mathrm{Re}(\nu)} \cos\left(\mathrm{Im}\left(\nu\right) \log\left(r\right) + \varphi_b\right), \end{aligned} \tag{2.69}$$

where $\varphi_{a/b}$ are constant phases. Notice that for $\alpha \to 0$, the imaginary part of ν blows up, so these perturbations do not decouple in the two-derivative limit. Figure 7 shows the asymptotic behavior of one of our numerical solutions (parameter set #1). One can clearly see that a and b oscillate according to (2.69), while ϕ simply decreases monotonically.

As it turns out, the oscillating nature of our solutions makes it necessary to switch to a "stiff" method when trying to find exact numerical solutions in the UV. In addition, the

attractor-mechanism of the Lifshitz stage tends to "wipe out" initial conditions, which makes it more and more difficult to exactly hit AdS_4 numerically as the scaling stage gets wider. We therefore content ourselves with presenting the asymptotic behavior for a solution with a relatively narrow scaling stage. A more efficient way of studying the UV-asymptotics would be to directly shoot from the UV.

2.4 Summary and Discussion

In this chapter, we first showed that Lifshitz backgrounds are renormalized in the presence of higher derivative corrections, and in particular Weyl-squared corrections, according to (2.24)-(2.26). We then demonstrated in a toy model that higher curvature corrections, such as those that arise from the string α' expansion, may resolve the Lifshitz horizon into $AdS_2 \times \mathbb{R}^2$. In particular, we have constructed numerical flows from AdS_4 to an intermediate Lifshitz region and finally to $AdS_2 \times \mathbb{R}^2$ in the deep IR in the Einstein-Maxwell-dilaton system with a four-derivative correction of the form

$$\delta\mathcal{L} = \frac{3}{4}(\alpha + \beta e^{\lambda_2 \phi}) C^2_{\mu\nu\rho\sigma}. \tag{2.70}$$

The dilaton coupling β is introduced to stabilize the dilaton, so that an emergent $AdS_2 \times \mathbb{R}^2$ may appear in the IR.

The existence of flows to $AdS_2 \times \mathbb{R}^2$ is not universal, but depends on the parameters α, β, λ_1 and λ_2. For $\alpha < 1$, there is at most one irrelevant dilaton perturbation that can induce a flow from $AdS_2 \times \mathbb{R}^2$ in the deep IR to an intermediate Lifshitz region. We have presented a numerical example of such a flow for $\alpha = 0.9$. On the other hand, for $\alpha \geq 1$, if any irrelevant dilaton perturbations exist, then they necessarily come as a pair. Furthermore, in this case there are two possible dynamical exponents, $\tilde{z}_1$ and $\tilde{z}_2$ (where we take $\tilde{z}_1 < \tilde{z}_2$), allowed in the Lifshitz region. We have constructed a numerical example for $\alpha = 3$ that flows from $AdS_2 \times \mathbb{R}^2$ in the deep IR to an intermediate $\text{Lif}_4^{\tilde{z}_2}$. However, we were unable to

find numerical flows to $\text{Lif}_4^{\tilde{z}_1}$. It remains unclear whether such flows are possible. From a simple counting of irrelevant perturbations, we expect that these flows should indeed exist. In any case, the natural question that arises is whether or not the additional irrelevant perturbation that appears for $\alpha \geq 1$ leads to an interesting geometry. To make a definitive statement about the flows that are allowed, a study of perturbations around the different Lifshitz backgrounds would be required. A similar analysis was carried out for the massive vector case in [55, 56]. It would also be interesting to see if one can find numerical solutions that interpolate between the two Lifshitz solutions.

It would be desirable to explore whether a realistic string model would lead to either α' or string loop corrections of the form needed to resolve the Lifshitz horizon. The α' corrections extend beyond the gravitational sector, and for example may include RF^2 terms at the four derivative level. Even in the gravitational sector, one would expect to have a more general form of the four-derivative corrections, similar to (2.19), but also with possible dilaton couplings. We expect that the mechanism to resolve the Lifshitz singularity in the IR will also work in the more general case with $\alpha_{\text{R}} \neq 0$ and $\alpha_{\text{GB}} \neq 0$. However, the smooth flow to AdS_4 in the UV observed here relies on the fact that the Weyl tensor vanishes quickly enough so that it does not source the dilaton for small r. It is unclear whether the UV asymptotics would remain unchanged for *generic* higher derivative corrections.

In the case of an electrically charged brane considered here, there is another source of corrections that might modify the UV dynamics: Since the dilaton runs towards strong coupling, we expect quantum corrections to the gauge kinetic function $f(\phi)$ to become important and modify the effective potential in this regime. In addition, there is a priori no reason why magnetic solutions should not be equally sensitive to α'-corrections. We therefore expect our mechanism to be relevant also in the magnetic case. Since in this case the dilaton runs towards strong coupling in the IR, a consistent approach would be to consider both α' and quantum corrections at the same time.

We expect that our analysis can be easily extended to geometries with hyperscaling

violation. These backgrounds can be parametrized by a metric of the form

$$ds^2_{d+1} = e^{2\gamma r}(-e^{2zr/L}dt^2 + e^{2r/L}d\vec{x}^2 + dr^2). \tag{2.71}$$

For $\gamma \neq 0$ this metric is invariant under the scale transformation (1.2) only up to a rescaling of ds. One may construct solutions of this type by choosing an exponential potential for the dilaton, which as a result runs linearly with r. Flows to $\mathrm{AdS}_2 \times \mathbb{R}^2$ were constructed using a quantum corrected gauge kinetic function $f(\phi)$ in [53].

Finally, although an emergent $\mathrm{AdS}_2 \times \mathbb{R}^2$ geometry provides a non-singular resolution of the Lifshitz scaling solution, the presence of a non-contracting transverse $\mathbb{R}^2$ leads to non-zero entropy density at zero temperature in the dual non-relativistic system, thus violating the third law of thermodynamics. A more satisfying situation where the entropy density vanishes at zero temperature may potentially be obtained by flowing into AdS_4 in the deep IR. Thus one may imagine constructing flows from AdS_4 to Lifshitz to AdS_4. This would be a special case of an AdS to AdS domain wall solution, in which case the holographic c-theorem would apply [57, 58, 59]. It would be interesting to see whether such flows may be constructed in a toy model admitting AdS_4 solutions with two distinct AdS radii.

Chapter 3

Boundary-to-Bulk Correlators

In the previous chapter, we provided evidence that Lifshitz spacetime is indeed a physically meaningful geometry by showing that the potential IR divergences can be resolved in a UV complete theory of quantum gravity. Having gained more confidence in Lifshitz spacetime as a consistent geometry, we are now ready to ask interesting questions about the details of holography for non-relativistic field theories. In particular, we would like to continue to develop the holographic dictionary, a mapping between observables on the bulk and boundary site of the duality.

In the well studied case of relativistic AdS/CFT, an important part of this dictionary is the correspondence between normalizable modes, which scale as r^{Δ_+} near the boundary, and states in the Hilbert space of the dual field theory. In particular, a quantized bulk field ϕ can be mapped to its corresponding boundary operator O via

$$\phi \mapsto O = \lim_{r\to 0} r^{-\Delta_+}\phi. \tag{3.1}$$

The remarkable fact here is that both operators can be quantized in terms of the same creation/annihilation operators, which implies an isomorphism between the Fock space representations of bulk and boundary Hilbert spaces [60, 61]. Moreover, the map (3.1) can be inverted in position space. As a result, local quantum fields in the bulk can be ex-

pressed in terms of boundary operators with the help of a so-called smearing function K [62, 63, 64]. Consequently, we can study CFTs to learn something about their gravitational duals [65, 66, 67].

If AdS/CMT is to be understood as a true equivalence between a field theory and a gravitational theory, rather then just a set of prescriptions to compute condensed matter quantities, one should expect that a similar statement can be made for non-relativistic systems. In other words, the field theory should somehow contain all the relevant information about the gravitational theory. In this chapter, we address this issue by investigating the extent of reconstructability of bulk information from boundary data in non-relativistic spacetimes. Specifically, we examine the equivalent of the map (3.1) for such spacetimes, and show that it is in general not invertible in position space.

A simple argument why this reconstruction procedure is not straightforward can be made by studying geodesics in the corresponding backgrounds. For Lifshitz spacetime, the effective potential is given by

$$V_{\text{eff}}(r) = \left(\frac{L}{r}\right)^{2z} \kappa + \left(\frac{L}{r}\right)^{2(z-1)} \vec{k}^{\,2}. \tag{3.2}$$

Null geodesics ($\kappa = 0$) with nonzero transverse momentum k turn around at finite r and never reach the boundary (see Figure 8). This is a result of the non-relativistic nature of the dual theory, which manifests itself in the fact that the effective speed of light g_{tt}/g_{xx} diverges as $r \to 0$. Therefore, in the classical (i.e. geometric optics) limit, information about the transverse direction of the bulk geometry can never reach an observer at the boundary.

Quantum mechanically the picture is different. In general, wavefunctions are allowed to tunnel through any classically forbidden region to reach the boundary, so there is hope that bulk reconstruction is possible after all. However, as we will demonstrate, at large momenta the imprint these tunneling modes leave at the boundary is exponentially small and as a consequence, a smearing function cannot be constructed. Our arguments closely follow those of [68, 69], where first steps towards generalizing smearing functions to spaces other than pure AdS were made.

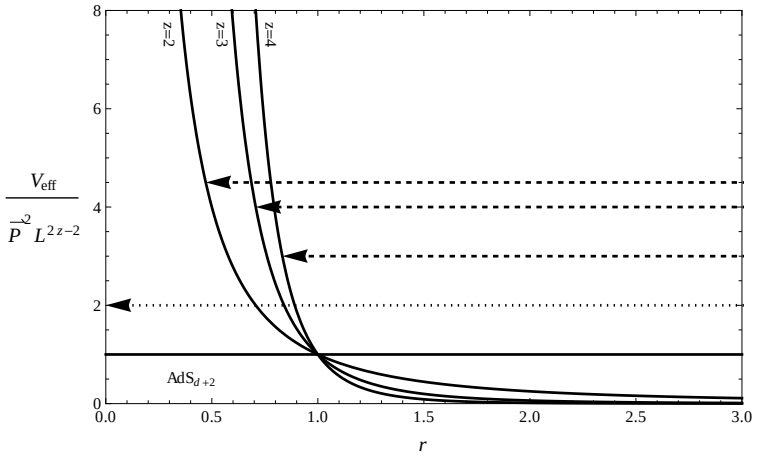

Figure 8: Effective potential (3.2) for null geodesics ($\kappa = 0$) in AdS ($z = 1$) and Lifshitz spacetimes ($z = 2, 3, 4$). In Lifshitz, light rays sent from the bulk in any nonradial direction have to turn around at finite r and can never reach the boundary.

Our analysis for the case of pure Lifshitz spacetime can be easily generalized to show that smearing functions do not exist for any geometry that allows for "trapped modes", that is, modes that have to tunnel through a momentum-barrier in the potential to reach the boundary. In [69], the authors show that the smearing function in their spherically symmetric spacetimes can indeed become well-defined, at least in some bulk region, once they change from an AdS-Schwarzschild solution to a nonsingular asymptotically AdS spacetime. Our case, however, does not allow such a resolution. Importantly, the smearing function in Lifshitz remains ill-defined everywhere if we resolve the tidal singularity into an $\text{AdS}_2 \times \mathbb{R}^d$ region, as we did in chapter 2. Similarly, the replacement of the near-boundary region with an asymptotic AdS_{d+2} region does not resolve the issue either.

The problem we encounter when trying to construct a smearing function is related to modes with large transverse momentum. At the end of this chapter, we will argue that we can make limited sense of smearing functions in Lifshitz spacetime after all, provided we are willing to introduce a momentum-cutoff Λ. This of course has the consequence that we forego the idea of using Lifshitz spacetime to calculate holographic observables at arbitrarily small transverse length scales. We will see in section 4.3 that a cutoff at large momenta (or equivalently small frequencies) is forced upon us when considering the effect of higher

derivative corrections.

3.1 Scalars in Planar Backgrounds

The geometric optics picture of figure 8 shows that a classical observer sitting at the boundary of Lifshitz spacetime cannot receive light signals from an observer in the bulk that carry nonzero transverse momentum. This indicates a potential difficulty of reconstructing bulk informatino purely from boundary data, in the spirit of AdS/CFT. However, to fully analyze the problem, we need to go beyond the classical approximation and consider the reconstruction of scalar field modes via a boundary-to-bulk correlator.

Instead of focussing only on Lifshitz spacetime, let us consider a more generall class of planar backgrounds, given by the following metric:

$$ds^2_{d+2} = e^{2B(r)}[-e^{2W(r)}dt^2 + d\vec{x}_d^2] + e^{2C(r)}dr^2. \tag{3.3}$$

For $W = 0$, the $(d+1)$-dimensional metric at constant r is Lorentz invariant. This encompasses the pure AdS case as well as Lorentz invariant domain wall flows. The $W \neq 0$ case allows for 'non-relativistic' backgrounds such as pure or asymptotic Lifshitz backgrounds as well as for planar black holes. In this case, we may interpret e^{-W} as the gravitational redshift factor[1]. The global behavior of the metric is constrained by the null energy condition (subsequently NEC; for previous work see [70, 56]). The two independent conditions are

$$-R^t_t + R^r_r = de^{W-C}\partial_r\left(-e^{-W-C}\partial_r B\right) \geq 0, \tag{3.4}$$

$$-R^t_t + R^{x_1}_{x_1} = e^{-W-(d+1)B-C}\partial_r\left(e^{W+(d+1)B-C}\partial_r W\right) \geq 0. \tag{3.5}$$

Here x_1 is any one of the $\vec{x}$ transverse directions. If we choose a gauge where $A = C$, or

[1]Note that this assumes that there is an asymptotic reference region where $W = 0$, so that $(d+1)$-dimensional Lorentz invariance is restored. This would occur, for example, in an AdS to Lifshitz flow.

equivalently $W = C - B$, these conditions simplify to

$$\left((e^{-B})'e^{-2W}\right)' \geq 0, \tag{3.6}$$

$$\left(W'e^{dB}\right)' \geq 0, \tag{3.7}$$

We now consider a minimally coupled scalar in the background (3.3). The Klein-Gordon equation is given by

$$[e^{-W-(d+1)B-C}\partial_M e^{W+(d+1)B+C}g^{MN}\partial_N - m^2]\phi = 0. \tag{3.8}$$

Since the metric (3.3) has Killing vectors $\frac{\partial}{\partial t}$ and $\frac{\partial}{\partial x^i}$, the wave equation above is separable and we can write

$$\phi(t, \vec{x}, r) = e^{i(\vec{k}\cdot\vec{x}-Et)}f(r). \tag{3.9}$$

The Klein-Gordon equation (3.8) then becomes

$$\left[e^{2(W+B-C)}\left(\partial_r^2 + \frac{d(W+(d+1)B-C)}{dr}\partial_r\right) + E^2 - e^{2W}\vec{k}^{\,2} - e^{2(W+B)}m^2\right]f = 0. \tag{3.10}$$

Let us choose a gauge where $A = C$, or $W = C - B$. Equivalently, starting in any given gauge we can introduce a new radial coordinate ρ such that

$$e^{C-B-W}dr = d\rho. \tag{3.11}$$

Note that ρ is a tortoise coordinate for our metric ansatz. This gives

$$[\partial_\rho^2 + dB'\partial_\rho + E^2 - e^{2W}\vec{k}^{\,2} - e^{2(W+B)}m^2]f = 0, \tag{3.12}$$

where primes denote derivatives with respect to ρ. If we now let

$$f = e^{-dB/2}\psi, \tag{3.13}$$

we end up with a Schrödinger-type equation

$$-\psi'' + U\psi = E^2\psi, \tag{3.14}$$

where

$$U = V_m + V_k + V_{\cos}, \tag{3.15}$$

with

$$V_m = e^{2(W+B)}m^2, \qquad V_k = e^{2W}\vec{k}^{\,2}, \qquad V_{\cos} = (d/2)B'' + (d/2)^2 B'^2. \tag{3.16}$$

The effective potential U can be interpreted as a potential that timelike/null geodesics would see, plus an additional "cosmological" pontential $V_{\cos}$. To see this, note that we can simplify the geodesic equation by defining conserved quantities along the Killing directions,

$$E \equiv e^{2A}\dot{t}, \qquad \vec{k} \equiv e^{2B}\dot{\vec{x}}, \tag{3.17}$$

where a dot indicates a derivative with respect to the affine parameter λ. Geodesics then obey

$$-m^2 = \left(\frac{ds}{d\lambda}\right)^2 = -e^{-2(W+B)}E^2 + e^{-2B}\vec{k}^{\,2} + e^{2C}\dot{r}^2. \tag{3.18}$$

If we define

$$V_{\text{eff}} \equiv e^{2(W+B)}m^2 + e^{2W}\vec{k}^2, \tag{3.19}$$

with $m^2 = 1$ for timelike and $m^2 = 0$ for null geodesics, then we find

$$e^{2(W+B+C)}\dot{r}^2 = E^2 - V_{\text{eff}}. \tag{3.20}$$

This is of the form of an energy conservation equation, $E_{\text{tot}} = E_{\text{kin}} + V_{\text{eff}}$, where

$$E_{\text{kin}} = e^{2(W+B+C)}\dot{r}^2. \tag{3.21}$$

and the effective potential is given by $V_{eff} = V_m + V_k$, see (3.16). The additional potential $V_{\text{cos}}$is a familiar correction term for the scalar potential in curved space. In AdS; it plays a crucial role in the derivation of the Breitenlohner-Freedman bound [71].

3.2 Scalars in Lifshitz Spacetime

For Lifshitz backgrounds, the Schrödinger potential can be written as

$$U = \left(\frac{L}{z\rho}\right)^2 \left(m^2 + \frac{d(d+2z)}{4L^2}\right) + \left(\frac{L}{z\rho}\right)^{2(1-1/z)} \vec{k}^2, \tag{3.22}$$

where we introduced a new radial coordinate according to (3.11), to bring the metric to the form (1.5). Explicitly, we have

$$\rho = \frac{L}{z}\left(\frac{r}{L}\right)^z. \tag{3.23}$$

Note that both V_m and the entirety of V_{cos} contribute to the $1/\rho^2$ blowup as $\rho \to 0$ (corresponding to the boundary). The fact that these two pieces scale with the same power of ρ is a feature of Lifshitz spacetime; it will not continue to be true for more complicated spacetimes such as the AdS-Lifshitz flows studied in chapter 2.

The qualitative behavior of solutions to the Schrödinger equation is roughly as follows: The wavefunction starts out oscillating deep in the bulk ($\rho \to \infty$) and crosses the potential barrier at the classical turning point ρ_0. For $\rho < \rho_0$, the mode must tunnel under the barrier, and thus the wavefunction will in general be a superposition of exponentially growing and suppressed modes. We will only be interested in the mass ranges where the growing solution is non-normalizable. In this range, the normalizable modes relevant for canonical quantization are exponentially suppressed in the area of this barrier at small ρ.

For $z = 1$, V_k is a constant, but for $z > 1$ it blows up near the boundary, although less fast than the other terms in the potential. Specifically, $V_k/V_m \propto e^{-2B}$. For spacetimes with Lifshitz asymptotics,

$$\partial_\rho \left(e^{-B}\right)\Big|_{\rho_{\rm bdy}} = \partial_\rho \left(\frac{z\rho}{L}\right)^{1/z}\Big|_{\rho_{\rm bdy}} > 0 \tag{3.24}$$

Consequently, $\partial_\rho e^{-B} > 0$ throughout the spacetime. Near the boundary, the mass term V_m will always dominate, but V_k will increase in relative importance as we head in towards the IR region. Because of the different behavior of the mass/cosmological and momentum-dependent terms, it is crucial to distinguish between two qualitatively different "types" of tunneling. If at a given energy, the momentum $\vec{k}$ is sufficiently small, the wavefunction crosses the barrier at a point where V_k is subdominant compared to the other terms in the potential. Consequently, the $1/\rho^2$ part of U will control the suppression near the boundary. We shall refer to those modes as *free modes*. This name is justified, because even though they are tunneling, classically they correspond to null geodesics that can reach the boundary.

If $\vec{k}$ is large, the wavefunction crosses the barrier already at a point where $U \approx V_k$, and the wavefunction will receive an additional suppression by an exponential in $\vec{k}$, due to tunneling through this thicker barrier. We shall refer to this class of solutions as *trapped modes*. They play a crucial role in our analysis, as they are the quantum equivalent to nonradial null-geodesics that cannot reach the boundary, which we encountered in the introduction to this chapter.

We may study the behavior of these free and trapped modes by solving the Schrödinger equation (3.14) in a Lifshitz background. It is convenient to scale out the energy E by introducing the dimensionless coordinate

$$\zeta = E\rho. \tag{3.25}$$

Then (3.14) becomes $-\psi''(\zeta) + (U-1)\psi(\zeta) = 0$ where

$$U = \frac{\nu_z^2 - 1/4}{\zeta^2} + \frac{\alpha}{\zeta^k}, \tag{3.26}$$

with

$$\nu_z = \frac{1}{z}\sqrt{(mL)^2 + (d+z)^2/4}, \qquad \alpha = \left(\frac{EL}{z}\right)^\gamma \left(\frac{\vec{k}}{E}\right)^2, \qquad \gamma = 2(1-1/z). \tag{3.27}$$

Since the null energy condition demands $z \geq 1$, we generally focus on the case $0 < \gamma < 2$. (The $\gamma = 0$, or pure AdS, case is familiar and can be treated by standard methods.) In this case, the boundary ($\zeta \to 0$) behavior of U is $\sim 1/\zeta^2$, while the horizon ($\zeta \to \infty$) behavior is $\sim 1/\zeta^\gamma$.

Near the boundary, we have

$$-\psi'' + \frac{\nu^2 - 1/4}{\zeta^2}\psi \approx 0 \qquad \Rightarrow \qquad \psi \sim A\zeta^{1/2-\nu} + B\zeta^{1/2+\nu}. \tag{3.28}$$

Using (3.23), (3.25) and (3.13), we can express the behavior of the original Klein-Gordon field in terms of the original coordinate r as

$$\phi \sim \hat{A}\left(\frac{r}{L}\right)^{\Delta_-} + \hat{B}\left(\frac{r}{L}\right)^{\Delta_+}, \tag{3.29}$$

where

$$\hat{A} = A\left(\frac{EL}{z}\right)^{1/2-\nu}, \quad \hat{B} = B\left(\frac{EL}{z}\right)^{1/2+\nu}, \quad \Delta_\pm = \frac{d+z}{2} \pm \sqrt{(mL)^2 + \left(\frac{d+z}{2}\right)^2}. \tag{3.30}$$

We will consider only the mass range where the first solution (related to A) is non-normalizable with respect to the Klein-Gordon norm, while the second solution (related to B) is normalizable. Via the AdS/CFT correspondence, non-normalizable modes represent classical sources of an operator O at the boundary, which redefine the Hamiltonian of the field theory [1, 3, 2].

Normalizable fluctuations are placed on top of these classical sources and they correspond to different states in the field theory, or equivalently expectation values of O [61, 60]. We will only be interested in the situation where the boundary Hamiltonian is fixed, so we will consequently treat non-normalizable solutions as non-fluctuating. The fluctuating modes to be quantized are thus the normalizable modes given by B. As a result, we will end up setting $A = 0$ and investigating the consequences of doing so. Note that this is in contrast with the computation of AdS/CFT correlators, which we will discuss in chapter 4. In this case, B is interpreted as the response to turning on a source A.

Turning now to the horizon, we see that both terms in (3.26) fall off as $\zeta \to \infty$. Hence the horizon behavior is given by[2]

$$-\psi'' - \psi \approx 0 \qquad \Rightarrow \qquad \psi \sim ae^{i\zeta} + be^{-i\zeta}. \tag{3.31}$$

In terms of the original r coordinate, this becomes

$$\psi \sim a \exp\left(i\frac{EL}{z}\left(\frac{r}{L}\right)^z\right) + b \exp\left(-i\frac{EL}{z}\left(\frac{r}{L}\right)^z\right), \tag{3.32}$$

so that

$$\phi \sim a\left(\frac{r}{L}\right)^{d/2} \exp\left(i\frac{EL}{z}\left(\frac{r}{L}\right)^z\right) + b\left(\frac{r}{L}\right)^{d/2} \exp\left(-i\frac{EL}{z}\left(\frac{r}{L}\right)^z\right). \tag{3.33}$$

The horizon modes correspond to infalling and outgoing waves, given by a and b, respectively. Since the wave equation is second order and linear, the boundary data (A, B) must be linearly related to the horizon data (a, b). AdS/CFT correlators are generally computed by taking infalling conditions at the horizon, corresponding to $b = 0$, while bulk normalizable modes are given instead by taking $A = 0$ at the boundary. Of course, the precise relation between boundary and horizon data can only be obtained by solving the wave equation. While this

[2]For simplicity, we have assumed $1 < k < 2$. For $0 < k \leq 1$, the horizon falloff $\sim 1/\zeta^k$ is insufficiently fast, and the potential becomes long-ranged. This introduces a correction to the horizon behavior of the wavefunction. However, this is unimportant for our discussion, as we have no need for the asymptotic phase of ψ in the classically allowed region.

cannot be performed in general, the exact solution is known for $z = 2$, where the potential U is analytic. We now turn to this case, as it provides a clean example of the behavior of trapped modes and in particular the exponential suppression that they receive when tunneling under the barrier in the potential.

3.2.1 A Specific Example: $z = 2$ Lifshitz

For a pure Lifshitz background with $z = 2$, or $\gamma = 1$, the potential (3.26) is analytic in ζ and the Schrödinger equation takes the form

$$-\psi'' + \left(\frac{\nu^2 - 1/4}{\zeta^2} + \frac{\alpha}{\zeta} - 1\right)\psi = 0, \tag{3.34}$$

where $\alpha = \vec{k}^2 L/2E$. As this is essentially Whittaker's equation, the solution can be written in terms of the Whittaker functions $M_{-i\alpha/2,\nu}(-2i\zeta)$ and $W_{-i\alpha/2,\nu}(-2i\zeta)$, or equivalently in terms of confluent hypergeometric functions [20]. Expanding for $\zeta \to 0$ and demanding that ψ satisfies the boundary asymptotics (3.28) for normalizable and nonnormalizable modes gives

$$\begin{aligned}\psi = &\left[\left(\frac{i}{2}\right)^{\frac{1}{2}+\nu} B - \left(\frac{i}{2}\right)^{\frac{1}{2}-\nu} \frac{\Gamma(-2\nu)\Gamma(\frac{1}{2}+\nu+\frac{i\alpha}{2})}{\Gamma(2\nu)\Gamma(\frac{1}{2}-\nu+\frac{i\alpha}{2})} A\right] M_{-i\alpha/2,\nu}(-2i\zeta) \\ &+ \left[\left(\frac{i}{2}\right)^{\frac{1}{2}-\nu} \frac{\Gamma(\frac{1}{2}+\nu+\frac{i\alpha}{2})}{\Gamma(2\nu)} A\right] W_{-i\alpha/2,\nu}(-2i\zeta).\end{aligned} \tag{3.35}$$

For the horizon, we expand for large ζ and compare with (3.31) to obtain

$$\begin{aligned}\psi \;=\; &\left[e^{-\pi\alpha/4}\frac{\Gamma(\frac{1}{2}+\nu+\frac{i\alpha}{2})}{\Gamma(1+2\nu)} 2^{-i\alpha/2} b\right] M_{-i\alpha/2,\nu}(-2i\zeta) \\ &+ \left[e^{\pi\alpha/4} 2^{i\alpha/2} a + e^{i\pi(\frac{1}{2}-\nu)} e^{\pi\alpha/4} \frac{\Gamma(\frac{1}{2}+\nu+\frac{i\alpha}{2})}{\Gamma(\frac{1}{2}+\nu-\frac{i\alpha}{2})} 2^{-i\alpha/2} b\right] W_{-i\alpha/2,\nu}(-2i\zeta).\end{aligned} \tag{3.36}$$

Comparing (3.35) with (3.36) gives the relation between horizon and boundary coefficients

$$\begin{aligned} A &= (2i)^{\frac{1}{2}-\nu}\frac{\Gamma(2\nu)}{\Gamma(\frac{1}{2}+\nu-\frac{i\alpha}{2})}e^{\pi\alpha/4}\left(2^{-i\alpha/2}b - e^{i\pi(\frac{1}{2}+\nu)}\frac{\Gamma(\frac{1}{2}+\nu-\frac{i\alpha}{2})}{\Gamma(\frac{1}{2}+\nu+\frac{i\alpha}{2})}2^{i\alpha/2}a\right), \\ B &= (2i)^{\frac{1}{2}+\nu}\frac{\Gamma(-2\nu)}{\Gamma(\frac{1}{2}-\nu-\frac{i\alpha}{2})}e^{\pi\alpha/4}\left(2^{-i\alpha/2}b - e^{i\pi(\frac{1}{2}-\nu)}\frac{\Gamma(\frac{1}{2}-\nu-\frac{i\alpha}{2})}{\Gamma(\frac{1}{2}-\nu+\frac{i\alpha}{2})}2^{i\alpha/2}a\right). \end{aligned} \tag{3.37}$$

Although we are primarily interested in normalizable modes in the Lifshitz bulk, we first note that the usual computation of the retarded Green's function proceeds by taking infalling boundary conditions at the horizon, namely $b = 0$. Then (3.36) immediately gives

$$\psi_{\text{infalling}} \sim W_{-i\alpha/2,\nu}(-2i\zeta). \tag{3.38}$$

We now demand that the coefficient of $M_{-i\alpha/2,\nu}(-2i\zeta)$ in (3.35) vanishes, from which we obtain

$$G_R(E,\vec{p}) \sim \frac{\hat{B}}{\hat{A}} = \left(\frac{EL}{2}\right)^{2\nu}\frac{B}{A} = \left(\frac{EL}{i}\right)^{2\nu}\frac{\Gamma(-2\nu)\Gamma(\frac{1}{2}+\nu+\frac{i\alpha}{2})}{\Gamma(2\nu)\Gamma(\frac{1}{2}-\nu+\frac{i\alpha}{2})}, \tag{3.39}$$

in agreement with [20] when continued to Euclidean space. Note that in the large momentum limit, $k \to \infty$ (or more precisely for $\alpha \gg \nu$), the Whittaker function $W_{-i\alpha/2,\nu}(-2i\zeta)$ is only large near the boundary, and decays exponentially into the bulk. This matches with the heuristic picture of AdS/CFT, where the CFT "lives" on the boundary. In the relativistic case, corresponding to an AdS geometry, the boundary data has a power law falloff as it penetrates into the bulk. However, for this Lifshitz geometry, the falloff is exponential.

Of course, for the bulk reconstruction that we are interested in, we actually want to consider the space of normalizable modes, as they are the ones that span the Hilbert space in the bulk. From the Hamiltonian picture, the natural norm is the Klein-Gordon norm, which is in fact compatible with the norm for the Schrödinger equation (3.14). Normalizable modes correspond to taking $A = 0$, so that

$$\psi_{\text{normalizable}} \sim M_{-i\alpha/2,\nu}(-2i\zeta). \tag{3.40}$$

Comparing (3.35) with (3.36) then gives the relation between bulk and boundary coefficients for normalizable modes

$$\frac{B}{b} = 2^{-i\alpha/2}\left(\frac{2}{i}\right)^{\frac{1}{2}+\nu}\frac{\Gamma(\frac{1}{2}+\nu+\frac{i\alpha}{2})}{\Gamma(1+2\nu)}e^{-\pi\alpha/4}. \tag{3.41}$$

Note that $M_{-i\alpha/2,\nu}(-2i\zeta)$ is essentially a standing wave solution in the classically allowed region $\zeta > \zeta_0$, where ζ_0 is the classical turning point. Since this interval is semi-infinite, the wavefunction must be normalized by fixing the amplitude b of these oscillations. Hence the ratio B/b is a direct measure of the amplitude of properly normalized wavefunctions at the boundary.

Recall our previous distinction between the two different types of tunneling solutions: "free" vs. "trapped" modes. Modes with small momenta k at fixed E ($\alpha \ll \nu$) are "free modes". For these modes, we have, up to an overall phase

$$\frac{|B|}{|b|} \approx \frac{2^{\nu+\frac{1}{2}}\Gamma\left(\frac{1}{2}+\nu\right)}{\Gamma(1+2\nu)}. \tag{3.42}$$

The tunneling process produces the typical scaling behavior $\sim \rho^{\Delta_+}$ at the boundary, but there is no exponential suppression. For large momenta ($\alpha \gg \nu$) the modes are "trapped", and we find instead

$$\frac{|B|}{|b|} \approx \frac{\sqrt{4\pi}e^{-\left(\nu+\frac{1}{2}\right)}}{\Gamma(1+2\nu)}\alpha^{\nu}e^{-\pi\alpha/2}. \tag{3.43}$$

These modes have to tunnel not only through the $1/\rho^2$ potential near the boundary, but also through the wider momentum barrier $V_k \sim k^2/\rho$ at larger ρ. This causes the solution to be exponentially suppressed when it reaches the boundary. We conclude that the $z = 2$ Lifshitz metric allows for trapped modes, which have arbitrarily small boundary imprint for large k.

Clearly, we could have obtained the exponential suppression factor $e^{-\pi\alpha/2}$ in (3.43) by simply setting $V_m = V_{\cos} = 0$ in the Schrödinger potential. More generally, since the size of V_k is controlled by k^2, in any interval $[\rho_1,\rho_2]$ away from the boundary, i.e. in any region

where the potential U is bounded, at large enough k the difference in amplitudes between the points ρ_1 and ρ_2 will always be governed by an exponential relation like (3.43). For the purpose of determining whether or not trapped modes exist in a given spacetime, it will therefore be enough to study the equivalent tunneling problem in the potential $U \equiv V_k$. We will come back to this issue later.

3.3 WKB Approximation

In order to study the existence of trapped modes in spacetimes beyond exact $z = 2$ Lifshitz, it will be useful to have a formalism that provides a qualitative description of the behavior of tunneling modes even for cases where an analytic solution might not exist. This will allow us to study Lifshitz with $z \neq 2$, as well as more general backgrounds (3.3) with nontrivial W, B and C. The WKB method provides us with just such a formalism.

Applying the WKB approximation to the effective Schrödinger equation in Lifshitz spacetime, and other spacetimes in which the potential falls of as $1/\rho^2$ near the origin, is not straightforward, and some subtleties arise. It is therefore necessary to carefully develop a formalism that will allow us to find approximate solutions, and furthermore to quantify its shortcomings by performing an error analysis.

We would like to find approximate solutions to equations of the form

$$\psi'' + \Omega^2(\zeta)\psi = 0, \tag{3.44}$$

with $\Omega^2 > 0$ as $\zeta \to \infty$ and $\Omega^2 \sim -\zeta^{-2}$ as $\zeta \to 0$. Furthermore, we shall assume that for a given energy, there exists only one classical turning point with $\Omega^2(\zeta_0) = 0$. To capture all of these properties explicitly, we may write

$$\Omega^2 = K^2 - \frac{1}{\zeta^2}\left(\nu^2 - \frac{1}{4} + \mu(\zeta)\right), \tag{3.45}$$

with $\lim_{\zeta\to 0}\mu(\zeta)=0$ and $\nu>1/2$. Notice that for $\nu\leq 1/2$ the qualitative picture would change considerably: The wavefunction becomes oscillating again close to the boundary, which requires a different treatment. For Lifshitz spacetime, we have $K=1$ and $\mu=\alpha\zeta^{2-\gamma}$, where $\zeta\equiv Ex$ (see (3.26)). We now make the standard WKB-ansatz

$$\psi\sim\frac{1}{\sqrt{P(\zeta)}}e^{i\int d\zeta' P(\zeta')}. \tag{3.46}$$

Plugging into (3.44), we arrive at a differential equation for $P(\zeta)$:

$$P^2-\Omega^2+\frac{1}{2}\frac{P''}{P}-\frac{3}{4}\left(\frac{P'}{P}\right)^2=0. \tag{3.47}$$

This equation can be solved perturbatively, assuming that the frequency Ω^2 is slowly-varying:

$$P^2=Q_0+\epsilon Q_1+\epsilon^2 Q_2+\cdots, \tag{3.48}$$

where

$$\begin{aligned} Q_0 &\equiv \Omega^2,\\ Q_1 &\equiv \frac{3}{4}\left(\frac{\Omega'}{\Omega}\right)^2-\frac{1}{2}\frac{\Omega''}{\Omega},\\ &\text{etc.,} \end{aligned} \tag{3.49}$$

and we introduced an explicit parameter ϵ that counts the number of derivatives and needs to be set to 1 at the end. To lowest order, $P^2\approx\Omega^2$ and the error can be estimated by comparing the size of the first order to the zeroth order term. Away from the classical turning point ζ_0, the full solution can be written as:

$$\psi(\zeta)=\begin{cases}(-\Omega^2)^{-\frac{1}{4}}\left[Ce^{-\int_{\zeta_0}^{\zeta}d\zeta'\sqrt{-\Omega^2}}+De^{\int_{\zeta_0}^{\zeta}d\zeta'\sqrt{-\Omega^2}}\right], & \zeta<\zeta_0;\\ (\Omega^2)^{-\frac{1}{4}}\left[ae^{i\int_{\zeta_0}^{\zeta}d\zeta'\sqrt{\Omega^2}}+be^{-i\int_{\zeta_0}^{\zeta}d\zeta'\sqrt{\Omega^2}}\right], & \zeta>\zeta_0.\end{cases} \tag{3.50}$$

As is obvious from (3.49), the WKB approximation always breaks down near the turning point. As usual, this can be dealt with by approximating the potential in the region close to ζ_0 by a linear function

$$\Omega^2 \approx \beta\left(\zeta-\zeta_0\right), \qquad \beta \equiv \frac{d\Omega^2}{d\zeta}\left(\zeta_0\right) > 0. \tag{3.51}$$

In this region, the solution is then given in terms of Airy functions:

$$\psi_0 \approx E_1 \mathrm{Ai}\left(\beta^{\frac{1}{3}}\left(\zeta_0-\zeta\right)\right) + E_2 \mathrm{Bi}\left(\beta^{\frac{1}{3}}\left(\zeta_0-\zeta\right)\right). \tag{3.52}$$

It has the following asymptotics:

$$\psi_0 \approx \begin{cases} \frac{\left(\zeta_0-\zeta\right)^{-\frac{1}{4}}}{2\beta^{\frac{1}{12}}\sqrt{\pi}}\left[E_1 e^{-\frac{2}{3}\sqrt{\beta}\left(\zeta_0-\zeta\right)^{\frac{3}{2}}} + 2E_2 e^{\frac{2}{3}\sqrt{\beta}\left(\zeta_0-\zeta\right)^{\frac{3}{2}}}\right], & \zeta \ll \zeta_0; \\ \frac{\left(\zeta-\zeta_0\right)^{-\frac{1}{4}}}{2\beta^{\frac{1}{12}}\sqrt{\pi}}\left[\left(E_2-iE_1\right)e^{i\left(\frac{\pi}{4}+\frac{2}{3}\sqrt{\beta}\left(\zeta-\zeta_0\right)^{\frac{3}{2}}\right)} + \left(E_2+iE_1\right)e^{-i\left(\frac{\pi}{4}+\frac{2}{3}\sqrt{\beta}\left(\zeta-\zeta_0\right)^{\frac{3}{2}}\right)}\right], & \zeta \gg \zeta_0. \end{cases} \tag{3.53}$$

On the other hand, for ζ close to, but not too close to ζ_0, the exponent in (3.50) can be written as

$$\int_{\zeta_0}^{\zeta} d\zeta' \sqrt{|\Omega^2|} \approx \begin{cases} -\frac{2}{3}\sqrt{\beta}\left(\zeta_0-\zeta\right)^{\frac{3}{2}}, & \zeta < \zeta_0; \\ \frac{2}{3}\sqrt{\beta}\left(\zeta-\zeta_0\right)^{\frac{3}{2}}, & \zeta > \zeta_0. \end{cases} \tag{3.54}$$

Matching (3.53) and (3.50), we find

$$\begin{aligned} C &= \left(e^{-i\frac{\pi}{4}}a + e^{i\frac{\pi}{4}}b\right), \\ D &= \frac{i}{2}\left(e^{-i\frac{\pi}{4}}a - e^{i\frac{\pi}{4}}b\right). \end{aligned} \tag{3.55}$$

Near the boundary ($\zeta \ll 1$), we then have

$$\psi(\zeta) = \frac{\zeta^{\frac{1}{2}}}{\left(\nu^2-\frac{1}{4}\right)^{\frac{1}{4}}}\left(Ce^{S_0(\zeta)} + De^{-S_0(\zeta)}\right), \tag{3.56}$$

where

$$S_0(\zeta) \equiv \int_{\zeta}^{\zeta_0} d\zeta' \sqrt{-\Omega^2}. \tag{3.57}$$

Hence the solution near the boundary is determined entirely in terms of S_0, which is given as an integral over the effective potential.

As a check of the validity of the WKB approximation, let us determine whether Q_1 in (3.48) remains small compared to Q_0 for all ζ. Consider the slightly more general case where $\Omega^2 \sim -\zeta^{-s}$ as $\zeta \to 0$. We find

$$Q_1 = -\frac{s\,(s-4)}{16\zeta^2}. \tag{3.58}$$

For $s \neq 0, 4$, this term blows up near the boundary. For $s < 2$, it blows up faster than $Q_0 = \Omega^2$ itself, thus rendering the WKB approximation invalid. For $s > 2$, it blows up slower than Ω^2, so the relative error approaches zero and we should expect WKB to yield accurate results. In the borderline case $s = 2$, which is the one that is interesting for us, the first order correction is in general comparable to the zero-th order term. Hence the lowest order approximation will a priori not give very accurate results.

Stated differently, for $s = 2$ the perturbative expansion (3.48) of P is not consistent, since in general the order n and order $n+1$ terms will mix. To avoid this mixing, we need to find a way to explicitly move the term $Q_1 = -1/(4\zeta^2)$ to one lower order in the expansion. Obviously, we could just declare

$$P^2 = \Omega^2 - \frac{1}{4\zeta^2} + O\left(\epsilon\right). \tag{3.59}$$

This is equivalent to making the somewhat ad-hoc substitution $\nu^2 \to \nu^2 + 1/4$ in (3.48). A more rigorous way is to perform the following change of variables:

$$\begin{aligned} \zeta &\equiv e^w, \\ \psi &\equiv e^{\frac{w}{2}} u. \end{aligned} \tag{3.60}$$

The Schrödinger equation then reads

$$u'' + \omega^2 u = 0, \tag{3.61}$$

where

$$\omega^2 \equiv e^{2w} - \nu^2 - \mu(w). \tag{3.62}$$

It is easy to see that in these coordinates, the effective frequency is indeed slowly varying both in the deep UV and the deep IR. In fact, one can check that the first order term Q_1 becomes much smaller than Ω^2 in both limits. We see that in the new variables (3.60), the expansion (3.48) is consistent and the WKB solution is a good approximation everywhere, except in the vicinity of the turning point.

Repeating the steps (3.50) through (3.56) for (3.61) and changing back to our previous variables we arrive at

$$\psi = \left(\frac{\zeta}{\nu}\right)^{\frac{1}{2}} \left(Ce^{S(\zeta)} + De^{-S(\zeta)}\right), \tag{3.63}$$

with

$$S(\zeta) \equiv \int_{\zeta}^{\zeta_0} d\zeta' \sqrt{-\Omega^2 + \frac{1}{4\zeta'^2}}\,. \tag{3.64}$$

Not surprisingly, the effect of the coordinate transformation (3.60) is indeed to add an effective potential $\Delta U = 1/(4\zeta^2)$ to (3.45). Therefore, all we need to do in practice is to replace $\nu^2 \to \nu^2 + 1/4$. Let us emphasize that (3.61) is in fact equivalent to (3.44), so this substitution is now on a rigorous footing.

The exponential growth/decay of the solution in the classically forbidden region is manifest in the dependence on S in (3.63), which roughly corresponds to the area of the tunneling barrier. The wider/higher the barrier, the larger the corresponding factor e^S is. We are only interested in the normalizable, or decaying solution near the boundary, so we will have to set $C = 0$. Up to a finite error, the WKB approximation then accurately captures the boundary behavior of this solution, and in particular the exponential suppression between bulk and

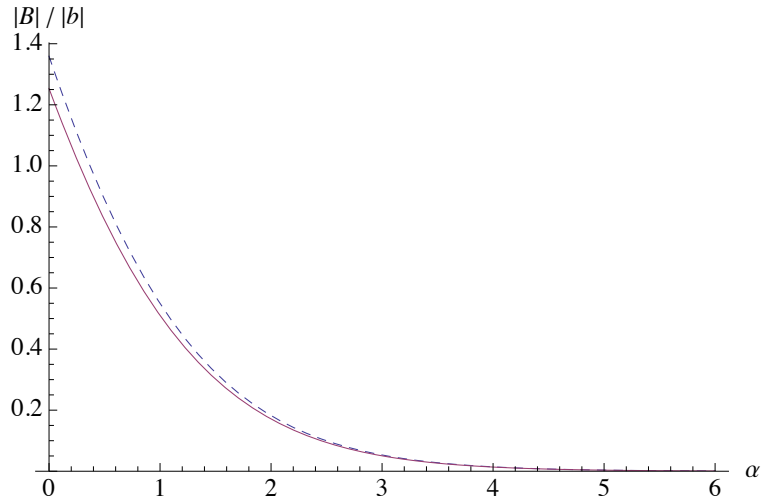

Figure 9: Plot of the WKB (dashed) and exact (solid) boundary normalization factor $|B|/|b|$ as a function of α. Here we have taken $z = 2$ and $\nu = 1$. The large α behavior is exponentially suppressed, $|B|/|b| \sim \alpha^{\nu} e^{-\pi\alpha/2}$.

boundary amplitudes.

We can compare this WKB approximation with the exact solution for $z = 2$ from section 3.2.1. Figure 9 shows a plot of the WKB solution for $z = 2$ Lifshitz, compared to the exact solution. As we can see, the WKB approximation accurately captures the exponential momentum-suppression at large α. In section 3.5, we will use the WKB formalism to investigate for which spacetimes smearing functions exist.

3.3.1 Example: AdS ($z = 1$)

We can use the WKB approximation to analyze the near-boundary behavior in various planar spacetimes. For AdS, $z = 1$ and we have

$$\Omega^2 = 1 - \frac{\nu^2 - \frac{1}{4}}{\zeta^2}, \tag{3.65}$$

where

$$\zeta = \sqrt{E^2 - k^2}\rho. \tag{3.66}$$

Computing the integral (3.64), we find

$$S(\zeta) = -\sqrt{\nu^2 - \zeta^2} - \frac{\nu}{2} \log\left(\frac{\nu - \sqrt{\nu^2 - \zeta^2}}{\nu + \sqrt{\nu^2 - \zeta^2}}\right). \tag{3.67}$$

Near the boundary ($\zeta \ll \nu$),

$$e^S \approx \left(\frac{e}{2\nu}\right)^{-\nu} \zeta^\nu. \tag{3.68}$$

Plugging this result into (3.63) and rescaling back to the original field ϕ we arrive at the familiar-looking result

$$\phi(x) = A\rho^{d-\Delta} + B\rho^{\Delta}, \tag{3.69}$$

where $\Delta \equiv (d+1)/2 + \nu$, and

$$\begin{aligned} A &= Ce^{-\nu} 2^\nu \nu^{\nu - \frac{1}{2}} \left(E^2 - k^2\right)^{\frac{1}{4} - \frac{\nu}{2}}, \\ B &= iDe^{\nu} 2^{-\nu-1} \nu^{-\nu - \frac{1}{2}} \left(E^2 - k^2\right)^{\frac{1}{4} + \frac{\nu}{2}}. \end{aligned} \tag{3.70}$$

Notice that the inclusion of the correction term ΔU was crucial to obtain the correct boundary behavior.

3.3.2 Example: $z = 2$ Lifshitz

For Lifshitz with $z = 2$, we have

$$\Omega^2 = 1 - \frac{\nu^2 - \frac{1}{4}}{\zeta^2} - \frac{\alpha}{\zeta}. \tag{3.71}$$

The classical turning point is at

$$\zeta_0 = \frac{\alpha}{2}\left(1 + \sqrt{1 + \left(\frac{2\nu}{\alpha}\right)^2}\right). \tag{3.72}$$

In this case, the WKB integral (3.64) can be evaluated to give

$$S = -\sqrt{\nu^2+\alpha\zeta-\zeta^2} - \nu\log\left(\frac{\zeta\left(2\nu^2+\alpha\zeta_0\right)}{\zeta_0\left(2\nu^2+\alpha\zeta+2\nu\sqrt{\nu^2+\alpha\zeta-\zeta^2}\right)}\right) + \frac{\pi\alpha}{4} + \frac{\alpha}{2}\arcsin\left(\frac{\alpha-2\zeta}{\sqrt{4\nu^2+\alpha^2}}\right). \tag{3.73}$$

In the near-boundary limit $\zeta/\nu \to 0$, with α/ν held fixed, we find

$$e^S \approx \left(\frac{\sqrt{\alpha^2+(2\nu)^2}}{(2\nu)^2}\right)^{-\nu} \exp\left[-\nu+\frac{\alpha}{2}\left(\pi-\arctan\left(\frac{2\nu}{\alpha}\right)\right)\right]\zeta^{-\nu}. \tag{3.74}$$

For $\alpha/\nu \ll 1$ this can be approximated as

$$e^S \approx \left(\frac{e}{2\nu}\right)^{-\nu}\zeta^{-\nu}, \tag{3.75}$$

which is exactly what we found in the AdS case.

Hence high energy/low momentum modes do not "feel" the Lifshitz background, but instead behave like they would in the AdS case. Those are precisely the "free modes", defined in section 3.2, which only have to tunnel through the ρ^{-2}-part of the potential. Notice that for finite momenta, the definitions of ζ in AdS (3.66) and Lifshitz (3.25) differ slightly. They do however agree in the $\alpha \to 0$ limit.

We are interested in the normalizable mode, which may be obtained by setting $C = 0$; this furthermore implies $D = e^{-i\frac{\pi}{4}}b$. Using (3.63), we see that

$$\left.\frac{|B|}{|b|}\right|_{\text{WKB}} = \frac{e^\nu}{\sqrt{\nu}(2\nu)^{2\nu}}(\alpha^2+4\nu^2)^{\nu/2}\exp\left[-\frac{\alpha}{2}\left(\pi-\arctan\left(\frac{2\nu}{\alpha}\right)\right)\right]. \tag{3.76}$$

This may be compared with the exact $z = 2$ solution (3.41)

$$\frac{|B|}{|b|} = 2^{\frac{1}{2}+\nu}\frac{|\Gamma(\frac{1}{2}+\nu+i\frac{\alpha}{2})|}{\Gamma(1+2\nu)}e^{-\pi\alpha/4}. \tag{3.77}$$

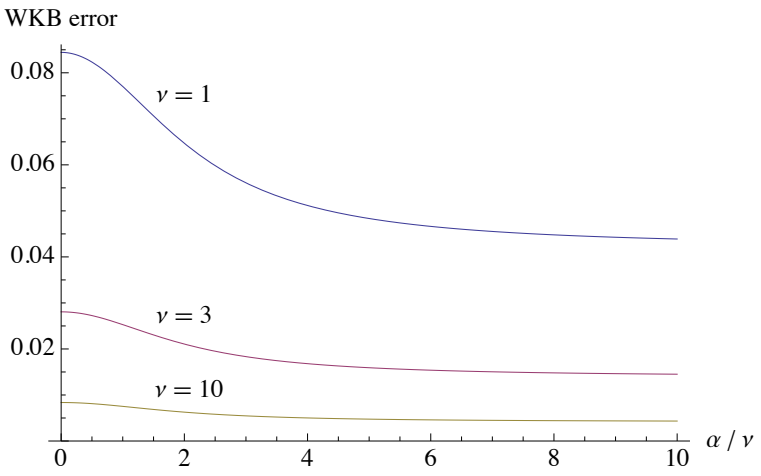

Figure 10: Comparison of the WKB amplitude factor with the exact result for $z = 2$ and $\nu = 1$, 3 and 10. The fractional WKB error is given by $(\eta_{\rm WKB} - \eta_{\rm exact})/\eta_{\rm exact}$, where $\eta = |B|/|b|$.

As an example, we show the behavior of the WKB and exact solution as a function of α for $\nu = 1$ in Figure 9.

It is straightforward to examine the behavior of the WKB and exact solutions in the small and large α limits. The $\alpha/\nu \ll 1$ limit was already considered above. In the opposite limit $\alpha/\nu \gg 1$, we find instead

$$e^S \approx \left(\frac{e}{2\nu}\right)^{-2\nu} \alpha^{-\nu} e^{\frac{\alpha\pi}{2}} \zeta^{-\nu}. \tag{3.78}$$

Thus we obtain

$$\left.\frac{|B|}{|b|}\right|_{\rm WKB} \approx \begin{cases} \left(\frac{e}{2}\right)^{\nu} \nu^{-\left(\nu+\frac{1}{2}\right)}, & \text{for } \frac{\alpha}{\nu} \ll 1; \\ \frac{e^{2\nu}}{\sqrt{\nu}(2\nu)^{2\nu}} \alpha^{\nu} e^{-\frac{\pi\alpha}{2}}, & \text{for } \frac{\alpha}{\nu} \gg 1. \end{cases} \tag{3.79}$$

This may be compared with the exact solution in the same limits

$$\frac{|B|}{|b|} \approx \begin{cases} \frac{2^{\nu+\frac{1}{2}}\Gamma\left(\frac{1}{2}+\nu\right)}{\Gamma(1+2\nu)}, & \text{for } \frac{\alpha}{\nu} \ll 1; \\ \frac{\sqrt{4\pi}}{\Gamma(1+2\nu)} \alpha^{\nu} e^{-\frac{\pi\alpha}{2}}, & \text{for } \frac{\alpha}{\nu} \gg 1. \end{cases} \tag{3.80}$$

Our result demonstrates that the WKB solution gives the correct α behavior for both small

and large α. Note that the ν dependent prefactors are different for finite ν, although they coincide in the large ν limit. This is illustrated in Figure 10, where we plot the fractional difference between the WKB result and the exact solution for several values of ν. In particular, while the asymptotic behavior $|B|/|b| \sim \alpha^\nu e^{-\pi\alpha/2}$ is reproduced as $\alpha/\nu \to \infty$, the fractional error approaches a constant for fixed ν

$$\frac{\delta(|B|/|b|)}{|B|/|b|} \to \frac{\Gamma(1+2\nu)e^{2\nu}}{\sqrt{4\pi\nu}(2\nu)^{2\nu}} - 1 = \frac{1}{24\nu} + \frac{1}{1152\nu^2} + \cdots . \tag{3.81}$$

One should keep in mind, however, that this will not affect our results on the absence of smearing functions for the Lifshitz background, as what is important is the exponential suppression near the boundary, and not the exact form of the prefactor.

3.4 General Lifshitz Spacetime

For the general Lifshitz case, we consider the effective potential

$$\Omega^2 = 1 - \frac{\nu^2}{\zeta^2} - \frac{\alpha}{\zeta^\gamma}, \tag{3.82}$$

where we recall that γ is related to the critical exponent by $\gamma = 2(1 - 1/z)$. We restrict to the case $z > 1$, corresponding to $0 < \gamma < 2$. While the exact WKB integral may be performed numerically, it is in fact possible to extract the asymptotic behavior in the large α limit.

More precisely, we note that Ω^2 introduces several scales for ζ, depending on the relative importance of the three terms. In the UV, as $\zeta \to 0$, the ν^2/ζ^2 term will dominate, while in the IR, as $\zeta \to \infty$, the constant term will dominate. If $\alpha < \nu^\gamma$, then the α/ζ^γ term is not important. In this case, the $1/\zeta^2$ piece of the potential leads to power law behavior in the UV, but no exponential suppression in the wavefunction. On the other hand, for $\alpha > \nu^\gamma$, an intermediate region $(\nu^2/\alpha)^{1/(2-\gamma)} < \zeta < \alpha^{1/\gamma}$ opens up, where the α/ζ^γ term leads to

tunneling behavior.

For $\alpha \gg \nu^\gamma$, the UV and IR regions are well separated, and we may approximate the WKB integral according to

$$S = \int_\zeta^{\zeta_0} d\zeta' \sqrt{\frac{\nu^2}{\zeta'^2} + \frac{\alpha}{\zeta'^\gamma} - 1} \approx \int_\zeta^{\zeta_*} d\zeta' \sqrt{\frac{\nu^2}{\zeta'^2} + \frac{\alpha}{\zeta'^\gamma}} + \int_{\zeta_*}^{\zeta_0} d\zeta' \sqrt{\frac{\alpha}{\zeta'^\gamma} - 1} = S_1 + S_2, \quad (3.83)$$

where $(\nu^2/\alpha)^{1/(2-\gamma)} \ll \zeta_* \ll \alpha^{1/\gamma}$. The first integral may be performed by making the change of variables $u = (\alpha/\nu^2)\zeta^{2-\gamma}$. The result is

$$S_1 = \frac{\nu}{2-\gamma} \left[2\sqrt{1+u} + \log \frac{\sqrt{1+u}-1}{\sqrt{1+u}+1} \right] \Bigg|_{(\alpha/\nu^2)\zeta^{2-\gamma}}^{(\alpha/\nu^2)\zeta_*^{2-\gamma}}. \quad (3.84)$$

Expanding for the lower limit near zero and the upper limit near infinity gives

$$S_1 = \frac{\nu}{2-\gamma} \log\left(\frac{4\nu^2}{\alpha e^2}\right) - \nu \log\zeta + \frac{2\sqrt{\alpha}}{2-\gamma} \zeta_*^{1-k/2} \left(1 - \frac{\nu^2}{2\alpha\zeta_*^{2-\gamma}} + \cdots\right). \quad (3.85)$$

This gives the correct near-boundary behavior

$$\psi_{\text{WKB}} \sim \zeta^{1/2} e^{-S} \sim \zeta^{\nu+1/2}. \quad (3.86)$$

For the second integral, we let $u = \alpha/\zeta^\gamma$, so that

$$S_2 = \frac{\alpha^{1/\gamma}}{\gamma} \int_1^{\alpha/\zeta_*^\gamma} u^{-1-1/\gamma} \sqrt{u-1}\, du. \quad (3.87)$$

Although this integral can be expressed in terms of the incomplete Beta function, we only need the expansion for large α/ζ_*^γ. The result is

$$S_2 = \frac{\sqrt{\pi}\Gamma(1/\gamma - 1/2)}{2\Gamma(1/\gamma)} \alpha^{1/\gamma} - \frac{2\sqrt{\alpha}}{2-\gamma} \zeta_*^{1-\gamma/2} \left(1 - \frac{2-\gamma}{2(2+\gamma)} \frac{\zeta_*^\gamma}{\alpha} - \cdots\right). \quad (3.88)$$

When S_1 and S_2 are added together, the leading terms in ζ_* cancel, while the rest vanish in

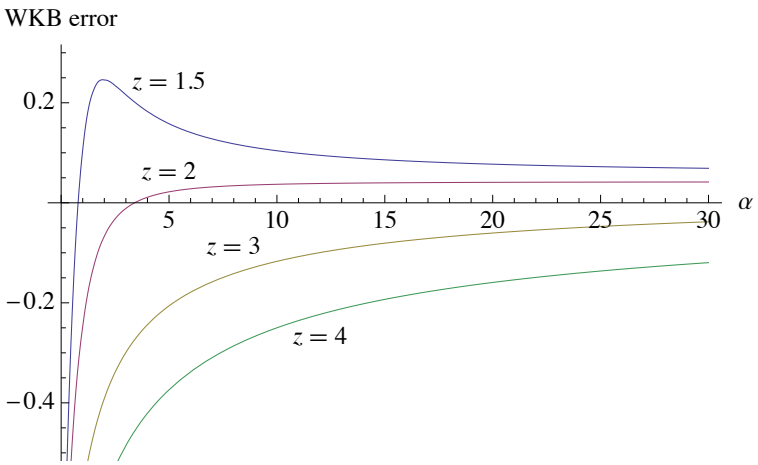

Figure 11: Comparison of the asymptotic WKB amplitude factor with the exact (numerical) result for $\nu = 1$, and $z = 1.5$, 2, 3 and 4. The fractional WKB error is given by $(\eta_{\text{WKB}} - \eta_{\text{exact}})/\eta_{\text{exact}}$, where $\eta = |B|/|b|$. Note that the asymptotic WKB result (3.89) is only valid in the large α limit. The fractional error approaches a constant (dependent on ν) as $\alpha \to \infty$.

the asymptotic limit. We thus obtain

$$\psi_{\text{WKB}} \sim \sqrt{\frac{\zeta}{\nu}} e^{-S} \sim \zeta^{\nu+1/2} \frac{1}{\sqrt{\nu}} \left(\frac{\alpha e^2}{4\nu^2}\right)^{\nu/(2-\gamma)} \exp\left(-\frac{\sqrt{\pi}\Gamma(1/\gamma - 1/2)}{2\Gamma(1/\gamma)} \alpha^{1/\gamma}\right). \tag{3.89}$$

This agrees with (3.78) for $\gamma = 1$, corresponding to $z = 2$. We have confirmed numerically that this WKB result for $\alpha \gg \nu^\gamma$ reproduces the correct asymptotic behavior in α. As an example, we show the fractional error for several values of z at fixed $\nu = 1$ in Figure 11. As in the $z = 2$ case discussed above, for fixed ν, the exact prefactor is not reproduced by WKB. However, the exponential suppression is confirmed.

3.4.1 Error Analysis

In addition to the explicit numerical analysis of the previous section, we would like to investigate the domain of validity of the WKB approximation analytically. In particular, this allows us to identify potentially problematic regions that yield a large error when integrated over, and identify when and where the WKB approximation breaks down.

In the coordinates (3.60), the effective frequency is given by

$$\omega^2 = e^{2w} - \alpha e^{(2-\gamma)w} - \nu^2. \tag{3.90}$$

The relative error can be estimated by

$$\begin{aligned}\frac{Q_1}{Q_0} = \frac{1}{\omega^6}\Bigg[&\frac{1}{4}e^{4w} + \nu^2 e^{2w} + \frac{1}{16}\alpha^2\left(2-\gamma\right)^2 e^{2(2-\gamma)w} \\ &+ \frac{1}{4}\alpha\left(\gamma^2+\gamma-2\right)e^{(4-\gamma)w} - \frac{1}{4}\nu^2\alpha\left(2-\gamma\right)^2 e^{(2-\gamma)w}\Bigg].\end{aligned} \tag{3.91}$$

Clearly, $Q_1/Q_0 \to 0$ as $w \to -\infty$, so the WKB approximation is always valid in the deep UV. The matching procedure near the turning point is only valid if there is some finite overlap between the matching region, where ω^2 is approximately linear, and the semiclassical region, where $|Q_1|/|Q_0| \ll 1$. Let us consider two separate cases:

1. $\alpha \ll \nu$: We can write $\omega^2 \approx e^{2w} - \nu^2$. The condition for the potential to be approximately linear is

$$\frac{\left(\omega^2\right)''\left(w_0\right)}{\left(\omega^2\right)'\left(w_0\right)}\left(w - w_0\right) \ll 1. \tag{3.92}$$

   Since the left hand side is of order $|w - w_0|$, the matching region is approximately given by $e^w \in [\nu e^{-1}, \nu e]$. To check if there is some overlap of this interval with the semiclassical region, let us plug the upper and lower bound into our error estimate:

$$\frac{|Q_1|}{|Q_0|} \approx \begin{cases} \frac{0.08}{\nu^2}, & e^w = \nu e^{-1}; \\ \frac{0.21}{\nu^2}, & e^w = \nu e. \end{cases} \tag{3.93}$$

   We see that for small ν (more precisely, for $\nu \lesssim 1/2$), the error becomes of order one and there is no overlap between the matching region and the semiclassical region. In this case, the matching procedure fails.

2. $\alpha \gg \nu$: We can write $\omega^2 \approx e^{2w} - \alpha e^{(2-k)w}$ for w near the turning point at $e^{w_0} \approx \alpha^{1/\gamma}$.

The condition (3.92) now gives $e^w \in \left[\alpha^{1/\gamma}e^{-1}, \alpha^{1/\gamma}e\right]$ and the error at the boundary points is $Q_1/Q_0 \sim \alpha^{-2/\gamma} \cdot \text{const}$. Hence for α large enough the matching always yields good results.

Even though for large α the matching procedure works for all ν, one needs to be more careful: As we have seen previously, there are three different regimes of ζ, corresponding to each of the three terms in (3.90) dominating. In the region where $\alpha e^{(2-\gamma)w}$ dominates, the relative error grows as w decreases (see (3.58)). If $\nu = 0$, the error continues to grow to infinity as we approach the boundary. However, for $\nu \neq 0$, the ν^2/ρ^2 part of the potential takes over at $\alpha e^{(2-\gamma)w} \sim \nu^2$, and the relative error decreases again. Hence there is a local maximum of order

$$\frac{|Q_1|}{|Q_0|} \approx \frac{3}{32\nu^2}. \tag{3.94}$$

For small ν, the WKB approximation breaks down in this region. We speculate that since $\alpha e^{(2-\gamma)w} \sim \nu^2$ is precisely where the potential changes from k^2/ρ to ν^2/ρ^2 behavior, there is some nontrivial mixing between growing and decaying modes that the WKB approximation cannot account for. This mixing is stronger for small ν, as the difference between the relevant exponents, $\Delta_+ - \Delta_- = 2z\nu$, becomes small. Nevertheless, we can conclude that our WKB approximation can be trusted as long as $\nu \gtrsim 1/2$. Most importantly, the approximation becomes more and more accurate at large α/ν, which is precisely the regime we are interested in.

3.5 Smearing Functions in Lifshitz Spacetimes

In this section, we introduce smearing functions as a way to reconstruct bulk physics from boundary dynamics. Using the WKB formalism developed previously, we will show that for Lifshitz spacetimes, and more generally for any flow involving Lifshitz, such reconstruction is not possible.

First, recall that the normalizable solutions of the Klein Gordon equation can be used

to construct the Hilbert space of the bulk theory in the following way: We decompose the scalar as

$$\phi\left(t,\vec{x},r\right)=\int dEd^{d}k\frac{1}{N_{E,k}}\left(\phi_{E,k}\left(t,\vec{x},r\right)a_{E,k}+\phi_{E,k}^{*}\left(t,\vec{x},r\right)a_{E,k}^{\dagger}\right), \tag{3.95}$$

where $a_{E,k}$ are operators, $N_{E,k}\equiv\left\langle \phi_{E,k},\phi_{E,k}\right\rangle ^{\frac{1}{2}}$and $\left\langle \cdot,\cdot\right\rangle$ is the Klein-Gordon inner product, defined by

$$\left\langle f,g\right\rangle \equiv i\int_{\Sigma}d^{d}xdr\sqrt{-g}g^{00}\left(f^{*}\partial_{t}g-\left(\partial_{t}f^{*}\right)g\right). \tag{3.96}$$

Here, the integral is to be taken over a spacelike slice Σ. This norm is designed to be preserved by the effective Schrödinger equation in (3.14).

If we choose $\left\langle \phi_{E,k},\phi_{E,k}^{*}\right\rangle =0$, i.e. pick definite frequency solutions, the a and $a^{\dagger}$ are the usual creation/annihilation operators for particles with wavefunction $\phi_{E,k}$. We can create all possible states in the Fock space by repeatedly acting with $a^{\dagger}$ on the vacuum $\left|0\right\rangle _{\text{AdS}}$. In Lorentzian AdS/CFT, the bulk-boundary dictionary states that there exists a boundary operator defined by

$$O\left(t,\vec{x}\right)\equiv\lim_{r\to0}r^{-\Delta_{+}}\phi\left(t,\vec{x},r\right), \tag{3.97}$$

which is sourced by the classical, non-normalizable solution ϕ_{cl} behaving as $r^{\Delta_{-}}$ at the boundary. Taking the above limit in (3.95), we arrive at

$$O\left(t,\vec{x}\right)=\int dEd^{d}k\frac{1}{N_{E,k}}\left(\varphi_{E,k}\left(t,\vec{x}\right)a_{E,k}+\varphi_{E,k}^{*}\left(t,\vec{x}\right)a_{E,k}^{\dagger}\right). \tag{3.98}$$

Here $\varphi_{E,k}\equiv\lim_{r\to0}r^{-\Delta_{+}}\phi_{E,k}$. The remarkable fact is that the boundary operator can be expanded in terms of *the same* a,$a^{\dagger}$ as the bulk field. Thus, to create an arbitrary state in the bulk we can use either bulk operators or boundary operators that are "smeared" over $\vec{x}$ and t in an appropriate way. For example, for a single-particle state we have

$$a_{E,k}=\int dt'd^{d}x'N_{E,k}\varphi_{E,k}^{*}\left(t',\vec{x}'\right)O\left(t',\vec{x}'\right), \tag{3.99}$$

so the state $|E,k\rangle_{\text{AdS}}$ can be built entirely out of boundary operators, and so on. Here we need to assume that the φ are normalized such that

$$\int dEd^dk\varphi^*_{E,k}\left(t,\vec{x}\right)\varphi_{E,k}\left(t',x'\right)=\delta\left(t-t'\right)\delta\left(\vec{x}-\vec{x}'\right). \tag{3.100}$$

Notice that (3.100), and not (3.96), is the relevant inner product here. This is because the $\varphi_{E,k}$ are not solutions to any equation of motion at the boundary; rather, they are a set of complete functions[3]. The condition (3.100) is not in tension with the Klein-Gordon normalization condition in the bulk, since we have explicitly factored out $N_{E,k}$ in (3.95).

Equation (3.99) induces an isomorphism between the Fock-space representations of the bulk and boundary Hilbert spaces. The question we would like to answer is whether we can express any operator in the bulk entirely in terms of boundary operators. In particular, we would like to reconstruct ϕ from its corresponding boundary operator O. We make the ansatz

$$\phi\left(t,\vec{x},r\right)=\int dt'd^dx'K\left(t,\vec{x},r|t',\vec{x}'\right)O\left(t',\vec{x}'\right), \tag{3.101}$$

where K is called a smearing function. We can plug (3.99) back into (3.95) to obtain:

$$K\left(t,\vec{x},r|t',\vec{x}'\right)=\int dEd^dk\phi\left(t,\vec{x},r\right)\varphi^*_{E,k}\left(t',\vec{x}'\right). \tag{3.102}$$

Note that this K differs from the usual bulk-to-boundary propagator in that it is a relationship among normalizable modes. Throughout this chapter, we will assume that K has a well-defined Fourier transform, which allows us to interchange the order of integration above. We will comment on some mathematical details and the precise definition of K in section 3.7.

[3]In other words: O is an off-shell operator.

In Lifshitz spacetime, the normalizable solutions are given by

$$\phi_{E,k} = e^{-i\left(Et-\vec{k}\cdot\vec{x}\right)} f_{E,k} = e^{-i\left(Et-\vec{k}\cdot\vec{x}\right)} e^{-\frac{d}{2}B} \psi_{E,k}. \tag{3.103}$$

Near the boundary,

$$\psi \approx B_{E,k}\zeta^{\frac{1}{2}+\nu} \equiv \hat{B}_{E,k} r^{z\left(\frac{1}{2}+\nu\right)}, \tag{3.104}$$

so that

$$\varphi_{E,k} = \lim_{r\to 0} r^{-\Delta_+}\phi = e^{-i\left(Et-\vec{k}\cdot\vec{x}\right)}\hat{B}_{E,k}. \tag{3.105}$$

The normalization condition (3.100) then requires $|\hat{B}_{E,k}| = (2\pi)^{-(d+1)/2}$. Let us now use the WKB approximation. For normalizable solutions, we have $C = 0$, or $a = -ib$, so the normalization of the wavefunction is fixed by

$$|b| = \nu^{\frac{1}{2}} z^{\frac{1}{2}+\nu} (2\pi)^{-\frac{d+1}{2}} \lim_{y\to 0} y^{\nu} e^{S(y)}. \tag{3.106}$$

The properly normalized WKB solution is then given by

$$\psi_{E,k}(\rho) = \begin{cases} (2\pi)^{-\frac{d+1}{2}} \nu^{\frac{1}{2}} z^{\frac{1}{2}+\nu} \left(U+\Delta U-E^2\right)^{-\frac{1}{4}} \lim_{y\to 0} y^{\nu} e^{S(y)-S(\rho)}, & \rho < \rho_0; \\ e^{i\frac{\pi}{4}} (2\pi)^{-\frac{d+1}{2}} \nu^{\frac{1}{2}} z^{\frac{1}{2}+\nu} \left(E^2-U-\Delta U\right)^{-\frac{1}{4}} \lim_{y\to 0} y^{\nu} e^{S(y)} \left[e^{-i\Phi(\rho)} - ie^{i\Phi(\rho)}\right], & \rho > \rho_0, \end{cases} \tag{3.107}$$

where $S(\rho) = \int_{\rho}^{\rho_0} d\rho' \sqrt{U+\Delta U-E^2}$, $\Phi(\rho) = \int_{\rho_0}^{\rho} d\rho' \sqrt{E^2-U-\Delta U}$ and $\Delta U \equiv 1/(2\rho')^2$ (see appendix D).

Using this result, we can write our candidate smearing function as

$$K = e^{-\frac{d}{2}B} \int \frac{dE}{(2\pi)^{\frac{1}{2}}} \frac{d^d p}{(2\pi)^{\frac{d}{2}}} e^{i\left(E(t'-t)-\vec{k}\cdot(\vec{x}'-\vec{x})\right)} \psi_{E,k}. \tag{3.108}$$

We recognize this integral as the inverse Fourier transform of $\psi_{E,p}$. We will now show that this object does not exist[4] because ψ grows exponentially with momentum p.

[4]For a precise definition of what we mean by nonexistence, see section 3.7.

First, let E and ρ be fixed. We then choose k large enough so $\rho < \rho_0$, i.e. so the ρ we are considering is in the tunneling region. This choice is possible for any ρ. For concreteness, we can choose

$$k^2 > E^2 \rho^\gamma. \tag{3.109}$$

Then

$$\left| \lim_{y\to 0} y^\nu e^{S(y)-S(\rho)} \right| = \lim_{y\to 0} y^\nu \exp\left(\int_y^\rho d\rho' \sqrt{\frac{\nu^2}{(\rho')^2} + \frac{k^2}{(\rho')^\gamma} - E^2} \right), \tag{3.110}$$

and the integral is real-valued. Now let $0 < \lambda < 1$ such that $y < \lambda\rho < \rho$ and split the integral accordingly:

$$\int_y^\rho = \int_y^{\lambda\rho} + \int_{\lambda\rho}^\rho. \tag{3.111}$$

Roughly speaking, the first integral provides the boundary data with the correct asymptotic y-dependence, while the second integral is responsible for the exponential behavior in p. In the first integral, using (3.109), we find

$$\int_y^{\lambda\rho} d\rho' \sqrt{\frac{\nu^2}{(\rho')^2} + \frac{k^2}{(\rho')^\gamma} - E^2} > \nu \log\left(\frac{\lambda\rho}{y}\right). \tag{3.112}$$

In the second integral, for p large enough[5] we can find a constant $0 < c < 1$ such that

$$\int_{\lambda\rho}^\rho d\rho' \sqrt{\frac{\nu^2}{(\rho')^2} + \frac{k^2}{(\rho')^\gamma} - E^2} > \int_{\lambda\rho}^\rho d\rho' \frac{ck}{(\rho')^{\frac{\gamma}{2}}} = cz\rho^{\frac{1}{z}} \left(1 - \lambda^{\frac{1}{z}}\right) k. \tag{3.113}$$

Putting everything together, we conclude that for E and ρ fixed, there exist $c, \lambda \in (0,1)$ and k_0 such that

$$\left| \lim_{y\to 0} y^\nu e^{S(y)-S(\rho)} \right| > (\lambda\rho)^\nu \exp\left[cz\rho^{\frac{1}{z}} (1 - \lambda^{\frac{1}{z}}) k \right], \tag{3.114}$$

for all $k > p_0$. Hence the function $\psi_{E,k}$ grows exponentially with k and the smearing function defined in (3.102) does not exist[6].

[5] For concreteness, choose e.g. $p^2 > E^2\rho^k/(1-c^2)$.

[6] This exponential behavior in p is distinct from the behavior of $|B|/|b|$ in α (see e.g. (3.43)), since here we are interested in the amplitude of the wavefunction at a fixed radial location ρ, and not its overall

The inability to construct a smearing function is due to the existence of trapped modes, which have to tunnel through V_k to reach the boundary. The boundary imprint of these modes is suppressed by a factor of e^{-ck}, where c is some positive constant depending on the geometry. However, the normalization condition (3.100) turns this suppression into an exponential amplification: For any given mode the smearing function takes the corresponding boundary data and amplifies it by an appropriate factor to reconstruct bulk information. Consequently, trapped modes receive a contribution e^{+ck} in the smearing function integral. As $k \to \infty$, the boundary imprint of trapped modes becomes arbitrarily small, and as a result the smearing function integral diverges.

The splitting of the domain of integration into a near-boundary region $[0, \lambda\rho]$ and a bulk region $[\lambda\rho, \rho]$ is crucial for our proof: In the near-boundary region, we use the fact that no matter how large k is, we can make ρ' small enough such that the cosmological- and mass-terms in the potential dominate over V_k and we can approximate $U \approx \nu^2/(\rho')^2$. Modes that tunnel through this part do not contribute an exponential factor $\sim e^k$, but rather produce the correct boundary scaling $y^{-\nu}$. This scaling is consequently stripped off by the y^ν factor in (3.110). In the bulk region near ρ, however, there is a minimum value that ρ' can take, so as we drive k to infinity, eventually $U \approx k^2/(\rho')^\gamma$ becomes a very good approximation. This is what produces the exponential factor in (3.114).

We see that there are two qualitatively different limits of the potential: $\rho \to 0$ and $k \to \infty$. Both of them are important for understanding the behavior of (3.110), which is why we need to pick $0 < \lambda < 1$ to get a lower bound that reflects this behavior. Simply setting $\lambda = 0$ corresponds to approximating $U \approx k^2/(\rho')^\gamma$ everywhere. However, in doing so we would be neglecting the boundary scaling $y^{-\nu}$, and consequently the lower bound (3.114) would be zero. Similarly, $\lambda = 1$ corresponds to approximating $U \approx \nu^2/(\rho')^2$ everywhere. While this is certainly true for small ρ', we would be missing the fact that the momentum part V_k of the potential can still dominate in any interval away from the boundary (i.e.

normalization.

close to ρ) and lead to exponential growth. The bound (3.114) would just be a constant independent of k and we would not be able to make the same conclusion about the smearing function.

3.5.1 Momentum-space Analysis

It is instructive to analyze the behavior of the integral (3.108) at large momenta in the (E,$|k|$)-plane. We already saw that for fixed energy E, the smearing function diverges exponentially with $|k|$, as the tunneling barrier becomes arbitrarily large at high momenta. However, this is not necessarily the only direction along which the integral diverges. Let us introduce polar coordinates

$$\begin{aligned} |k| &= q\cos\theta \\ E &= q\sin\theta. \end{aligned} \tag{3.115}$$

Figure 12 shows a sketch of the spectrum in the (E,$|k|$)-plane: The solid line divides trapped modes, which have to tunnel through V_k from free modes, which only tunnel through $U \sim 1/\rho^2$. If we imagine cutting off Lifshitz at some small value $\lambda\rho$ with $\lambda < 1$, all modes with $E < (\lambda\rho)^{-\frac{1}{2}}\,|k|$ (yellow region) are trapped modes[7]. Let us study the integral which defines the smearing direction. If we perform this integral along any direction θ over these modes (i.e. $\tan\theta < (\lambda\rho)^{-\frac{1}{2}}$), the exponential term in the integrand behaves as

$$\mathrm{Re}\left(S\left(y\right) - S\left(\rho\right)\right) = \int_y^\rho d\rho' \sqrt{\frac{\nu_z^2}{(\rho')^2} + \left(\frac{1}{(\rho')^\gamma} - \tan^2\theta\right) q^2\cos^2\theta}. \tag{3.116}$$

For q large enough, this term grows linearly and the smearing function is exponentially divergent. We see that the variable that controls the suppression (or amplification) due to

[7]Notice that the choice of λ is arbitrary. In particular, along any line $E = \tan\theta|k|$, there is a choice of λ such that all modes are below the momentum-barrier for large enough $|k|$. Nevertheless, because of the subtleties discussed at the end of the previous section, we should not simply take $\lambda \to 0$ but instead work with a small but finite value.

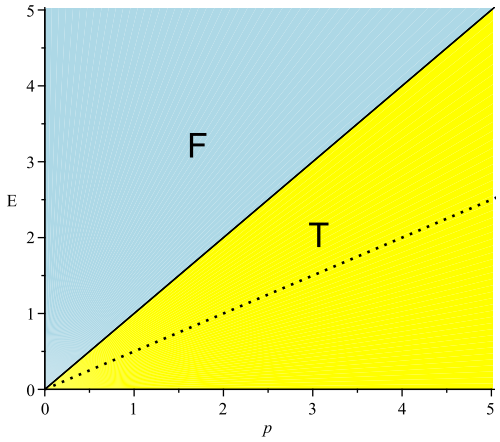

Figure 12: Sketch of free (F) and trapped (T) modes for general case (energy E vs. momentum $p \equiv |\vec{k}|$). Deforming the geometry in the IR may introduce a cutoff (dotted line), but this line will always remain below the solid line, and some trapped modes survive.

tunneling is in fact $q = \sqrt{E^2 + k^2}$, as opposed to just $|k|$.

3.5.2 No Smearing Function $\Leftrightarrow$ Singularities?

The divergence of the smearing function is due to trapped modes, which correspond to classical geodesics that cannot reach the boundary. However, those are precisely the trajectories that start and end at the tidal singularity at $\rho \to \infty$, so their fate is not well-understood even on the classical level. Therefore, one might wonder if the inability to construct smearing functions is simply due to the presence of singularities. This question has been raised before in the case of black hole solutions in AdS[8] [68, 69]. Fortunately, as we have seen in chapter 2, in our case there are known ways to resolve the singularity in the IR, so we can directly test the conjecture that non-existence of smearing functions is related to singularities. Thus we can use the numerical flows constructed earlier to test whether resolving the singularity can make the smearing function well defined.

As a warm-up, consider the following analytical toy-model describing a flow from AdS_{d+2}

[8]However, we should point out that the two types of singularities encountered here are qualitatively different. In the Lifshitz case, the singularity is 'mild', in the sense that all curvature invariants remain finite. It is, however, felt by strings that fall towards the horizon [43].

to Lifshitz to $AdS_2 \times \mathbb{R}^d$:

$$\begin{aligned} e^{2A} &= \frac{1}{\rho^2}, \\ e^{2B} &= \begin{cases} \frac{1}{\rho^2}, & 0 < \rho < R_1; \\ \frac{1}{R_1^\gamma \rho^{2-\gamma}}, & R_1 < \rho < R_2; \\ \frac{1}{R_1^\gamma R_2^{2-\gamma}}, & R_2 < \rho, \end{cases} \\ C &= A. \end{aligned} \tag{3.117}$$

The last condition is a gauge choice, which fixes our radial coordinate to be ρ, as defined in (3.11). The potential is given by

$$U(\rho) = \begin{cases} \frac{\nu_1^2 - \frac{1}{4}}{\rho^2} + k^2, & 0 < \rho < R_1; \\ \frac{\nu_z^2 - \frac{1}{4}}{\rho^2} + k^2 \left(\frac{R_1}{\rho}\right)^\gamma, & R_1 < \rho < R_2; \\ \frac{\nu_\infty^2 - \frac{1}{4}}{\rho^2} + k^2 \left(\frac{R_1}{R_2}\right)^\gamma \left(\frac{R_2}{\rho}\right)^2, & R_2 < \rho, \end{cases} \tag{3.118}$$

where ν_z was defined in (3.27), and $0 < \gamma < 2$. All modes with $k > E$, or equivalently $\tan\theta < 1$ are trapped. It is interesting to note that since the potential goes to zero as $\rho \to \infty$, there are now modes that are below the barrier in the AdS_{d+2} region. For pure AdS, this is not possible, as the wavefunction cannot be below the barrier everywhere.

Let us see if a smearing function exists for any point ρ in the bulk. For $0 < \rho < R_1$, we need to compute

$$\left| \lim_{y \to 0} y^\nu e^{S(y) - S(\rho)} \right| = \lim_{y \to 0} y^\nu \exp\left(\mathrm{Re} \int_y^\rho d\rho' \sqrt{\frac{\nu_1^2}{\rho'^2} + (1 - \tan^2\theta)\, q^2 \cos^2\theta} \right). \tag{3.119}$$

Naively, one might expect that since we are integrating all the way up to the boundary at $\rho = 0$, the $1/\rho^2$-term will eventually dominate and there is no q-divergence. However, we have seen before that it is necessary to split the integral into a near-boundary region

and a bulk region, according to (3.111). The near boundary integral will then produce the typical boundary scaling $y^{-\nu}$, while the bulk integral will grow linearly for trapped modes. In complete analogy with (3.114) we find that there exist constants $q_0, c > 0$ and $\lambda \in (0,1)$ such that

$$\left| \lim_{y\to 0} y^{\nu_1} e^{S(y)-S(\rho)} \right| > (\lambda\rho)^{\nu_1}\, e^{cq}, \tag{3.120}$$

for all $q > q_0$. Again, even though the $1/\rho^2$ part of the potential dominates near the boundary, there is still an exponential divergence due to trapped modes, and the smearing function does not exist in the AdS region.

For points within the Lifshitz region ($R_1 < \rho < R_2$), the relevant integral contains an integral over the AdS_{d+2} region, which is divergent by itself, plus an additional term

$$\int_{R_1}^{\rho} d\rho' \sqrt{\frac{\nu_z^2}{\rho'^2} + \left(\left(\frac{R_1}{\rho'}\right)^k - \tan^2\theta \right) q^2 \cos^2\theta}. \tag{3.121}$$

This integral gives a real contribution for $\tan\theta < (R_1/\rho)^{\gamma/2}$, which grows linearly with large q. Hence the smearing function still grows like $e^{c'q}$, but now $c' > c$ and it diverges even faster than in the AdS_{d+2} part.

The same logic can be applied to a point within the $\mathrm{AdS}_2 \times \mathbb{R}^d$ region in the IR ($\rho > R_2$). In this case there is a contribution from both AdS_{d+2} and Lifshitz, plus a contribution

$$\int_{R_2}^{\rho} d\rho' \sqrt{\frac{\nu_\infty^2}{\rho'^2} + \left(\left(\frac{R_1}{R_2}\right)^k \left(\frac{R_2}{\rho'}\right)^2 - \tan^2\theta \right) q^2 \cos^2\theta}. \tag{3.122}$$

Modes with $\tan\theta < (R_1/R_2)^{\gamma/2}\, R_2/\rho$ begin to tunnel already in the $\mathrm{AdS}_2 \times \mathbb{R}^d$ part of the potential, and so the smearing function will diverge even faster at large q. The final result is that there is no smearing function for any point ρ in the bulk. The trapped modes lead to an exponential divergence which becomes worse the deeper we try to reach into the bulk.

Let us now check that the result obtained for the toy-model (3.117) is indeed correct also

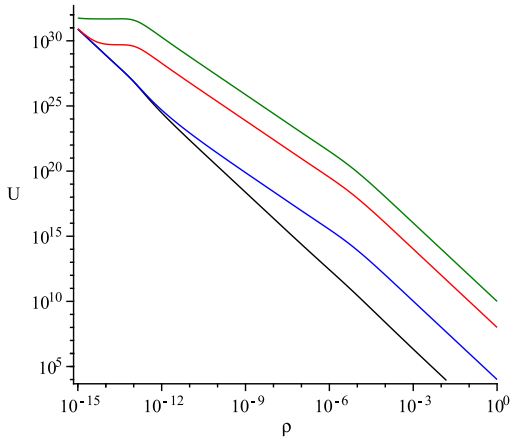

Figure 13: Effective potential U for the numerical flow found in section 2.3.2, for $m = 1$ (note that $p \equiv |\vec{k}|$. The momentum increases from bottom to top, with $k = 0$ (black), 10^2 (blue), 10^4 (red), 10^5 (green). At large momenta, the potential is well approximated by $V_k = e^{2W}k^2$.

for the exact numerical solution found in section 2.3.2 (here $d = 2$). The effective potential is plotted in Figure 13. As k increases, the potential becomes better and better approximated by V_k (shown in Figure 14). The metric coefficients and potential are of the form given in (3.117) and (3.118), except that now there is a smooth transition between the three regions.

Figures 15-17 show the real part of $S(y) - S(\rho)$ in the (E,$|k|$)-plane. Instead of taking y to zero we choose $y \approx 10^{-15}$, which we may think of as disregarding the near-boundary region of the ρ'-integral and starting at $y = \lambda\rho$. The thick line divides free (blue) modes from trapped (yellow) modes. The contours represent lines along which $\mathrm{Re}\,(S(y) - S(\rho))$ is constant. If we keep E fixed and increase p, we cross the contours at approximately equal distances, so the integral grows linearly in p. This is not only true for lines of constant E, but for any line within the trapped region (i.e. any line that stays below the black solid line). Hence the integral indeed diverges linearly with $q = \sqrt{E^2 + k^2}$, as was anticipated in section 3.5.1.

Figure 18 shows $\mathrm{Re}\,(S(y) - S(\rho))$ for three points representing AdS_4, Lifshitz and $AdS_2 \times \mathbb{R}^2$. The energy is held fixed at $E = 10^{16}$, such that at small p, the wavefunction is oscillating everywhere. As we increase p, the mode eventually becomes trapped and the real part of the integral grows linearly. Note that in the log-log plot used here, the three curves lie nicely

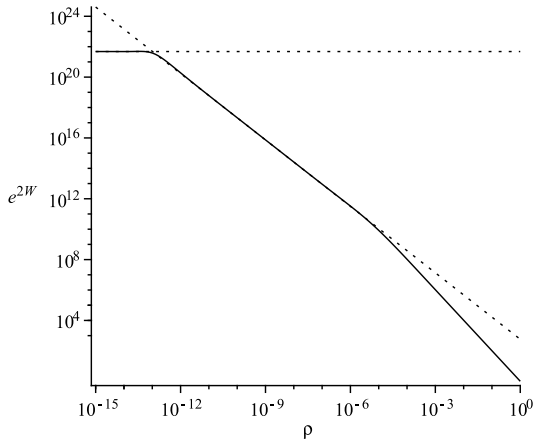

Figure 14: The factor e^{2W} for the same numerical solution. The solution flows from AdS_4 ($e^{2W} \approx$ const.), to Lifshitz ($e^{2W} \sim \rho^{1.45}$, corresponding to $z \approx 3.68$) to $AdS_2 \times \mathbb{R}^2$ ($e^{2W} \sim \rho^{-2}$).

on top of each other. This fact confirms our prediction that the smearing function diverges faster the deeper we try to reach into the bulk.

We conclude that resolving the tidal singularity is not enough to make the smearing function well defined. The $AdS_2 \times \mathbb{R}^2$ region in the IR can be thought of as the $z \to \infty$ limit of Lifshitz spacetime. As a consequence, $V_k \sim \rho^{-2}$, and there are still trapped modes with arbitrarily small boundary imprint.

It is also worth commenting on the addition of an AdS region in the UV, as in (3.117), which may seem desirable to make the holographic renormalization procedure better-defined. We have seen explicitly that the integral over (3.119) is still divergent at large momenta and a smearing function does not exist, even for points close to the boundary.

3.5.3 Other Flows Involving Lifshitz

The $AdS_2 \times \mathbb{R}^d$ geometry considered in the previous section is not the only possible IR endpoint of the RG-flow for Lifshitz solutions. Ref. [55, 72, 73] have considered flows from Lifshitz an AdS_{d+2} fixed point in the IR. These flows are of particular interest to us, since V_p does not go to zero as $\rho \to \infty$, but reaches a constant value corresponding to the AdS geometry at the horizon. Consequently, some of the problematic trapped modes never oscil-

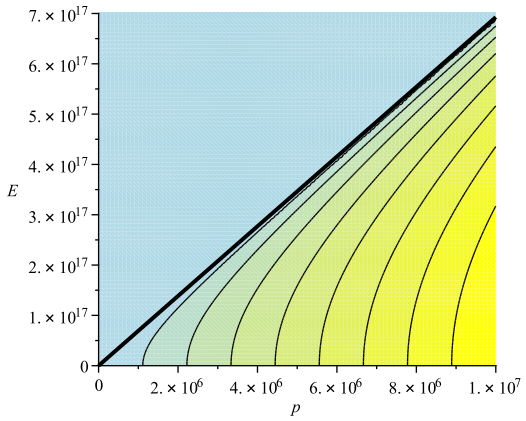

Figure 15: Plot of $\mathrm{Re}\,(\mathrm{S(y)} - \mathrm{S}(\rho))$ for a point within the AdS_4 region ($\rho \approx 1.3 \cdot 10^{-15}$). The black solid line represents $V_k = E^2$ and divides free (blue) from trapped modes (yellow). Contours indicate lines of constant $\mathrm{Re}\,(\mathrm{S(y)} - \mathrm{S}(\rho))$, with a linear increase between different contours.

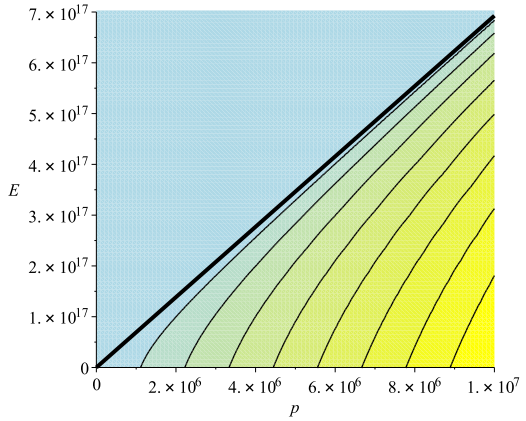

Figure 16: Plot of $\mathrm{Re}\,(\mathrm{S(y)} - \mathrm{S}(\rho))$ for a point within the Lifshitz region ($\rho \approx 9 \cdot 10^{-8}$).

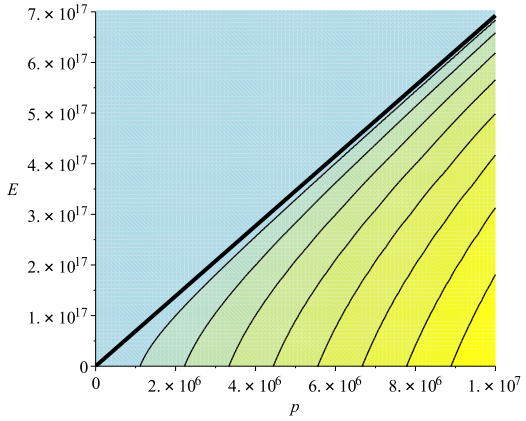

Figure 17: Plot of $\mathrm{Re}\,(\mathrm{S(y)} - \mathrm{S}(\rho))$ for a point within the $\mathrm{AdS}_2 \times \mathbb{R}^2$ region ($\rho \approx 1$).

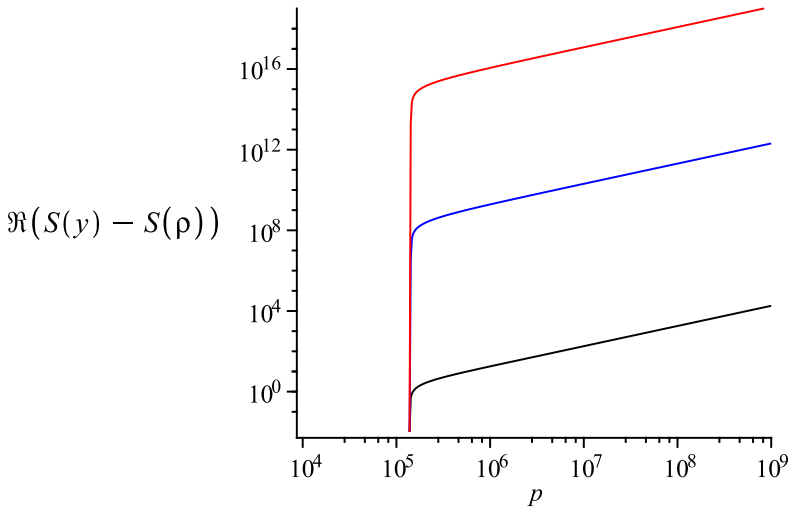

Figure 18: Plot of the real part of $S(y) - S(\rho)$ vs. $p \equiv |\vec{k}|$ at three different positions within the AdS_4 ($\rho \approx 1.3 \cdot 10^{-15}$), Lifshitz ($\rho \approx 9 \cdot 10^{-8}$) and $AdS_2 \times \mathbb{R}^2$ ($\rho \approx 1$) regions (from bottom to top). The energy is fixed at $E = 10^{16}$ and we chose $m = 1$. For large momenta, the solution begins to tunnel and contributes an exponential factor in K.

late, and are thus removed from the spectrum. To see how this works, consider the following toy-model of such a Lifshitz to AdS_{d+2} flow:

$$\begin{aligned} e^{2A} &= \frac{1}{\rho^2}, \\ e^{2B} &= \begin{cases} \frac{1}{\rho^{2-\gamma}}, & 0 < \rho \leq R_1; \\ \frac{R_1^\gamma}{\rho^2}, & \rho > R_1, \end{cases} \\ C &\equiv A. \end{aligned} \tag{3.123}$$

The potential is given by

$$U(\rho) = \begin{cases} \frac{\nu_z^2 - \frac{1}{4}}{\rho^2} + \frac{k^2}{\rho^\gamma}, & 0 < \rho \leq R_1; \\ \frac{\nu_1^2 - \frac{1}{4}}{\rho^2} + \frac{k^2}{R_1^k}, & \rho > R_1. \end{cases} \tag{3.124}$$

To compute the smearing function at some fixed $\rho \leq R_1$ we again split the interval $[0,\rho]$ into a near-boundary region $[0, \lambda\rho]$ and a bulk region $[\lambda\rho,\ \rho]$, where $\lambda < 1$. In the bulk region, the potential can be approximated by $V_k = k^2/\rho^\gamma$ for p large enough. Then, modes with $k > (\lambda\rho)^{\gamma/2}\, E$ are trapped by V_k. For $\rho > R_1$, the potential takes a constant value. In pure Lifshitz, modes with $k < R_1^{\gamma/2} E$ would have been oscillating in this region. However, these modes are now completely under the barrier and therefore have to be excluded from the spectrum. The AdS_{d+2} region in the IR thus introduces a natural (energy-dependent) momentum cutoff.

Nevertheless, there is still a finite wedge of trapped modes with $R_1^{-\gamma/2} < \tan\theta < (\lambda\rho)^{-\gamma/2}$ (cf. Figure 12) and integrating up to $q = \infty$ will produce the same divergent behavior as before. In section 3.6.1, we will give a general argument as to why this has to be the case, and show that no smooth IR-deformation can remove all trapped modes from the spectrum.

3.6 Smearing Functions for General Planar Backgrounds

We have seen that the construction of smearing functions can fail if there are modes that have to tunnel through a momentum barrier in the potential. The integral (3.102) diverges if such modes exist at arbitrarily large $q = \sqrt{E^2 + k^2}$. In this section, we will generalize our previous findings to prove that smearing functions do not exist for any geometries that allow trapped modes.

Consider a background that satisfies

$$\partial_\rho e^W < 0 \text{ for } \rho \in [\rho_1, \rho_2]. \tag{3.125}$$

We would like to compute the smearing function at a bulk point $\rho > \rho_1$. All modes with $V_k(\rho_1) > E^2$ have to tunnel through some part of V_k and are therefore trapped modes. Let us write the integral defining the smearing function in (3.102) as $\int dE d|k| \int d\Omega_{d-1}$ and focus on the integral in the $(E,|k|)$-plane. The domain of integration is shown in Figure 12,

where free and trapped modes are separated by the solid line $E^2 = V_k(\rho_1)$. Choosing polar coordinates (3.115), we find that the exponential part of the integrand satisfies

$$\mathrm{Re}\,(S(y) - S(\rho)) > \mathrm{Re}\int_{\rho_1}^{\rho_2} d\rho' \sqrt{V_{\mathrm{m}}(\rho') + V_{\cos}(\rho') + (e^{2W(\rho')} - \tan^2\theta)\cos^2\theta q^2}. \tag{3.126}$$

Since the integration domain does not include the boundary, the first two terms under the square root are bounded. Thus, for $\tan\theta < e^{W(\rho_1)}$, the integral grows linearly with large q and the smearing function diverges exponentially. The divergence appears not only at fixed E, but under any angle in the yellow region of Figure 12.

Consequently, if a geometry has trapped modes that are below the barrier at some ρ_1, a smearing function does not exist for any $\rho > \rho_1$. Using the null energy condition (3.7), one can show that once $\partial_\rho e^W$ is negative for some ρ_1, it cannot be positive for any $\rho < \rho_1$. Thus, once the wavefunction is below the V_k barrier, it will stay below it as we go towards the boundary. Using the terminology introduced earlier, trapped modes cannot become free near the boundary. Therefore, when computing the smearing function $K(t, x, \rho|t', x')$, there is an exponential contribution from trapped modes regardless of which bulk point ρ we consider.

The condition (3.125) makes it is easy to identify geometries without smearing functions. Clearly, Lifshitz has $\partial_\rho e^W < 0$ everywhere, and as we saw earlier, K does not exist. If we instead consider flows that involve only a finite region with broken Lorentz invariance, such that (3.125) is satisfied in some region, we still have trapped modes, and the smearing function will not exist. This analysis includes flows involving a Lifshitz region, as well as hyperscaling geometries with Lifshitz scaling. Our analysis above shows that none of these geometries admit smearing functions, provided the spacetime satisfies the NEC.

3.6.1 Removing Trapped Modes via Deformations

In our discussion above, we always assumed that the momentum-space integral (3.102) does in fact include trapped modes with arbitrarily large q on some set of nonzero measure. This is

clearly the case in the examples mentioned above. On the other hand, the smearing function for AdS converges because modes with $k^2 > E^2$ are simply not part of the spectrum, as the corresponding wavefunction would have to be below the potential globally.

One might wonder if it is possible to 'fix' a geometry which a priori does not admit a smearing function, by removing all trapped modes from the spectrum in a physical way. The AdS example gives us a hint on how one might accomplish this task: If the geometry is deformed in the deep IR such that would-be trapped modes never actually oscillate, they would simply not be allowed. Using the null energy condition (3.6) and (3.7) , it is easy to show that there are only three relevant IR asymptotics that we need to consider:

1. e^W decreases monotonically to a constant value $\mu > 0$.

2. e^W attains a minimum value $\mu > 0$, but then goes to constant $M > \mu$.

3. e^W attains a minimum value $\mu > 0$, but then goes to infinity.

Trapped states are equivalent to tunneling states in the potential $V_k = k^2 e^{2W}$. For p large enough, these states always exist [74]. This can be seen heuristically by bounding the potential from above with an appropriate square-well potential $\widetilde{U}(\rho)$ (see Figure 19). Therefore, no smooth deformation can ever remove all trapped modes from the spectrum.

As an example, consider case 1, which captures the case of the Lifshitz to AdS_{d+2} flow discussed in section 3.5.3. The AdS region introduces an energy-dependent momentum cutoff $k < E/\mu$. However, since μ is by definition a global minimum and (3.125) holds, we clearly have $\mu < e^{W(\rho_1)}$. Although the cutoff may remove some trapped modes from the spectrum, there will always remain a wedge of trapped modes that gives a divergent contribution when integrated over (see Figure 12). We conclude that spaces without a smearing function cannot be deformed smoothly to make the smearing function well-defined.

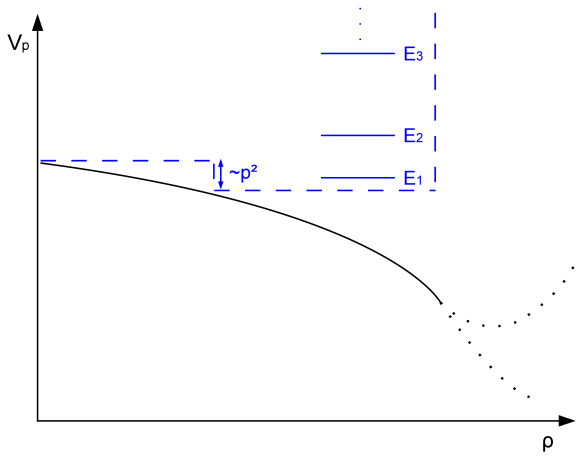

Figure 19: Sketch of V_k for a potential satisfying (3.125). This includes deformations of AdS and flows involving Lifshitz. Using the min-max principle, the energy levels are bounded from above by those of a square-well potential. In the large k limit, there are always trapped modes. The near-horizon behavior of the potential is irrelevant for our discussion.

3.6.2 Adding Trapped Modes via Deformations

Another interesting question is what happens if we take a geometry with a smearing function, such as AdS [62, 63, 64], and add a small (planar) perturbation in the IR. It can be seen from (3.7) that e^W must start with non-positive slope at the boundary for any background that is asymptotically AdS[9]. Since the potential scales with k, such a perturbation will always introduce new trapped modes. In particular, the momentum-potential $V_k = k^2 e^{2W}$ can always be bounded from above by a semi-infinite square-well potential of width l and height $h = k^2 h_0$, where h_0 is some constant (see Figure 19). For large enough k, the square-well always admits bound states with $k^2(1 - h_0) < E^2 < k^2$ and, via the min-max principle, so will V_k. As a result, the smearing function would be destroyed anytime the metric is deformed by such a perturbation.

This result is interesting, as it opens up the possibility that "small" perturbations of AdS can make the smearing function ill-defined by introducing new trapped states. However, we

[9]If we do not insist on AdS asymptotics, then we could choose e^W to immediately have a positive slope. If e^W has positive slope at some ρ_+, the NEC dictates that e^W cannot begin to decrease at some larger ρ. Thus, in this scenario no trapped modes are introduced, and the smearing function will continue to exist everywhere. In particular, we cannot have a situation akin to Figure 5 in [69], where the potential has a dip allowing trapped modes to become oscillating again close to the boundary.

should keep in mind that our ansatz only allows for planar perturbations; we cannot consider localized disturbances. It would be interesting to study the effect of such perturbations in a more general setup. Again, notice that the ultimate IR fate of the geometry with AdS behavior in the UV is not important for this discussion. In particular, whether or not there is a singularity at $r \to \infty$ does not change the qualitative result.

3.6.3 Relativistic Domain Wall Flows

Given the above considerations, one may get the impression that the smearing function no longer exists for any geometry other than pure AdS. However, it is important to realize that such a conclusion is in fact unwarranted. What we have seen is that the non-existence of the smearing function is intimately tied to the presence of trapped modes with exponentially small imprint on the boundary. Since such modes arise from the large k limit of $V_k = e^{2W}\vec{k}^2$, they are naturally absent when $W = 0$, corresponding to flows preserving $(d+1)$-dimensional Lorentz symmetry

$$ds^2_{d+2} = e^{2B(r)}[-dt^2 + d\vec{x}_d^2] + e^{2C(r)}dr^2. \tag{3.127}$$

In this case, the Schrödinger equation (3.14) is more naturally written as

$$-\psi'' + (V_m + V_{\cos})\psi = (E^2 - \vec{k}^2)\psi. \tag{3.128}$$

In particular, the effective potential $\hat{U} = V_m + V_{\cos}$ no longer scales with k.

In general, $\hat{U}$ may admit bound states and/or modes trapped at the horizon. Although bound states fall off exponentially outside the classically allowed region, since such states occur only at fixed values of $Q^2 \equiv E^2 - \vec{k}^{\,2}$, they will always have a non-vanishing (although small) amplitude at the boundary. Hence the presence of such states do not present an obstruction to the existence of a smearing function. Trapped modes at the horizon, on the other hand, are potentially more troubling, as they may form a continuum spectrum with a limit of vanishing amplitude on the boundary. However, it turns out that this possibility does

not prevent the construction of a well-defined smearing function $K(t, x, r|t', x)$ for any fixed value of r. The point here is that since $\hat{U}$ is independent of Q, the maximum suppression factor to tunnel from the boundary to r is bounded by setting $Q = 0$ in (3.128). As a result, it is impossible to make the suppression arbitrarily small. Hence we conclude that the smearing function exists for finite r in the case of relativistic domain wall flows, although the $r \to \infty$ limit of K may not exist if there are trapped modes that live arbitrarily far from the boundary.

We see that it is generally possible to define a smearing function only for relativistic flows, where $W = 0$ along the entire flow. Furthermore, for the case of $\mathrm{AdS}_{d+2} \to \mathrm{AdS}_{d+2}$ flows, the effective potential $\hat{U}$ falls off as $1/\rho^2$ both in the UV and the IR. Since this potential is too steep to admit trapped modes in the deep IR, there are no modes completely removed from the boundary, and hence the $r \to \infty$ limit of the smearing function is well-defined. Thus in this case the entire bulk may be reconstructed.

3.7 Modifying the Bulk-Boundary Dictionary

We have seen that for transverse Lorentz-breaking spacetimes with locally decreasing transverse speed of light, the smearing function is not well defined, even after resolving potential singularities. Thus, we are left with the option of loosening some of our initial assumptions about this function and its corresponding entry in the bulk-boundary dictionary. In particular, we need to reexamine our implicit assumption that K can reconstruct the bulk up to arbitrarily small transverse length scales.

Let us be a bit more precise about what kind of mathematical object the smearing function really is, and what we mean by saying that K does or does not exist. The most general possible definition is to let the smearing function be any map from boundary operators to bulk fields. However, a reasonable condition is that K defines a continuous, linear functional on the space of boundary operators. Continuity means that for any convergent sequence of

boundary operators O_n we have

$$\lim_{n\to\infty} K\left[O_n\right] = K\left[\lim_{n\to\infty} O_n\right]. \tag{3.129}$$

The difficulty in constructing such a K is due to the fact that the two limits are defined with respect to very different norms. The bulk norm relevant for the left hand side is the Klein-Gordon norm (3.96), while the boundary norm for O is given by (3.100). We have seen that in spacetimes with $\partial_\rho e^W < 0$ locally, there exist nonzero bulk solutions that have exponentially small boundary imprint, which provide an obstruction for constructing continuous smearing functions.

Our strategy in this chaper was to calculate a candidate smearing function $\widehat{K}$ in momentum space, and ask whether it defines a well-behaved object in position space. The problematic case is when the function defined in this way grows exponentially, i.e. $\widehat{K} \approx e^{ck}$. Its action on a boundary field can be written in momentum space as

$$K\left[O\right] \sim \int dk\, \widehat{K}\left(k\right) \widehat{O}\left(k\right). \tag{3.130}$$

Whether or not this integral is well-defined clearly depends on what we allow $\widehat{O}$ to be: If $\widehat{O}$ is a square-integrable function, the smearing function has to be square-integrable as well, which is clearly not the case here.

What if we impose a stricter fall-off condition at $k \to \infty$? One rather strict condition would be that $\widehat{O}$ falls off faster than any inverse power of k at infinity[10]. A classic example of such a function is a Gaussian $\sim e^{-k^2}$. However, e^{ck} is not a well-defined functional on this space either. This can be seen by explicitly constructing a sequence of functions with arbitrarily small boundary imprint, i.e. a sequence that goes to zero in the boundary norm. For example, consider

$$\widehat{O}_n\left(k\right) \equiv e^{-cn}\Psi\left(k-n\right), \tag{3.131}$$

[10]In other words: O is a Schwartz-function and K is a tempered distribution.

where Ψ is some bump-function. Attempting to reconstruct the corresponding bulk solution yields $K[O_n] \sim \int dk \Psi(k)$, which is independent of n, and in particular never equal to zero. Using (3.129), this means that the smearing function is not continuous.

The only way to make sense of the smearing function is to completely avoid configurations with arbitrarily small boundary imprint. This can only be achieved by introducing a hard momentum cutoff Λ. In other words, we attempt to invert the bulk-boundary map $\phi \mapsto O$ only for configurations with $\widehat{O}(k > \Lambda) = 0$. Acting on these functions, the exponential e^{ck} is indeed a well-defined continuous functional, and the integral (3.130) converges. There is, however, a price to pay: as is well-known, the Fourier transform of such compactly supported functions does not have compact support. The position space wavefunction necessarily has to leak out to infinity, and thus full localization in the transverse direction can never be achieved.

3.8 Summary and Discussion

In this chapter, we studied the possibility of bulk reconstruction from boundary information in Lifshitz and more general non-relativistic spacetimes. At the classical level, the presence of non-radial null geodesics that do not reach the Lifshitz boundary suggests that much of the bulk data is inaccessible from the boundary. We have confirmed this heuristic picture by studying smearing functions for a bulk scalar field and demonstrating that they do not exist for Lifshitz spacetimes with $z > 1$. The reason for this is that there will always be trapped modes in the bulk that have exponentially vanishing imprint on the boundary. It is these modes and the information that they contain that cannot be reconstructed from any local boundary data.

Of course, as we discussed in chapter 2, Lifshitz spacetime has a tidal singularity at the horizon. Since the trapped modes begin and end in the tidal singularity, one might conjecture that resolving the Lifshitz singularity would remove such modes and lead to a

well defined smearing function. However, this is not the case, as we have seen; even with a regular horizon such as $\mathrm{AdS}_2 \times \mathbb{R}^d$ or AdS_{d+2}, there will be trapped modes with vanishing imprint on the boundary as the transverse momentum is taken to infinity. Thus the existence or non-existence of a smearing function is independent of the nature of the horizon, and in particular whether it is singular or not.

More generally, we have seen that the constructibility of the smearing function depends crucially on whether there exists a family of trapped modes with arbitrarily small suppression on the boundary. The only way this can arise is if the momentum dependent part of the effective Schrödinger potential $V_k = e^{2W}\vec{k}^2$ has a local minimum or a barrier that grows as $k \to \infty$. Thus the question of whether or not the smearing function exists is closely related to the behavior of the gravitational redshift factor e^{-W}. In general, all non-relativistic backgrounds such as Lifshitz and ones with hyperscaling violation (including flows with such regions) do not admit smearing functions. The same is true for geometries such as Schwarzschild-AdS, where e^{2W} starts out as unity on the boundary, but vanishes at the horizon [69]. On the other hand, smearing functions are expected to exist for backgrounds with $W = \text{const.}$, i.e those preserving $(d+1)$-dimensional Lorentz invariance along the entire flow.

The scaling of V_k with $\vec{k}^2$ has the important consequence that any trapped mode will always be completely suppressed on the boundary with a factor $\sim e^{-cq}$ as $q \to \infty$, where $q^2 = E^2 + \vec{k}^2$ and c is a geometry and radial location dependent positive constant. This gives rise to the perhaps somewhat unexpected feature that, with the existence of trapped modes, the smearing function $K(t, x, r|t', x)$ cannot exist even near an asymptotic AdS_{d+2} region near the boundary, so long as r is at a fixed location. One may wonder why the presence of trapped modes living in the IR would destroy the possibility of reconstruction of the UV region near the boundary. The reason for this is that, while a trapped mode in the IR indeed has to tunnel to reach the boundary, its amplitude does not immediately vanish in the interior of the bulk geometry. Moreover, these modes can live at a finite distance from

the boundary. Hence they can have an imprint at any fixed r in the bulk, and yet vanish on the boundary. It thus follows that the bulk information corresponding to such modes cannot be obtained from the boundary, and thus the smearing function would not exist for any fixed value of r.

Since the existence of trapped modes with arbitrarily large values of q provides an obstruction to the construction of a smearing function, one way around this difficulty is to remove such modes by considering a hard momentum cutoff Λ. Another way to think about this is that it may indeed be possible to reconstruct the bulk data from the boundary information, but only up to a fixed momentum $k = \Lambda$. As Λ is taken larger, the reconstruction becomes more difficult, as there would be larger amplification in going from the boundary to the bulk due to the presence of trapped modes with larger values of q. With such a cutoff, one would have good control of the near boundary region in the bulk. However, one would lose complete localization in the transverse directions. The analysis in this chapter provides a first hint that non-relativistic spacetimes may have an intrinsic, built-in momentum-cutoff that has gone unnoticed in previous work. In fact, we will see in section 4.3 that such a cutoff is not an artificial construction, but arises naturally as soon as one considers the effect of higher derivative corrections to the bulk action of matter fields.

To summarize our discussion of smearing functions, if we limit ourselves to a minimum spatial resolution, local operators in the non-relativistic CFT do indeed contain all the relevant information about fields in the bulk of Lifshitz and other non-relativistic spacetimes. However, full locality in the transverse direction cannot be achieved using smearing functions only, due to the presence of modes with vanishing boundary imprint. If and how the missing local bulk information can be extracted from the field theory remains an interesting open question. One possibility that comes to mind is to make use of non-local operators in the field theory, such as Wilson-loops [75]. At the very least, our analysis demonstrates that some parts of the holographic dictionary for non-relativistic gauge/gravity dualities are more intricate than in the well-understood AdS/CFT case.

Chapter 4

Holographic Green's Functions

The AdS/CFT correspondence provides us with a powerful set of tools to make predictions for strongly coupled quantum field theories. The most striking feature of AdS/CFT is the fact that it is a weak-strong coupling duality. This has the consequence that calculations that might be difficult, or impossible, to carry out on the strongly coupled field theory side, might be relatively easy to carry out on the gravity side. Through the "holographic dictionary", AdS/CFT then provides us with a mathematical mapping between observables calculated on the gravity side to those on the field theory side.

An important such observable in any field theory is the 2-point correlation function of various operators. Instead of computing diagrams explicitly on the field theory side, we can use a "holographic" technique for calculating boundary Green's functions [25]. For Lifshitz spacetime, the holgraphic Green's function was first computed for scalar fields in [20], and later for fermions and other operators [76, 77, 78, 79, 80]. While the functional form of the Green's function in Lifshitz spacetime with $z = 2$ is known analytically, a few open questions still remain. First, given our discovery of "trapped modes" in the previous chapter, we are interested in how these modes affect the boundary Green's functions. Since trapped modes are exponentially suppressed near the boundary, one might suspect that their imprint on the Green's function is also small.

If the Green's function is in fact insensitive to a certain part of phase space containing trapped modes, this opens up the possibility for a notion of universality of Lifshitz Green's functions. If two spacetimes only differ by features that affect modes with high momentum, we expect the Green's functions of the corresponding field theories to be effectively the same.

The goal of this chapter is to explore precisely the effect of trapped modes on boundary correlators. We will first demonstrate that the holographic spectral function (the imaginary part of the Green's function) is indeed exponentially insensitive to modes with large momenta, or equivalently small energies. This is true not just for Lifshitz spacetime, but for a more general class of non-relativistic backgrounds. Finally, we will use the insensitivity of holographic Green's functions to trapped modes to proof that in any field theory with Lifshitz scaling symmetry, the spectral function exhibits a characteristic exponential suppression at small energies (or large momenta). We expect that this feature is robust with respect to changing the microscopic details of the theory. To provide concrete support for this conjecture, we will analyze how higher derivative corrections may effect the universal features of Green's functions. As we will show, the characteristic exponential suppression survives even when adding an infinite tower of correction terms that one would expect in any sensible effective field theory.

4.1 Green's Functions in Quantum Field Theories

To begin our discussion of holographic Green's functions, it is worthwile recalling some of the basic properties of Green's functions in quantum field theories. At zero temperature, one typically defines three different functions, namely the retarded, advanced, and time-ordered

(causal) Green's functions

$$\begin{aligned} G_R(\vec{x},t;\vec{x}',t') &= i\langle[\phi(\vec{x},t)\phi(\vec{x}',t')]\rangle\Theta(t-t'), \\ G_A(\vec{x},t;\vec{x}',t') &= -i\langle[\phi(\vec{x},t)\phi(\vec{x}',t')]\rangle\Theta(t'-t), \\ G_c(\vec{x},t;\vec{x}',t') &= i\langle T\phi(\vec{x},t)\phi(\vec{x}',t')\rangle. \end{aligned} \tag{4.1}$$

When Fourier transformed into $(\omega,\vec{k})$, unitarity and causality imply that G_R is analytic in the upper half of the complex ω-plane, while G_A is analytic in the lower half. These functions are not independent, but may be related by

$$G_R(\omega,\vec{k}) = [G_A(\omega,\vec{k})]^*, \tag{4.2}$$

as well as

$$G_c(\omega,\vec{k}) = G_R(\omega,\vec{k})\theta(\omega) + G_A(\omega,\vec{k})\theta(-\omega). \tag{4.3}$$

In general, these Green's functions can be obtained from a single real analytic function $G(\omega,\vec{k})$ satisfying $[G(\omega,\vec{k})]^* = G(\omega^*,\vec{k})$ (except for possible poles and branch cuts) by using an $i\epsilon$ prescription

$$\begin{aligned} G_R(\omega,\vec{k}) &= G(\omega+i\epsilon,\vec{k}), \\ G_A(\omega,\vec{k}) &= G(\omega-i\epsilon,\vec{k}), \\ G_c(\omega,\vec{k}) &= G(\omega+i\epsilon\,\mathrm{sign}\,\omega,\vec{k}). \end{aligned} \tag{4.4}$$

The substitution for the time-ordered Green's function is equivalent to taking $\omega^2 \to \omega^2 + i\epsilon$. For real ω, the spectral function is defined by

$$\chi(\omega,\vec{k}) = 2\,\mathrm{Im}\,G_R(\omega,\vec{k}) = -i[G_R(\omega,\vec{k}) - G_A(\omega,\vec{k})] = -i[G(\omega+i\epsilon,\vec{k}) - G(\omega-i\epsilon,\vec{k})]. \tag{4.5}$$

The spectral function may be interpreted as the density of states in phase space. Mathematically, non-vanishing spectral weight $\chi(\omega, \vec{k})$ arises either from poles or discontinuities across any branch cuts that lie on the real ω axis.

In the holographic calculation, the choice of Green's function is determined by choosing appropriate boundary conditions at the horizon. For example, choosing only solutions that are infalling (outgoing) at the horizon selects the retarded (advanced) Green's function.

4.2 Hidden Horizons in Non-relativistic AdS/CFT

4.2.1 Horizon Boundary Conditions and the Holographic Green's Function

In contrast with Euclidean AdS/CFT, in the Minkowski case, the Green's function has a richer analytic structure that is closely related to the causal propagation of information. For example, while the usual computation of the retarded Green's function involves taking infalling boundary conditions at the AdS horizon, one could equally well have obtained the advanced Green's function by taking outgoing boundary conditions. As we saw above, in the situation where time reversal invariance holds, the retarded and advanced Green's functions are related by complex conjugation. This is easy to understand in terms of boundary conditions at the horizon, since complex conjugation of the radial wavefunction interchanges infalling with outgoing boundary conditions.

More generally, the AdS/CFT Green's function probes the bulk, as its computation depends on our ability to relate horizon with boundary data. Consider, for example, the case of the scalar Green's function arising from the action

$$S = \int dt\, d^d x\, d\rho \sqrt{-g} \left[-\frac{1}{2} \partial_\mu \phi \partial^\mu \phi - \frac{1}{2} m^2 \phi^2 \right], \tag{4.6}$$

in a background of the form

$$ds^2_{d+2} = e^{2A(\rho)}(-dt^2 + d\rho^2) + e^{2B(\rho)}d\vec{x}^2_d. \tag{4.7}$$

As we have seen previously, the bulk solution takes the form

$$\phi(t, \vec{x}, \rho) = e^{i(\vec{k}\cdot\vec{x}-\omega t)} f_{\omega,\vec{k}}(\rho). \tag{4.8}$$

For metrics of the form (4.7), the Klein-Gordon equation $(\Box - m^2)\phi = 0$ can again be converted into a Schrödinger-like equation

$$-\psi''(\rho) + U(\rho)\psi(\rho) = \omega^2\psi(\rho), \tag{4.9}$$

where the effective potential is

$$U = e^{2A}m^2 + e^{2A-2B}\vec{k}^2 + \left(\frac{dB}{2}\right)'^2 + \left(\frac{dB}{2}\right)'', \tag{4.10}$$

and where $f_{\omega,\vec{k}}(\rho) = e^{-dB/2}\psi(\rho)$. Since the solution to the wave equation will depend on both the bulk geometry and the horizon boundary condition, the Green's function will similarly depend on the bulk and horizon data. Now, let us assume that the metric is asymptotically of the Lifshitz (non-relativistic scale-invariant) form (1.5),

$$ds^2_{d+2} \sim \left(\frac{L}{z\rho}\right)^2 \left(-dt^2 + d\rho^2\right) + \left(\frac{L}{z\rho}\right)^{2/z} d\vec{x}^2_d. \tag{4.11}$$

The asymptotic boundary solution to (3.14) has the form

$$\psi(\rho \to 0) \sim A\left(\frac{z\rho}{L}\right)^{\frac{1}{2}-\nu_z} + B\left(\frac{z\rho}{L}\right)^{\frac{1}{2}+\nu_z}, \tag{4.12}$$

where

$$\nu_z = \frac{1}{z}\sqrt{(mL)^2 + \left(\frac{d+z}{2}\right)^2}. \tag{4.13}$$

The holographic prescription for calculating boundary Green's functions of ϕ is [25]

$$G(\omega, \vec{k}) = K\frac{B}{A}, \tag{4.14}$$

where K is a numerical normalization constant. This result simply states that the AdS/CFT Green's function is proportional to the ratio of the normalizable to the non-normalizable mode.

The coefficients B and A are determined by solving the equation (3.14) subject to infalling or other appropriate boundary conditions at the horizon. For the case of Lisfhitz spacetime with $z = 2$, this was done in section 3.2.1. It is worthwile to discuss the form of the Green's function in the more general case of an effective potential of the form (4.10). Assuming $U(\rho)$ approaches a constant value U_0 at the horizon, the horizon solution has the form

$$\psi \sim ae^{i\sqrt{\omega^2 - U_0}\rho} + be^{-i\sqrt{\omega^2 - U_0}\rho}, \tag{4.15}$$

and is oscillatory in the classically allowed range of frequencies, $\omega^2 > U_0$. The a mode is infalling, while the b mode is outgoing for positive ω. In the forbidden range, we may take $\sqrt{\omega^2 - U_0} \to i\sqrt{U_0 - \omega^2}$, so the a mode is exponentially damped, while the b mode blows up. Although the retarded Green's function is obtained by taking $b = 0$, here we leave it arbitrary so that we can examine the effect of changing the horizon boundary conditions.

Since the wave equation is second order and linear, the horizon and boundary data are related by a linear transformation

$$\begin{pmatrix} A \\ B \end{pmatrix} = \mathcal{M}\begin{pmatrix} a \\ b \end{pmatrix} = \begin{pmatrix} \mathcal{M}_{Aa} & \mathcal{M}_{Ab} \\ \mathcal{M}_{Ba} & \mathcal{M}_{Bb} \end{pmatrix}\begin{pmatrix} a \\ b \end{pmatrix}, \tag{4.16}$$

where the connection matrix $\mathcal{M}$ depends on the bulk geometry connecting the horizon to the boundary through the effective potential (4.10). In terms of this matrix $\mathcal{M}$, the Green's function then has the form

$$G(\omega, \vec{k}) = K \frac{\mathcal{M}_{Ba} + \mathcal{M}_{Bb}(b/a)}{\mathcal{M}_{Aa} + \mathcal{M}_{Ab}(b/a)}. \tag{4.17}$$

This explicitly demonstrates how the Green's function connects the horizon (represented by the horizon data b/a) to the boundary via the bulk matrix $\mathcal{M}$. We can, in fact, say a bit more about the matrix $\mathcal{M}$. Since we are solving a real differential equation (3.14), any time ψ is a solution, so is its complex conjugate ψ^*. This allows us to relate the a and b modes in (4.15) whenever the solution is oscillatory at the horizon. In particular, $\mathcal{M}_{Ab} = \mathcal{M}^*_{Aa}$, and likewise $\mathcal{M}_{Bb} = \mathcal{M}^*_{Ba}$. In this case, we obtain the expression

$$G(\omega, \vec{k}) = K \frac{\mathcal{M}_{Ba}}{\mathcal{M}_{Aa}} \frac{1 + e^{-2i \arg \mathcal{M}_{Ba}}(b/a)}{1 + e^{-2i \arg \mathcal{M}_{Aa}}(b/a)}. \tag{4.18}$$

This expression highlights the dependence of the Green's function on the ratio b/a specifying the boundary condition at the horizon. The retarded Green's function is obtained by taking $b/a = 0$, while the advanced Green's function corresponds to $b/a \to \infty$. Since $\mathcal{M}_{Ba} e^{-2i \arg \mathcal{M}_{Ba}} = \mathcal{M}^*_{Ba}$ (and likewise for $\mathcal{M}_{Aa}$), we may explicitly see that $G_A(\omega, \vec{k}) = G_R(\omega, \vec{k})^*$. More generally, the Green's function expression (4.18) allows us to explore the sensitivity of the boundary behavior to small changes in the infrared. For example, a small change to the bulk geometry in the deep IR would induce a change to the effective potential U near the horizon. As a result, an infalling wave could scatter off the perturbation, so that at some distance outside the horizon (but still in the IR), the actual solution is mostly infalling, but now picks up a small outgoing component as well. In this case, the effect of the perturbation on the retarded Green's function can be modeled by taking b/a small but non-vanishing, so that a small outgoing component is introduced. Expanding to lowest order

in b/a, the result is

$$G(\omega,\vec{k}) = K\frac{\mathcal{M}_{Ba}}{\mathcal{M}_{Aa}}\left[1+(e^{-2i\arg\mathcal{M}_{Ba}}-e^{-2i\arg\mathcal{M}_{Aa}})\frac{b}{a}+\cdots\right]. \tag{4.19}$$

For generic values of the arguments, the sensitivity of the Green's function to b/a is of $\mathcal{O}(1)$. However, it becomes completely insensitive to b/a (and not just to leading order) in the limit $\arg\mathcal{M}_{Ba} = \arg\mathcal{M}_{Aa}$. Note that in this limit, the Green's function is purely real, as the ratio $\mathcal{M}_{Ba}/\mathcal{M}_{Aa}$ is real. Equivalently, the spectral function, defined by

$$\chi(\omega,\vec{k}) = 2\,\mathrm{Im}\,G_R(\omega,\vec{k}) = -i\left(G_R(\omega,\vec{k})-G_A(\omega,\vec{k})\right), \tag{4.20}$$

goes to zero. Throughout this chapter, we will therefore take an exponentially small χ as a signal for the insensitivity to a change of the near-horizon bulk state and/or geometry.

4.2.2 Tunneling Barriers and Decoupling of the IR

As we have seen above, when $\arg\mathcal{M}_{Ba} = \arg\mathcal{M}_{Aa}$, the Green's function becomes purely real and thus invariant under changing from retarded (infalling) to advanced (outgoing) boundary conditions. This is actually not surprising, as complex conjugation of a real function leaves it unchanged. What may appear more unusual is that in this case, since the dependence on b/a completely drops out, the Green's function is unaffected by any choice of horizon boundary conditions $0 \leq |b/a| \leq \infty$.

It is important to note, however, that since the second order wave equation admits two linearly independent solutions, the connection matrix $\mathcal{M}$ is necessarily invertible. What this means is that $\arg\mathcal{M}_{Ba}$ can never actually be degenerate with $\arg\mathcal{M}_{Aa}$. As a result, the Green's function is never real (in the classically allowed range of ω), although it can approach a real function in the limiting case. In this sense, the horizon boundary conditions never completely drop out of the Green's function computation. However, the dependence on the horizon can become highly suppressed whenever $\mathcal{M}$ becomes nearly degenerate.

Since the effective Schrödinger equation (3.14) governing the wavefunction is specified by the effective potential (4.10), the connection matrix $\mathcal{M}$ will depend on the explicit form of U as well as the frequency ω. Here it is important to note that, while the boundary is in a classically forbidden region, the asymptotic form of the potential $U \sim 1/\rho^2$ is too steep for tunneling. This is the reason we have power law behavior at the boundary, rather than exponential growth/decay. If the shape of the potential is such that there is no tunneling between the horizon and the boundary, then the entries in $\mathcal{M}$ are all of $\mathcal{O}(1)$, and generically there is no degeneracy. In this case, the UV and IR are tied together by an $\mathcal{O}(1)$ transformation, and perturbations in the IR are directly reflected in changes to the Green's function.

On the other hand, if the potential U admits a tunneling region and ω is below the barrier, then the connection matrix $\mathcal{M}$ will become nearly degenerate. This is exactly the situation where the Green's function becomes insensitive to the horizon boundary conditions. Heuristically, what is going on is that the tunneling barrier decouples the IR from the UV, so information at the horizon becomes hidden from the boundary.

We may once again use the WKB approximation (see section 3.3) to make the connection between tunneling of the wavefunction and the form of $\mathcal{M}$ more precise. Assuming asymptotically Lifshitz behavior, the potential U behaves near the boundary as

$$U\left(\rho \to 0\right) \sim \frac{\nu^2 - 1/4}{\rho^2}. \tag{4.21}$$

We assume that the effective Schrödinger energy ω^2 in (3.14) is such that the horizon falls into a classically allowed region. Since the potential increases without bound as we move towards the boundary, we will always encounter a classical turning point ρ_0. The wavefunction is thus oscillating in the classically allowed region $\rho > \rho_0$ (corresponding to the IR) and

growing/decaying in the forbidden region $\rho < \rho_0$

$$\psi_{\rm WKB} \approx \begin{cases} \sqrt{\nu}\left(U-\omega^2\right)^{-\frac{1}{4}}\left(Ce^{S(\rho,\rho_0)}+De^{-S(\rho,\rho_0)}\right), & \rho<\rho_0; \\ \sqrt{\nu}\left(\omega^2-U\right)^{-\frac{1}{4}}\left(ae^{i\Phi(\rho_0,\rho)}+be^{-i\Phi(\rho_0,\rho)}\right), & \rho>\rho_0. \end{cases} \tag{4.22}$$

where

$$S\left(\rho,\rho_0\right) \equiv \int_{\rho}^{\rho_0} d\rho\sqrt{U-\omega^2}, \qquad \Phi\left(\rho_0,\rho\right) \equiv \int_{\rho_0}^{\rho} d\rho\sqrt{\omega^2-U}. \tag{4.23}$$

and we perform the shift $\nu^2 \to \nu^2 + 1/4$ to make the WKB approximatino consistent. The coefficients in (4.22) are tied together via the connection formulae

$$\begin{pmatrix} C \\ D \end{pmatrix} = \mathcal{M}'' \begin{pmatrix} a \\ b \end{pmatrix} = \begin{pmatrix} e^{-i\frac{\pi}{4}} & e^{i\frac{\pi}{4}} \\ \frac{1}{2}e^{i\frac{\pi}{4}} & \frac{1}{2}e^{-i\frac{\pi}{4}} \end{pmatrix} \begin{pmatrix} a \\ b \end{pmatrix}. \tag{4.24}$$

To relate the WKB coefficients C and D to the coefficients A and B in (4.12), we match $\psi_{\rm WKB}$ with the exact solution (4.12) at some UV cutoff $\rho = \epsilon$, which will be taken to zero at the end. The result can be written as another matrix equation:

$$\begin{pmatrix} A \\ B \end{pmatrix} = \mathcal{M}' \begin{pmatrix} C \\ D \end{pmatrix} = \begin{pmatrix} \mathcal{M}'_{AC} & \mathcal{M}'_{AD} \\ \mathcal{M}'_{BC} & \mathcal{M}'_{BD} \end{pmatrix} \begin{pmatrix} C \\ D \end{pmatrix}. \tag{4.25}$$

Combining this with (4.24), we then find that $\mathcal{M} = \mathcal{M}'\mathcal{M}''$, which can be used to find the Green's function (4.17) in the WKB approximation. To determine $\mathcal{M}'$ explicitly, let us write

$$\begin{aligned} \psi_{\rm exact} &= A\phi_1 + B\phi_2, \\ \psi_{\rm WKB} &= C\phi_3 + D\phi_4, \end{aligned} \tag{4.26}$$

with $\phi_{1/2}$ being the exact solution with boundary behavior $\phi_{1/2} \approx \rho^{\frac{1}{2}\mp\nu}$, and

$$\phi_{3/4} \equiv \sqrt{\nu}\left(U-\omega^2\right)^{-\frac{1}{4}} e^{\pm S(\rho,\rho_0)}. \tag{4.27}$$

The matching matrix is then given by

$$\mathcal{M}' = \frac{1}{W_{12}} \begin{pmatrix} W_{32} & W_{42} \\ W_{13} & W_{14} \end{pmatrix}, \quad \text{where} \quad W_{ij} \equiv \phi_i(\epsilon)\,\phi_j'(\epsilon) - \phi_i'(\epsilon)\,\phi_j(\epsilon). \tag{4.28}$$

Working near the boundary, this takes the explicit form

$$\mathcal{M}' = \begin{pmatrix} \epsilon^{\nu} e^{S(\epsilon,\rho_0)} & 0 \\ 0 & \epsilon^{-\nu} e^{-S(\epsilon,\rho_0)} \end{pmatrix}. \tag{4.29}$$

We can easily read off the imaginary part of the Green's function and find

$$2\,\mathrm{Im}\,G_{\mathrm{WKB}}(\omega,\vec{k}) = K\frac{\mathcal{M}'_{BD}}{\mathcal{M}'_{AC}}\frac{1-\left|\frac{b}{a}\right|^2}{1+\left|\frac{b}{a}\right|^2} = K\epsilon^{-2\nu}e^{-2S(\epsilon,\rho_0)}\frac{1-\left|\frac{b}{a}\right|^2}{1+\left|\frac{b}{a}\right|^2}. \tag{4.30}$$

In the case $b = 0$, corresponding to infalling conditions at the horizon, the above expression is simply the spectral function χ. As we show in appendix D, the error due to the WKB approximation can be kept under perturbative control. The dependence on the shape of the effective potential U is captured in the e^{-2S} term in (4.30). While the near-boundary $1/\rho^2$ behavior only leads to power-law scaling, any tunneling region with U falling off slower than $1/\rho^2$ leads to an exponential suppression factor in the spectral function.

More concretely, consider a spacetime that enjoys Lifshitz scaling in some region in the bulk. The potential takes the form (4.10), with a tunneling term $\vec{k}^2 e^{2(A-B)} \sim \vec{k}^2\rho^{2(1/z-1)}$. Tunneling of the wavefunction through this part of the potential leads to an exponential fall-off of the spectral function at large momenta $|\vec{k}|$:

$$\chi\left(\omega, \vec{k} \gg c^{-1}\right) = f(\omega)\, e^{-c|\vec{k}|}, \tag{4.31}$$

with some geometry-dependent constant c. For some special cases like pure Lifshitz, this constant can actually secretly carry an additional dependence on $\vec{k}$ and ω, making χ vanish

even faster. We will comment on this issue at the end of the next section. From (4.31), we see that changing from infalling to outgoing boundary conditions results only in an exponentially small change $\delta G \sim \chi \sim e^{-c|\vec{k}|}$. For $|\vec{k}| \to \infty$, $\chi \to 0$ and so the Green's function becomes purely real, completely decoupling the near-horizon boundary conditions. This establishes the insensitivity of the Green's function to IR physics. We will further illustrate the connection between horizon boundary conditions and IR physics in section 4.2.4.

4.2.3 Horizon Decoupling for Lifshitz Backgrounds

For general backgrounds, the connection matrix $\mathcal{M}$ and the resulting Green's function (4.17) will have to be obtained either numerically, or using approximation methods such as WKB. However, analytic solutions are known for simple backgrounds such as AdS and $\text{Lif}_{z=2}$. Here we highlight and contrast these two cases as an explicit demonstration of the decoupling of the IR in a Lifshitz background. In particular, we will confirm our prediction (4.31) for the exponential fall-off of χ in the Lifshitz case.

4.2.3.1 The $z = 1$ AdS Case

For a pure Lifshitz or AdS geometry, we can take the metric (4.11) to be exact throughout the bulk. In this case, the effective potential becomes:

$$U = \frac{\nu_z^2 - 1/4}{\rho^2} + \vec{k}^2 \left(\frac{L}{z\rho}\right)^{2-2/z} . \tag{4.32}$$

Let us first consider the AdS case, which corresponds to $z = 1$. Here the potential is purely $1/\rho^2$ on top of a constant offset, and there is no tunneling region (so long as $\omega \geq |\vec{k}\,|$). The $1/\rho^2$ potential is "too steep for tunneling", and the wavefunction grows or decays polynomially. The exact solution for $\psi(\rho)$ is well known, and is given by a linear combination

of Bessel functions

$$\psi = \sqrt{\rho}\left[\alpha J_\nu(q\rho) + \beta Y_\nu(q\rho)\right], \tag{4.33}$$

where $q = \sqrt{\omega^2 - \vec{k}^2} = \sqrt{-k_\mu k^\mu}$. In this case, it is straightforward to obtain

$$\mathcal{M}_{z=1} = \begin{pmatrix} \frac{\Gamma(\nu)}{\sqrt{\pi}}\left(\frac{qL}{2}\right)^{\frac{1}{2}-\nu} e^{i(\frac{\nu}{2}-\frac{1}{4})\pi} & \frac{\Gamma(\nu)}{\sqrt{\pi}}\left(\frac{qL}{2}\right)^{\frac{1}{2}-\nu} e^{-i(\frac{\nu}{2}-\frac{1}{4})\pi} \\ \frac{\Gamma(-\nu)}{\sqrt{\pi}}\left(\frac{qL}{2}\right)^{\frac{1}{2}+\nu} e^{-i(\frac{\nu}{2}+\frac{1}{4})\pi} & \frac{\Gamma(-\nu)}{\sqrt{\pi}}\left(\frac{qL}{2}\right)^{\frac{1}{2}+\nu} e^{i(\frac{\nu}{2}+\frac{1}{4})\pi} \end{pmatrix}, \tag{4.34}$$

at least for non-integer values of ν. Note that this has the form

$$\mathcal{M} = \begin{pmatrix} \mathcal{M}(\nu)e^{i\varphi(\nu)} & \mathcal{M}(\nu)e^{-i\varphi(\nu)} \\ \mathcal{M}(-\nu)e^{i\varphi(-\nu)} & \mathcal{M}(-\nu)e^{-i\varphi(-\nu)} \end{pmatrix}, \tag{4.35}$$

where $\varphi(\nu) = (\nu/2 - 1/4)\pi$. This form is related to the $\nu \to -\nu$ symmetry of the effective potential.

For $\omega \geq |\vec{k}\,|$, the AdS Green's function can be obtained from (4.18). Using relativistic notation, we find

$$G(q) = K\frac{\Gamma(-\nu)}{\Gamma(\nu)}\left(\frac{qL}{2}\right)^{2\nu} e^{-i\nu\pi}\frac{1 + e^{i(\nu+\frac{1}{2})\pi}(b/a)}{1 + e^{-i(\nu-\frac{1}{2})\pi}(b/a)}. \tag{4.36}$$

Recall that the retarded Green's function corresponds to taking $b/a = 0$. In order to examine the sensitivity to horizon boundary conditions, we may expand to first order in b/a

$$G(q) = K\frac{\Gamma(-\nu)}{\Gamma(\nu)}\left(\frac{qL}{2}\right)^{2\nu} e^{-i\nu\pi}\left(1 - 2\sin(\nu\pi)\frac{b}{a} + \cdots\right). \tag{4.37}$$

Since we have assumed ν to be non-integral, this shows that $G(q)$ has $\mathcal{O}(1)$ sensitivity to the choice of horizon boundary conditions b/a. Moreover, this sensitivity is present in both the real and imaginary parts of the Green's function. For the spectral function we find $\chi \sim q^{2\nu}$, as required by scale invariance, but no exponential suppression factor.

4.2.3.2 The $z = 2$ Lifshitz Case

We now turn to $z = 2$ Lifshitz as an analytic example of a non-relativistic system. Here the potential has a combination of $1/\rho^2$ and $1/\rho$ terms

$$U_{z=2} = \frac{\nu_2^2 - 1/4}{\rho^2} + \frac{\vec{k}^2 L}{2\rho}. \tag{4.38}$$

As is well known from quantum mechanics, the $1/\rho$ potential is shallow enough that it presents a tunneling barrier in the system. However, not all the modes have to tunnel through this part of the potential. Denoting the crossover scale between $1/\rho$ and $1/\rho^2$ behavior as $\rho_* = \frac{2\nu_2^2}{\vec{k}^2 L}$, the condition for a mode to tunnel is

$$\frac{\vec{k}^2 L}{2\rho_*} \gg \omega^2 \quad \Longrightarrow \quad \alpha \equiv \frac{\vec{k}^2 L}{2\omega} \gg \nu_2. \tag{4.39}$$

For these modes, we expect an exponential suppression in α, as sketched in Figure 20. Using our result (3.37), we see that the connection matrix does indeed take the form (4.35), however with

$$\mathcal{M}(\nu_2) e^{i\varphi(\nu_2)} = \Gamma(2\nu_2)(\omega L)^{\frac{1}{2}-\nu_2} e^{\pi\alpha/4} \frac{e^{i(\frac{\nu_2}{2}-\frac{1}{4})\pi} 2^{i\alpha/2}}{\Gamma(\frac{1}{2}+\nu_2+\frac{i\alpha}{2})}. \tag{4.40}$$

In contrast with the relativistic case, this function depends on the ratio of $\vec{k}^2$ and ω through the parameter α. Using (4.18), the Green's function is then [20]

$$G(\omega, \vec{k}) = K \frac{\Gamma(-2\nu_2)}{\Gamma(2\nu_2)} (\omega L)^{2\nu_2} \frac{\Gamma(\frac{1}{2}+\nu_2+\frac{i\alpha}{2})}{\Gamma(\frac{1}{2}-\nu_2+\frac{i\alpha}{2})} e^{-i\nu_2\pi} \frac{1 + e^{-2i\varphi(-\nu_2)}(b/a)}{1 + e^{-2i\varphi(\nu_2)}(b/a)}, \tag{4.41}$$

where

$$\varphi(\nu_2) = \left(\frac{\nu_2}{2} - \frac{1}{4}\right)\pi + \frac{\alpha}{2}\log 2 + \arg\Gamma(\frac{1}{2} + \nu - \frac{i\alpha}{2}). \tag{4.42}$$

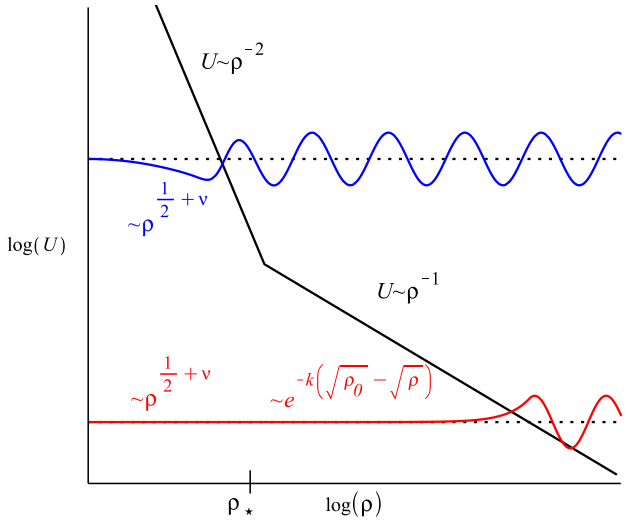

Figure 20: Sketch of the effective potential U for $z = 2$ Lifshitz spacetime. The potential changes from the near-boundary $1/\rho^2$ behavior to the tunneling potential $U \sim 1/\rho$ near the crossover scale $\rho_* \sim 1/|\vec{k}|^2$. A normalizable wavefunction with large energy ω and low momenta $|\vec{k}|$ crosses the barrier in the $1/\rho^2$ region and decays polynomially, according to (4.12) (blue curve). For low energies and large momenta the crossing point lies within the tunneling region and the wavefunction decays exponentially at first (red curve). This has the effect that states that are localized close to the horizon have an exponentially small amplitude at the boundary

For the non-tunneling modes with small α, we find (to first order in b/a)

$$\begin{aligned} G(\omega,\vec{k}) &= K\frac{\Gamma(-\nu_2)}{\Gamma(\nu_2)}\left(\frac{\omega L}{4}\right)^{2\nu_2} e^{-i\nu_2\pi}\left(1+\frac{i\pi\alpha}{2}\tan(\nu_2\pi)+\mathcal{O}(\alpha^2)\right) \\ &\quad\times\left[1-2\sin(\nu_2\pi)\left(1+\frac{i\alpha}{2}\left(i\pi-\log 4+\psi(\frac{1}{2}+\nu_2)+\psi(\frac{1}{2}-\nu_2)\right)+\mathcal{O}(\alpha^2)\right)\frac{b}{a}+\cdots\right], \end{aligned} \tag{4.43}$$

which matches the AdS Green's function (4.36) in the limit $\alpha \to 0$ once we identify $L \to 2L$, $\nu_2 \to \nu$ and $\omega \to q$. This should not be surprising because $\alpha \to 0$ can be achieved by taking $\vec{k} \to 0$. In this limit the transverse space becomes irrelevant, and the Lifshitz potential may be identified with the AdS potential. As a result, the Green's function at small α is sensitive to the horizon boundary conditions in essentially the same manner as given in (4.37).

What is more interesting is the $\alpha \gg \nu_2$ limit, where the horizon modes must tunnel under the $1/\rho$ potential to reach the boundary. For large α we first use Stirling's approximation to see that

$$\varphi(\nu_2) \sim \frac{\alpha}{2}\left(1-\log\frac{\alpha}{4}\right)-\frac{\pi}{4}+\mathcal{O}\left(\frac{1}{\alpha}\right). \tag{4.44}$$

A key observation is that, at leading order, the ν_2 dependence completely cancels out from the phase, and this is exactly what is required for the Green's function (4.41) to become insensitive to the horizon boundary conditions. Beyond leading order, we may use the identity

$$\varphi(\nu)-\xi(-\nu) = -\,\mathrm{Im}\,\log\left(1+e^{-2\pi i\nu-\pi\alpha}\right), \tag{4.45}$$

obtained by application of the reflection formula $\Gamma(1-z)\Gamma(z)=\pi\csc(\pi z)$, to see that $\varphi(\nu_2)$ is an even function of ν_2 to any finite order in the perturbative expansion in $1/\alpha$. Explicitly,

what we find is

$$G(\omega,\vec{k}) = K\frac{\Gamma(-2\nu_2)}{\Gamma(2\nu_2)}\left(\frac{|\vec{k}|L}{2}\right)^{4\nu_2}\left(1+e^{-i2\pi\nu_2}e^{-\pi\alpha}+\cdots\right) \times\left(1-2\sin(2\nu_2\pi)\left(\frac{\alpha}{4e}\right)^{i\alpha}e^{-\pi\alpha}\frac{b}{a}+\cdots\right). \quad (4.46)$$

This clearly demonstrates the insensitivity of the Green's function to the horizon boundary conditions in the tunneling (large α) regime. It is important to note that the magnitude of the Green's function is not necessarily small in this regime, and that it is only the dependence on b/a that is being exponentially suppressed.

The same conclusion can be drawn by looking at the spectral function:

$$\chi(\omega,\vec{k}) = 2K\frac{\Gamma(-2\nu_2)}{\Gamma(2\nu_2)}\left(\frac{|\vec{k}|L}{2}\right)^{4\nu_2}\sin\left(-2\pi\nu_2\right)e^{-\pi\alpha}. \quad (4.47)$$

At large α, $\chi(\omega,\vec{k})$ is exponentially small, as predicted in the previous section. In the $\alpha\to\infty$ limit, the spectral function vanishes and $G(\omega,\vec{k})$ becomes completely insensitive to changing boundary conditions.

One interesting aspect of pure Lifshitz spacetime is that the exponential suppression is in the variable $\alpha\sim\vec{k}^2/\omega$, instead of just $|\vec{k}|$. Again, the WKB approximation can help us understand this behavior. From (4.23), we can find the tunneling factor by evaluating

$$S\left(\epsilon,\rho_0\right) = \int_\epsilon^{\rho_0} d\rho\sqrt{\frac{\nu_2^2}{\rho^2}+\frac{\vec{k}^2L}{2\rho}-\omega^2}. \quad (4.48)$$

In the near boundary region $\epsilon\ll\rho_*$, the integral will just generate the expected power-law behavior $\epsilon^{2\nu_2}$, which is stripped off by the factor $\epsilon^{-2\nu_2}$ in (4.30). For large α, the tunneling region will contribute an additional term of order

$$S\sim k\int_{\rho_*}^{\rho_0} d\rho\sqrt{\frac{L}{2\rho}}\approx k\int_0^{\frac{\vec{k}^2L}{2\omega^2}} d\rho\sqrt{\frac{L}{2\rho}}\sim\frac{\vec{k}^2L}{\omega}\sim\alpha, \quad (4.49)$$

z	$2/\zeta$	$2/\zeta_{\text{num}}$
2	2	2.05
3	3/2	1.55
4	4/3	1.39

Table 2: Best fit results for numerically obtained spectral functions.

and the actual suppression term is $\sim e^{-\alpha}$ instead of just $e^{-|\vec{k}|}$. This result has a simple interpretation: For a finite tunneling region $[R_1, R_2]$, the barrier can be made arbitrarily high by taking $|\vec{k}| \to \infty$, resulting in exponential suppression $e^{-|\vec{k}|}$. However, for pure Lifshitz, the tunneling region can also be made arbitrarily wide by taking either $\omega \to 0$ at fixed $|\vec{k}|$, or $|\vec{k}| \to \infty$ at fixed ω. Since the WKB functional S is a measure for the area between the wavefunction and the tunneling potential, we end up with a suppression in $\alpha \sim |\vec{k}| \cdot (|\vec{k}|/\omega)$.

To demonstrate that similar results hold for Lifshitz with general z, we also computed the spectral function χ for $z = 2, 3, 4$ numerically. Figure 21 shows plots of the spectral function as a function of ω and $|\vec{k}|$ respectively. For AdS, modes with spacelike momenta $|\vec{k}|^2 > \omega^2$ have zero spectral weight. For Lifshitz, however, we can clearly see an exponential tail both at small ω and large $|\vec{k}|$ due to tunneling, indicating the by now familiar insensitivity to horizon boundary conditions. From the WKB approximation (4.30), we expect the asymptotic behavior $\chi \sim \exp\left(-\lambda \alpha^{1/\zeta}\right)$, with

$$\lambda = \frac{\sqrt{\pi}\Gamma(1/\zeta - 1/2)}{2\Gamma(1/\zeta)}, \qquad \alpha = \left(\frac{\omega L}{z}\right)^{\zeta} \left(\frac{\vec{k}}{\omega}\right)^{2}, \qquad \zeta = 2\left(1 - \frac{1}{z}\right). \tag{4.50}$$

Our numerical results confirm this behavior (see Table 2 for best-fit values).

4.2.4 Spectral Functions for Lorentz-breaking RG Flows

Our discussion so far has been focused on the insensitivity of the Green's function to a change of horizon boundary conditions. The goal of this section is to reformulate this statement in a more physical way. We do this by showing that for spacetimes with a tunneling barrier, the

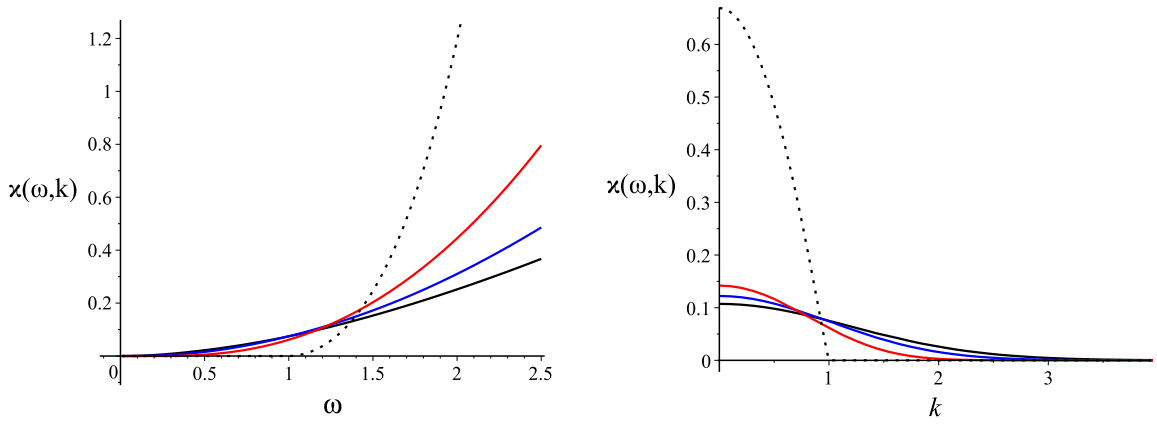

Figure 21: Plot of the spectral function $\chi(\omega, \vec{k})$ for Lifshitz with $z = 2, 3, 4$ (red, blue, black). The AdS spectral function is shown as a dotted line. Left: Varying ω while keeping $|\vec{k}| = 1/L$ fixed. Right: Varying $|\vec{k}|$ while keeping $\omega = 1/L$ fixed.

retarded Green's function is in fact exponentially insensitive to the near-horizon geometry itself. In terms of the corresponding RG flow, this has the somewhat surprising consequence that in the low energy, large momentum limit, the spectral function shows a universal behavior that depends only very weakly on the details of the IR theory. In that sense, flows with different IR fixed points are almost non-distinguishable.

To see explicitly how this arises, consider the case of an RG flow that interpolates between two different fixed points in the UV and IR. Since the dual spacetime interpolates between two different geometries at the horizon and the boundary, we introduce ρ_c as a cross-over scale between these two asymptotic geometries, and split the effective potential as

$$U = \begin{cases} U_{\text{UV}}, & \rho \ll \rho_c \\ U_{\text{IR}}, & \rho \gg \rho_c. \end{cases} \tag{4.51}$$

Although the potential near ρ_c depends on the precise way these two geometries are glued together, we will not need to know its explicit form in the intermediate region in order to study the general behavior of the spectral function. To simplify our discussion, let us assume that U decreases monotonically, so that there are no bound states, and that $U_{\text{UV}}(\rho \to 0) \sim$

$(\nu^2 - 1/4)/\rho^2$, as before.

We would like to extract information about IR physics from the spectral function. First, consider frequencies ω large enough so that the classical turning point $\rho_0(\omega)$ is in the UV, $\rho_0(\omega) \ll \rho_c$. Physically, since we are probing the geometry at high energies, χ is completely independent of the IR geometry. All that remains is the spectral function for the dual theory at the UV fixed point.

Next, let us use the WKB approximation to see what happens when we lower the energy far enough that the scalar wavefunction actually has to tunnel through part of the IR-potential, *i.e.* $\rho_0(\omega) \gg \rho_c$. We can approximate the WKB-integral as

$$S(\rho, \rho_0) \approx S_{\rm UV}(\rho, \rho_c) + S_{\rm IR}(\rho_c, \rho_0) + \cdots, \tag{4.52}$$

with $S_{\rm UV/IR} = \int d\rho \sqrt{U_{\rm UV/IR} - \omega^2}$. Here the ellipsis denotes terms that depend on the precise way the two geometries are glued together. Using (4.30), the spectral function now becomes

$$\chi \approx K \epsilon^{-2\nu} e^{-2S_{\rm UV}(\epsilon, \rho_c)} e^{-2S_{\rm IR}(\rho_c, \rho_0)}, \tag{4.53}$$

and the information about IR physics shows up in the factor $e^{-2S_{\rm IR}}$. For relativistic flows, one roughly gets $\chi \sim f(\omega)\,\mathcal{O}(1)\,e^{-2S_{\rm IR}(\rho_c, \rho_0)}$, and the IR geometry has an $\mathcal{O}(1)$ imprint on the spectral function. However, as we saw previously, if the UV fixed point has a Lifshitz scaling symmetry, the tunneling barrier will induce an exponential factor and we get

$$\chi \sim f(\omega)\,\mathcal{O}\left(e^{-c|\vec{k}|}\right) e^{-2S_{\rm IR}(\rho_c, \rho_0)}. \tag{4.54}$$

At large $|\vec{k}|$, all the information about IR physics is hidden under an exponentially small factor. In the limit $|\vec{k}| \to \infty$, a change of the geometry in the deep IR has no effect on the spectral function.

The factorization of χ into UV and IR factors in (4.53) allows us to make an even more

general statement: Consider any flow that breaks $(d+1)$-dimensional Lorentz-invariance somewhere in the bulk, *i.e.* $A \neq B$ in (4.10). At low frequencies ω and large momenta $|\vec{k}|$ the spectral function will have a universal exponential damping factor $e^{-c|\vec{k}|}$ due to the tunneling barrier $\vec{k}^2 e^{2A-2B}$.

We can demonstrate this behavior explicitly by considering holographic RG flows with $\mathrm{AdS}_2 \times \mathbb{R}^d$ near-horizon geometry. Examples of such geometryies are the nonsingular Lifshitz solutions constructed in chapter 2, as well as extremal charged black branes in AdS_{d+2}, which are holographically dual to theories at finite charge density [81]. Placing fermions on this background allows us to study Fermi surfaces in non-Fermi liquids [80, 82, 83, 84].

Of particular interest to us are flows with either AdS_{d+2} or Lif_z near-boundary behavior. For both cases, the Schrödinger potential can be written as

$$U = \begin{cases} \frac{\nu_z^2 - 1/4}{\rho^2} + \vec{k}^2 \left(\frac{L}{z\rho}\right)^{2-2/z}, & \rho \ll \rho_c; \\ \frac{\nu_\infty^2 - 1/4}{\rho^2}, & \rho \gg \rho_c, \end{cases} \tag{4.55}$$

where $\nu_\infty^2 = (mL_{\mathrm{IR}})^2 + \vec{k}^2 L_{\mathrm{IR}} + 1/4$, and the null energy condition requires $z \geq 1$. The near-horizon $\mathrm{AdS}_2 \times \mathbb{R}^d$ itself has a holographic dual, which is a CFT_1. In particular, there is a corresponding spectral function

$$\chi_{\mathrm{cft}} \approx K \epsilon^{-2\nu_\infty} e^{-2S_{\mathrm{IR}}(\epsilon, \rho_0)}. \tag{4.56}$$

Again, in the high energy limit the spectral function carries no information about the IR CFT. At low energies, specifically $\omega \ll \nu_\infty / \rho_c$ or equivalently $\rho_c \ll \rho_0(\omega)$, we can derive a direct relation between χ_{cft} and the full spectral function:

$$\chi\left(\omega \ll \frac{\nu_\infty}{\rho_c}, \vec{k}\right) \approx \epsilon^{-2\nu} e^{-2S_{\mathrm{UV}}(\epsilon, \rho_c)} \chi_{\mathrm{cft}}. \tag{4.57}$$

Let us evaluate this expression for large $|\vec{k}|$. The integral we have to perform is

$$S_{\rm UV}\left(\rho,\rho_c\right)=\int_{\rho}^{\rho_c}\sqrt{\frac{\nu^2}{\rho^2}+\vec{k}^2\left(\frac{L}{z\rho}\right)^{2-2/z}-\omega^2}. \tag{4.58}$$

The crossover scale from $1/\rho^2$ behavior to $1/\rho^{2(1-1/z)}$ behavior is at $\rho_*\equiv(\nu/p)^z$. We will assume that $|\vec{k}|\rho_c^{1/z}/\nu\gg 1$, so that this crossover still happens in the UV region, i.e. $\rho_*\ll\rho_c$. Since $\omega\ll\nu_\infty/\rho_c$, and the momentum is taken to be large, we can simply neglect the ω^2 term in (4.58). Introducing the new variable $u\equiv(p^2/\nu^2 z^{2(1-1/z)})\rho^{2/z}$, we can evaluate the integral:

$$S_{\rm UV}\left(\rho,\rho_c\right)\approx\frac{z\nu}{2}\left[2\sqrt{1+u}+\log\frac{\sqrt{1+u}-1}{\sqrt{1+u}+1}\right]_u^{u_c}. \tag{4.59}$$

Expanding this result around large u_c and small u, we find

$$e^{-2S_{\rm UV}(\epsilon,\rho_c)}\approx\epsilon^{2\nu}\left(\frac{|\vec{k}|}{2\nu z^{1-1/z}}\right)^{2z\nu}e^{-2(z\rho_c)^{\frac{1}{z}}|\vec{k}|}. \tag{4.60}$$

Plugging this back into (4.57), we see that the ϵ-dependent terms precisely cancel, and we are left with

$$\chi\big(\omega\ll\frac{\nu_\infty}{\rho_c},|\vec{k}|\gg\frac{\nu}{\rho_c^{1/z}}\big)\approx K\left(\frac{|\vec{k}|}{2\nu z^{1-1/z}}\right)^{2z\nu}e^{-2(z\rho_c)^{\frac{1}{z}}|\vec{k}|}\chi_{\rm cft}. \tag{4.61}$$

The spectral function at low energies is directly proportional to the IR spectral function $\chi_{\rm cft}$. At large $|\vec{k}|$, χ is exponentially small. It might seem surprising that this is true even for the case of asymptotically AdS spacetimes, where $z=1$. As we discussed in chapter 3, this is because even though pure AdS does not have a tunneling barrier, flowing to a non-relativistic $\mathrm{AdS}_2\times\mathbb{R}^d$ horizon necessarily breaks Lorentz invariance and introduces a tunneling barrier.

The relation (4.61) between UV and IR spectral functions has been obtained previously, using standard matching techniques [83]. Our calculation sheds new light on this result: While the spectral function is dominated by IR physics at low ω, the numerical coefficient

relating χ and χ_{cft} is exponentially small at large momenta. For a boundary observer, the signature of low-energy physics is hidden under an exponential tail.

4.2.5 Analytic Properties of the Green's Function

In section 4.1, we discussed how different types of Green's functions may be obtained from a single real analytic function $G(\omega, \vec{k})$ by using different $i\epsilon$ prescriptions. For a bulk scalar in AdS or Lifshitz, the Klein-Gordon equation, and hence effective Schrödinger-like equation (3.14), is quadratic in ω. However, the $\omega \to -\omega$ symmetry is broken by imposing infalling boundary conditions at the horizon. In other words, the holographic computation directly gives the retarded Green's function G_R without the need for any $i\epsilon$ prescription. Nevertheless, it is possible to analytically continue the resulting expressions to obtain $G(\omega, \vec{k})$ in the complex ω-plane.

As an example, we may start with the retarded AdS Green's function given by (4.36) with $b/a = 0$, and obtain

$$G(\omega, \vec{k}) = K \frac{\Gamma(-\nu)}{\Gamma(\nu)} \left(\frac{\vec{k}^2 - \omega^2}{4} \right)^{\nu}, \tag{4.62}$$

for non-integer values of ν; we have set $L = 1$ for notational ease throughout this section. This function has branch points at $\omega = \pm|\vec{k}|$, and as long as we take the principal branch of z^ν, the branch cuts will extend out as shown in Fig. 23. As a result, the spectral weight must vanish for $|\omega| < |\vec{k}|$. This region corresponds to the "energy" ω^2 lying completely under the AdS effective potential given by (4.32) with $z = 1$. In this case, the radial wavefunction never oscillates, and can be chosen to be real, which is consistent with the vanishing of $\chi(\omega, \vec{k})$. Furthermore, in this case there is no longer any freedom to modify the horizon boundary conditions, as one can only physically choose the exponentially decaying solution at the horizon. We give an example of the spectral function for AdS in Fig. 22.

We now turn to the $z = 2$ Lifshitz Green's function. Starting from (4.41), we find the

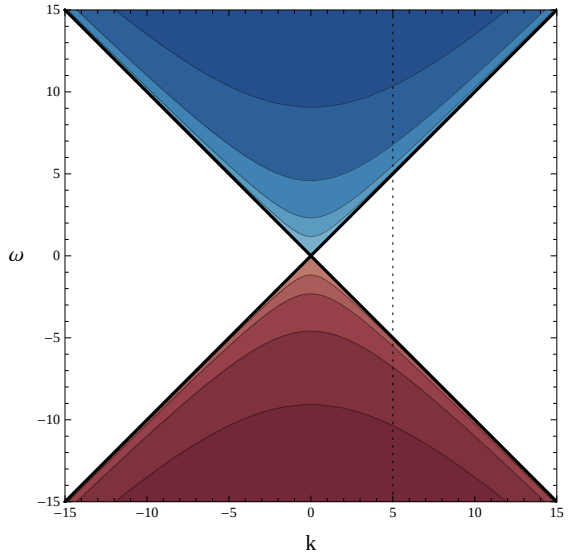

Figure 22: The spectral function for AdS (see (4.62), with $\nu = 1.1$). Note that $\chi(\omega, |\vec{k}|)$ vanishes identically for $|\omega| < |\vec{k}|$.

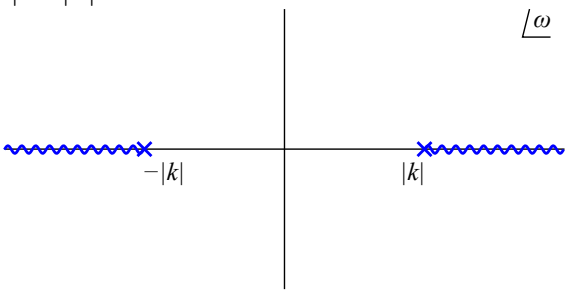

Figure 23: Branch cut structure in the complex ω-plane.

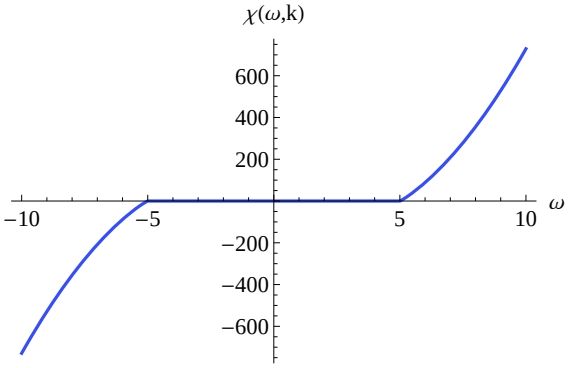

Figure 24: Spectral function $\chi(\omega, |\vec{k}|)$ for $|\vec{k}| = 5$.

appropriate analytic continuation to be

$$G(\omega,\vec{k}) = K\frac{\Gamma(-2\nu_2)}{\Gamma(2\nu_2)}(-\omega^2)^{\nu_2}\frac{\Gamma(\frac{1}{2}+\nu_2+\vec{k}^2/4\sqrt{-\omega^2})}{\Gamma(\frac{1}{2}-\nu_2+\vec{k}^2/4\sqrt{-\omega^2})}. \tag{4.63}$$

Again working with principal values, the factor $(-\omega^2)^{\nu_2}$ gives rise to a branch cut running from the origin to $+\infty$ as well as from the origin to $-\infty$. Thus χ is non-vanishing for any $\omega \neq 0$, although it becomes exponentially small for $|\omega| \ll \vec{k}^2/\nu_2$. Note that, while the Γ-function in the numerator introduces poles in $G(\omega,\vec{k})$, they all lie on the unphysical second Riemann sheet. Even though they are in the second sheet, the accumulation of these poles causes an essential singularity at $\omega = 0$. These features, along with the $z = 2$ Lifshitz spectral function, are shown in Fig. 25. In general, since the effective potential $U(\rho)$ in (4.32) vanishes at the horizon for any $z > 1$ Lifshitz geometry, the wavefunction will be oscillatory at the horizon. This in turn indicates that the retarded Green's function will be complex, and hence that $\chi(\omega,\vec{k})$ will be non-vanishing for any $\omega \neq 0$. Thus the structure of branch cuts running along the positive and negative real ω axis is universal for $z > 1$ Lifshitz.

4.2.6 Physical Interpretation of Horizon Insensitivity

We have found a region of momentum space ($\omega \ll 1$, $|\vec{k}| \gg 1$) in which the holographic Green's function of Lifshitz spacetime is exponentially insensitive to a change of horizon boundary conditions. As we argued previously, this implies that the two-point function is insensitive to the geometry in the deep IR itself. Our discussion provides a new perspective on the problem of finding the "true" IR endpoints of flows involving Lifshitz. We have seen in chapter 2 that the tidal singularity in Lifshitz spacetime can be resolved by constructing a flow to $\mathrm{AdS}_2 \times \mathbb{R}^d$ in the IR. However, the extensive ground state entropy of $\mathrm{AdS}_2 \times \mathbb{R}^d$ has led to the idea that the true IR endpoint of the flow may be a different geometry, such as a striped phase [85, 86, 87, 88, 89], a lattice [90], or a Bianchi-class geometry [91, 92]. Even though the ultimate fate of the theory in the deep IR is still unclear, it appears that

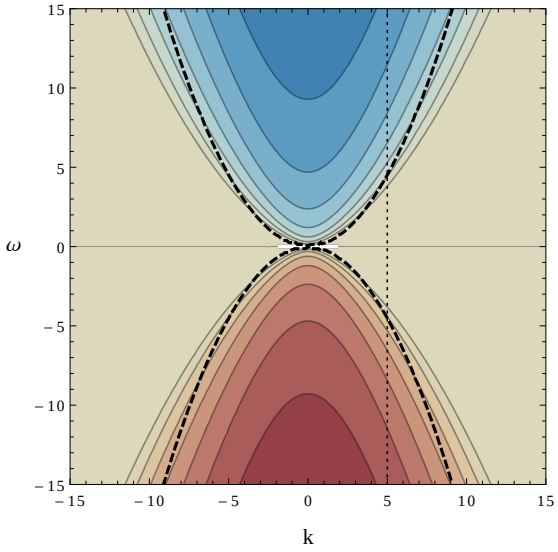

Figure 25: The spectral function for $z = 2$ Lifshitz (see (4.63), with $\nu = 1.1$). The spectral function is exponentially suppressed in the interior of the dashed circle shown in (a).

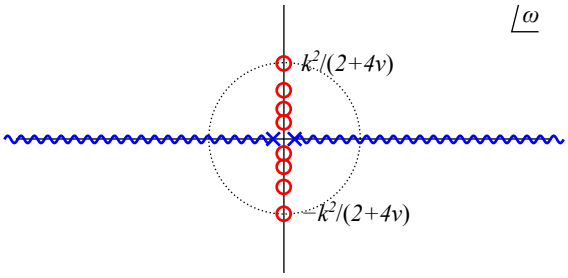

Figure 26: Analytic features in the complex ω-plane. The branch cuts extend from the origin to $\pm\infty$, and there are an infinite number of poles on the second sheet that accumulate at the origin.

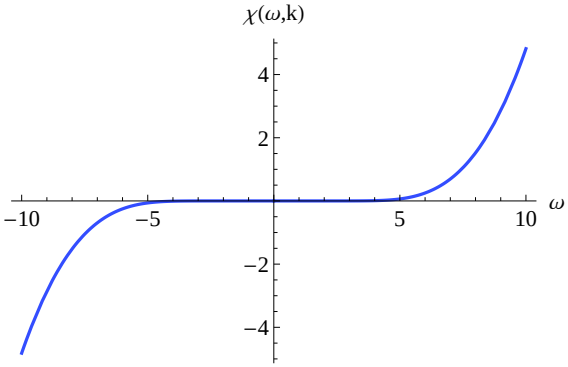

Figure 27: Spectral function $\chi(\omega, |\vec{k}|)$ for $|\vec{k}| = 5$. The spectral function is exponentially suppressed in the interior of the dashed circle in figure 26.

there is a variety of possible candidate groundstates, and thus a variety of different near-horizon geometries. From a boundary perspective, the geometric resolution of the horizon can be thought of as introducing a low-energy regulator. However, in the low energy, large momentum limit, the holographic Green's function becomes independent of the geometry in the deep IR, up to exponentially small corrections. In this sense, the field theory seems to care little about the exact mechanism that resolves the Lifshitz horizon. In particular, we may speculate that horizon features at small transverse length scales are practically invisible at the boundary. It would be interesting to confirm this for the case of striped phases/lattices, or a non-translationally invariant Bianchi geometry at the horizon.

Along the same lines, it would be interesting to understand how the tidal singularity at the horizon is reflected in field theory two-point functions. We can try to answer this question using what we learned about the relation between tunneling barriers and spectral functions: Consider a bulk state with fixed momentum $|\vec{k}|$, and send $\omega \to 0$. For a black hole geometry, this corresponds to a probe falling towards the horizon. Since the spectral function is proportional to $e^{-\alpha}$, with $\alpha \sim |\vec{k}|^2/\omega^{2/z}$, it is in fact not analytic at $\omega = 0$. Although this behavior is in principle allowed, it is certainly a peculiar feature. Moreover, as we saw in section 4.2.4, the non-analyticity is absent in the case of the nonsingular Lifshitz to $\mathrm{AdS}_2 \times \mathbb{R}^d$ flows - the spectral function only scales as $\chi \sim e^{-|\vec{k}|}$. Thus one may speculate that the tidal singularity in Lifshitz spacetime is mirrored in a non-analyticity of the holographic spectral function. In the next section, we will see that this non-analyticity is in fact not to be trusted, since higher derivative corrections to the bulk action will change the low energy behavior of the spectral function significantly.

The insight that tunneling barriers correspond to exponentially suppressed information at the boundary is not a new one. In particular, similar observations have been made in the context of finite temperature theories. Introducing a finite T may result in an effective tunneling barrier in the equations of motion, and as a result there are modes that are exponentially suppressed at the boundary [25, 93, 94]. A possible future direction would be

to explore the case of Lifshitz spacetime with $T \neq 0$, and study the interplay between the tunneling barriers discussed here and the effects of a nonzero temperature.

4.3 Universal Features of Lifshitz Green's Functions

Although the AdS/CFT dictionary provides us with an explicit prescription to calculate holographic Green's functions, it is interesting to note that in some cases, the functional form of the Green's function is in fact completely determined by spacetime symmetries. For example, consider the familiar picture of IIB theory on $\mathrm{AdS}_5 \times S^5$, which is dual to $\mathcal{N} = 4$ super-Yang Mills theory. In this case, the supergroup $\mathrm{SU}(2,2|4)$ is identical to the superconformal symmetry group of the four-dimensional CFT. As a result, all observables are constrained by the superconformal symmetry, and in particular the two-point functions are fully determined up to normalization. For example, the retarded scalar Green's function in momentum space must have the form

$$G_R(q^2) = A(-q^2)^{\Delta-2}, \qquad q^2 = \omega^2 - |\vec{k}\,|^2, \tag{4.64}$$

where A is an overall constant and Δ is the conformal dimension of the scalar operator $\mathcal{O}_\Delta$. We confirmed this result explicitly in (4.37).

The mapping between condensed matter systems and backgrounds with non-relativistic scaling symmetry is often less obvious. In this case, we must often fall back to the general strategy of constructing a holographic dual to a given field theory by matching symmetries and conserved quantities [20, 21, 22, 27]. Moreover, non-relativistic scale invariance is no longer sufficient to fully constrain the form of the two-point functions. Consider, for example, the case of Lifshitz scaling with dynamical exponent z, where energy and momentum scale as $\omega \to \lambda^z \omega$ and $\vec{k} \to \lambda \vec{k}$, respectively. This scaling symmetry only constrains the form of

the Green's function up to an arbitrary function of the scale-invariant quantity $\hat{\omega} = \omega/|\vec{k}\,|^z$:

$$G_R(\omega, \vec{k}\,) = |\vec{k}\,|^{2\nu z}\mathcal{G}(\hat{\omega}). \tag{4.65}$$

Here ν is the energy scaling dimension, and the momentum-dependent prefactor is chosen to give G_R the proper scaling dimension.

The form of the Green's function (4.65) holds for any (isotropic) scale-invariant theory, whether computed directly from the field theory or via the holographic dual. However, in general, $\mathcal{G}(\hat{\omega})$ cannot be fixed by matching symmetries alone. (If additional symmetries are imposed, such as $z = 2$ Schrödinger symmetry, then the Green's function may become fully determined.) This suggests that symmetries are not sufficient for connecting non-relativistic theories to their holographic duals, and in particular that the duality map must include additional dynamical information.

At the same time, the bulk theory yields a preferred choice of the Green's function obtained from the classical two-derivative bulk action [20]. For $z = 2$ Lifshitz, we calculated the holographic scalar Green's function in section 4.2.1. Moreover, our WKB calculation for arbitrary $z > 1$ revealed a characteristic exponential suppression of the spectral weight (i.e. the imaginary part of the Green's function) in the limit $\hat{\omega} \to 0$. We interpreted this feature as an "insensitivity" of the boundary theory to small changes of the geometry near the horizon. The same exponential behavior is responsible for making the smearing function of both Schwarzschild-AdS and Lifshitz spacetime a distribution rather than a true function (see chapter 3) and has been interpreted as a loss of bulk locality for such non-relativistic geometries [95].

It is natural to expect that different field theoretic models with the same dynamical exponent z will yield different Green's functions. This raises the issue as to how the holographic dual can distinguish among these models. For unbroken scaling symmetry, the bulk geometry is essentially fixed to be pure Lifshitz. Thus the background alone cannot distinguish

between different models, and we are mainly left with the dynamics of the bulk fields as the distinguishing characteristic. In particular, the addition of higher derivative terms to the bulk equations of motion will directly affect the form of the holographic Green's function. This is in contrast with the relativistic case, where higher derivative corrections may affect the constant A in (4.64), but will not otherwise modify the functional form of the retarded Green's function.

Once we allow for a higher derivative expansion in the bulk, it may seem that some predictive power is lost, since the holographic Green's function would in principle be sensitive to all of the infinitely many higher derivative terms. However, in this section we demonstrate that there are universal features that remain. In particular, the characteristic exponential suppression of the spectral function in the low frequency regime found previously is robust with respect to higher derivatives in the bulk, as long as the frequencies stay above a (momentum-dependent) cutoff.

We furthermore show that this exponential suppression arises in field theory models with $z = 2$ scaling. In particular, for the quadratic band crossing model of [96], a simple kinematical argument demonstrates that the exponential suppression arises because one has to go to higher and higher orders in the perturbative expansion to see non-zero spectral weight in the limit $\hat{\omega} \to 0$.

4.3.1 The Green's Function in a Scale Invariant Theory

In a translationally invariant theory, the retarded Green's function is naturally written in momentum space as $G_R(\omega, \vec{k})$. Furthermore, unitarity and causality demand that G_R is analytic in the upper half of the complex ω-plane. For a scale-invariant theory, the conditions on the Green's function are much stronger. In particular, for Lifshitz scaling symmetry with dynamical exponent z

$$\vec{x} \to \Lambda \vec{x}, \qquad t \to \Lambda^z t, \tag{4.66}$$

scale and rotational invariance demand that G_R cannot depend on ω and $\vec{k}$ separately, but must have the form

$$G_R(\omega, \vec{k}) = |\vec{k}|^{2\nu z} \mathcal{G}(\hat{\omega}) \quad \text{where} \quad \hat{\omega} \equiv \frac{\omega}{|\vec{k}|^z}. \tag{4.67}$$

Here ν is the energy scaling dimension and $\mathcal{G}(\hat{\omega})$ is analytic in the upper half $\hat{\omega}$ plane.

Non-relativistic scale invariance by itself does not further constrain the form of $\mathcal{G}(\hat{\omega})$. However, additional symmetries can fix it completely. For example, relativistic conformal invariance (for the case $z = 1$) constrains $G_R \sim (-q^2)^\nu$ where $q^2 = -k_\mu k^\mu = \omega^2 - |\vec{k}|^2$. This is equivalent to taking the function

$$\mathcal{G}_{\text{CFT}} = A(1 - \hat{\omega}^2)^\nu, \tag{4.68}$$

where A is a constant. Similarly, full Schrödinger symmetry (for $z = 2$) [21, 22, 27] requires

$$\mathcal{G}_{\text{Sch}} = A(1 - 2m\hat{\omega})^{2\nu}, \tag{4.69}$$

where A is again a constant, and m is the eigenvalue of the mass-operator of the Schrödinger algebra.

While the relativistic and Schrödinger cases are the most extensively studied, we are mainly interested in exploring the features of the function $\mathcal{G}(\hat{\omega})$ for Lifshitz models without additional symmetries using holographic methods. In general, $\mathcal{G}$ will depend on the details of the model. However, some universal properties can be deduced in both the small and large $\hat{\omega}$ limits. For $\hat{\omega} \to 0$, the only dimensionful quantity that remains is $|\vec{k}|$. Hence G_R must behave as $|\vec{k}|^{2\nu z}$, or equivalently

$$\mathcal{G}(\hat{\omega} \to 0) \sim \text{const.} \tag{4.70}$$

On the other hand, when $\hat{\omega} \to \infty$, the dependence on $|\vec{k}|$ drops out, and we must have

$$\mathcal{G}(\hat{\omega} \to \infty) \sim \hat{\omega}^{2\nu}. \tag{4.71}$$

As can be seen from (4.68) and (4.69), the $z = 1$ and Schrödinger $z = 2$ cases both satisfy these properties.

The retarded Green's function is in general complex, and this should be kept in mind when considering the limiting behaviors given above. Of particular interest is the general behavior of the spectral function $\chi(\omega, \vec{k}) = 2\,\mathrm{Im}\, G_R(\omega, \vec{k})$. For large ω, the spectral function scales as $\chi \sim \omega^{2\nu}$, consistent with (4.71), as well as the relativistic and Schrödinger cases. The small ω limit, on the other hand, is more subtle. While scaling symmetry demands $\chi \sim 2|\vec{k}|^{2\nu z}\ \mathrm{Im}\,\mathcal{G}(\hat{\omega})$, with $\mathrm{Im}\,\mathcal{G}(\hat{\omega})$ approaching a constant as $\hat{\omega} \to 0$, this constant is in fact zero for the $z = 1$ and $z = 2$ Schrödinger cases. Moreover, for these cases χ is identically vanishing for a range of $\hat{\omega}$ near zero. However, this no longer needs to be the case in theories with Lifshitz scaling, but without additional symmetries. Nevertheless, as we have shown in section 4.2.1, in the latter case the spectral function is at most exponentially small in the limit $\hat{\omega} \to 0$, at least in the two-derivative holographic theory. What we will show below is that this exponential suppression of χ remains robust, even when higher derivative corrections are included, as long as the perturbative expansion is kept under control.

4.3.2 Holographic Lifshitz Models

In this section, we repeat and refine the analysis of section 4.2.1, in particular introducing a more suitable radial coordinate $\hat{\rho}$ to determine the behavior of holographic Green's functions in the low/high frequency regime. We start by recalling the Lifshitz metric (1.5), with $L/z \equiv 1$:

$$ds^2_{d+2} = \frac{-dt^2 + d\rho^2}{\rho^2} + \frac{d\vec{x}^2}{\rho^{2/z}}. \tag{4.72}$$

The boundary of the bulk spacetime is located at $\rho = 0$, while the horizon is at $\rho = \infty$. For simplicity, we examine the scalar Green's function, which can be holographically computed from the action of a bulk scalar $\phi(t, \vec{x}, \rho)$.

At the two-derivative level, the minimally coupled equation of motion for ϕ is simply $(\Box - m^2)\phi = 0$. This system has been extensively studied, and the holographic computation of the retarded Green's function is by now standard [25]. Working in momentum space and taking

$$\phi(t, \vec{x}, \rho) = e^{i(\vec{k}\cdot\vec{x} - \omega t)} \rho^{d/2z} \psi(\rho), \tag{4.73}$$

we find that $\psi(\rho)$ satisfies the Schrödinger-like equation $-\psi'' + U_0 \psi = 0$ where

$$U_0 = \frac{\nu^2 - 1/4}{\rho^2} + \frac{|\vec{k}|^2}{\rho^{2-2/z}} - \omega^2. \tag{4.74}$$

and

$$\nu = \sqrt{m^2 + \left(\frac{d+z}{2z}\right)^2}. \tag{4.75}$$

We can highlight the scaling properties of the solution by defining the dimensionless coordinate

$$\hat{\rho} = \rho |\vec{k}|^z. \tag{4.76}$$

The Schrödinger-like equation now takes the form

$$-\psi''(\hat{\rho}) + \hat{U}_0(\hat{\rho})\psi(\hat{\rho}) = 0, \qquad \hat{U}_0(\hat{\rho}) = \frac{\nu^2 - 1/4}{\hat{\rho}^2} + \frac{1}{\hat{\rho}^{2-2/z}} - \hat{\omega}^2. \tag{4.77}$$

In order to apply the AdS/CFT prescription for calculating the retarded Green's function, we need to examine the solution near the boundary at $\hat{\rho} = 0$ and as it approaches the horizon at $\hat{\rho} = \infty$. In the limit $\hat{\rho} \to 0$, the Schrödinger potential is dominated by the $(\nu^2 - 1/4)/\hat{\rho}^2$ term, and we find the boundary behavior

$$\psi(\hat{\rho} \to 0) \sim A\hat{\rho}^{\frac{1}{2}-\nu} + B\hat{\rho}^{\frac{1}{2}+\nu}. \tag{4.78}$$

Here we have used the convention that B is the coefficient of the normalizable mode, while A is the coefficient of the non-normalizable mode. For $z > 1$, $\hat{U}_0$ approaches $-\hat{\omega}^2$ at the horizon, so the solution is oscillatory:

$$\psi(\hat{\rho} \to \infty) \sim a e^{i\hat{\omega}\hat{\rho}} + b e^{-i\hat{\omega}\hat{\rho}}. \tag{4.79}$$

For the retarded Green's function, we take infalling boundary conditions, which correspond to setting $b = 0$. In this case, we find

$$\mathcal{G}(\hat{\omega}) = \left.\frac{B}{A}\right|_{b=0}, \tag{4.80}$$

where the relation between $\{A, B\}$ at the boundary and $\{a, b\}$ at the horizon is obtained by solving the Schrödinger problem (4.77).

4.3.2.1 Bulk Higher Derivatives

At the two-derivative level, the solution for $\mathcal{G}(\hat{\omega})$ has been extensively studied, and analytic results may be obtained for $z = 1$ and $z = 2$ [25, 20]. However, as we emphasized in section 4.3.1, scaling symmetry by itself does not fully constrain the form of the Green's function. This raises the question of where the freedom of arbitrarily choosing the function $\mathcal{G}$ arises in the holographic dual. If we work within general relativity, there are two natural possibilities: the first is the choice of background metric, and the second is the form of the scalar equation. However, the metric (4.72) is essentially unique (up to coordinate transformations) once we have imposed Lifshitz scaling. This leaves us with modification of the equation of motion.

From a bulk effective field theory point of view, it is possible to include higher derivative terms in the scalar equation. In momentum space, non-radial derivatives in the effective action show up as powers of ω and $\vec{k}$, while additional ρ derivatives lead to a higher order differential equation for $\psi(\rho)$. If there are no additional ρ derivatives, then the momentum space equation remains second order and can be brought into Schrödinger form just as above.

This time, however, the effective Schrödinger potential in (4.77) generalizes to

$$\hat{U}(\hat{\rho}) = \frac{\nu^2 - 1/4}{\hat{\rho}^2} + \frac{1}{\hat{\rho}^{2-2/z}} - \hat{\omega}^2 + \frac{1}{\hat{\rho}^2} f(\hat{\omega}\hat{\rho}, \hat{\rho}^{1/z}), \tag{4.81}$$

where the function f encodes the presence of the higher derivative terms.

In principle, the procedure for extracting the holographic Green's function is unchanged from the prescription of (4.80). However, the higher derivative terms affect the shape of the potential, and hence may change the boundary and horizon asymptotics and possibly also introduce additional classical turning points in the bulk. In order to get a better understanding of the asymptotics, we write out the expansion

$$\frac{1}{\hat{\rho}^2} f(\hat{\omega}\hat{\rho}, \hat{\rho}^{1/z}) = \sum_{\substack{i,j \\ i+j>2}} \lambda_{i,j} \hat{\omega}^i \hat{\rho}^{i+j/z-2}, \tag{4.82}$$

where i and j count the number of temporal and spatial derivatives, respectively. The restriction $i + j > 2$ ensures that f only comprises the higher derivative contributions. Note that the coefficients $\lambda_{i,j}$ are dimensionless, although (after restoring units) we typically expect $\lambda_{i,j} \sim (\ell/L)^{i+j-2}$, where ℓ is some microscopic scale and L is the curvature scale of the Lifshitz bulk, such that $\ell \ll L$.

Focusing first on the boundary at $\hat{\rho} = 0$, we see that the behavior of the potential (4.81) remains dominated by the $1/\hat{\rho}^2$ term, since $i + j > 2$ in the derivative expansion. Thus the boundary scaling behavior remains unchanged from (4.78), and the relation of the scaling dimension to ν is unaffected by the higher order terms.

The horizon behavior, on the other hand, is considerably different. Since the horizon is located at $\hat{\rho} \to \infty$, and the expansion (4.82) in general contains positive powers of $\hat{\rho}$, the successive higher derivative terms will become more and more dominant at the horizon. Furthermore, the potential will generically go to $\pm\infty$ at the horizon, depending on the sign of $\lambda_{i,j}$ of the dominant term. As a result, strictly speaking, the perturbative expansion of

the scalar equation breaks down near the horizon. Nevertheless, we now argue that the holographic Green's function can be extracted from the solution of the higher derivative equation in a controlled manner.

4.3.2.2 Consistency of the Higher Derivative Expansion

At the two-derivative level, the Schrödinger potential (4.77) is monotonically decreasing as we move into the interior of the bulk, and there is a single classical turning point located at $\hat{\rho}_0$ where $\hat{U}_0(\rho_0) = 0$. For $\hat{\rho} < \hat{\rho}_0$, the solution connects to the power-law behavior (4.78) at the boundary, while for $\hat{\rho} > \hat{\rho}_0$, the solution is oscillatory, and infalling boundary conditions are chosen at the horizon.

Ignoring the shift of ν^2 in (4.77), there are two competing power laws in $\hat{U}$, namely $\nu^2/\hat{\rho}^2$ and $1/\hat{\rho}^{2-2/z}$, and the behavior of the solution depends on which of the power laws dominates at the classical turning point. We define the crossover point as $\hat{\rho}_* = \nu^z$, which is the location where the two terms become comparable. There are two distinct cases to consider:

1. For $\hat{\omega} \gg \nu^{1-z}$, the classical turning point is located at $\hat{\rho}_0 \approx \nu/\hat{\omega} \ll \hat{\rho}_*$. This point is close to the boundary, and the $1/\hat{\rho}^2$ potential ensures a power law behavior without exponential suppression. The holographic Green's function is "featureless", and behaves as $\mathcal{G} \sim \hat{\omega}^{2\nu}$.

2. For $\hat{\omega} \ll \nu^{1-z}$, the classical turning point is instead located at $\hat{\rho}_0 \approx \omega^{-z/(z-1)} \gg \hat{\rho}_*$. The Green's function now probes deep into the bulk, and can have non-trivial features. Note that the wavefunction has exponential behavior in the region $\hat{\rho}_* < \hat{\rho} < \hat{\rho}_0$, leading to an effective decoupling of the boundary from the horizon (see section 4.2).

We now consider the effect of the higher derivative terms, encoded in the function f in (4.82). Although this function dominates at the horizon, we nevertheless consider a formal perturbative expansion of the Schrödinger problem in the couplings $\lambda_{i,j}$. Of course, the higher order terms will dominate the wavefunction near the horizon. However, it is important to

realize that the holographic Green's function is not determined by the wavefunction at the horizon, but by its asymptotic behavior at the boundary. Infalling boundary conditions are needed at the horizon, but this can be imposed consistently at each order in the perturbative expansion. These infalling conditions will be seen in the boundary Green's function, but will not dominate over lower orders in the expansion.

Although a formal perturbative expansion can be used to solve the bulk scalar equation, the expansion of $\mathcal{G}$ in the couplings $\lambda_{i,j}$ will only be sensible if the corrections can be kept small. Obviously this cannot be true globally, as the higher derivative terms typically dominate near the horizon. However, as one can see for example by using the WKB approximation (see section 3.3), the holographic Green's function only gives us information about physics between the boundary and the classical turning point $\hat{\rho}_0$, where the wavefunction changes from exponential to oscillating behavior. Hence all that is necessary is to ensure that f remains small compared to the leading order potential $\hat{U}_0$ only for $\hat{\rho} \leq \hat{\rho}_0$. The specifics of this condition depend on whether we are in the high or low frequency regime. We consider these two cases separately:

1. In the high frequency regime ($\hat{\omega} \gg \nu^{1-z}$), the dominant term in $\hat{U}_0$ is $\nu^2/\hat{\rho}^2$. Since this term is decaying, while at the same time f becomes more important as we move away from the boundary, we only need to demand that f is small compared to $\nu^2/\hat{\rho}^2$ at the classical turning point. This gives rise to the condition $f(\hat{\omega}\hat{\rho}_0, \hat{\rho}_0^{1/z}) \ll \nu^2$, which may be satisfied by taking $(\ell/L)\nu \ll 1$, where we have assumed the expansion (4.82) along with the behavior of the couplings $\lambda_{i,j} \sim (\ell/L)^{i+j-2}$. As we may see from (4.75), the scale of ν is set by mL. Therefore, the condition for a valid expansion is equivalent to demanding $m\ell \ll 1$. We conclude that in this case, higher derivative corrections are under perturbative control provided the bulk couplings satisfy $m\ell \ll 1$. This behavior is very much like the relativistic $z = 1$ case, since in both situations the $\nu^2/\hat{\rho}^2$ potential dominates up to the classical turning point.

2. In the low frequency regime ($\hat{\omega} \ll \nu^{1-z}$), we need to compare f with the $1/\hat{\rho}^{2-2/z}$ term

in $\hat{U}_0$. Once again, we only need to consider the magnitude of f at the classical turning point. The condition is now $f(\hat{\omega}\hat{\rho}_0, \hat{\rho}_0^{1/z}) \ll \hat{\rho}_0^{2/z}$, which gives rise to the requirement

$$\hat{\omega} \gg \left(\frac{\ell}{L}\right)^{z-1}. \tag{4.83}$$

As $\hat{\omega}$ is taken smaller and smaller, we need to take higher and higher order corrections into account. As a result, the perturbative expansion breaks down at small $\hat{\omega}$, and results computed in this regime will not be robust against higher derivative corrections. Physically, what happens is that as $\hat{\omega} \to 0$, we probe closer and closer to the horizon, and it is precisely there where the higher derivative corrections dominate.

Hence, as long as the scale of the bulk higher derivative corrections satisfies $m\ell \ll 1$, the perturbative expansion of the boundary Green's function makes sense for dimensionless frequencies $\hat{\omega} \gg (\ell/L)^{z-1}$. For lower frequencies, the higher derivative terms start dominating.

This feature of higher derivative terms becoming more pronounced at the horizon is not restricted to the Lifshitz background, but is in fact fairly general and shows up in, *e.g.*, the pure AdS and Schwarzschild-AdS cases. While the pure AdS case tends to be robust against higher derivatives because of conformal invariance, more care may be needed in the case of holography at non-zero temperature [97, 98, 99, 25, 100, 101, 10, 102]. Transport coefficients, such as the shear viscosity, may be extracted using the Kubo formula, which is evaluated at $|\vec{k}| = 0$ before sending $\omega \to 0$. Since this is consistent with (4.83), the perturbative expansion for transport coefficients is valid. At the same time, however, more care may be needed when analyzing general hydrodynamic modes, which are defined for both ω and $\vec{k}$ small, but nonzero (see e.g. [103]).

4.3.3 WKB Analysis of the Spectral Function

In this section, we study the holographic spectral function of a probe scalar in Lifshitz spacetime, in the presence of higher derivative corrections. To determine the effect of higher

derivatives on the retarded Green's function, we consider a probe scalar with an effective potential of the form

$$\hat{U} = \frac{\nu^2 - 1/4}{\hat{\rho}^2} + \frac{1}{\hat{\rho}^{2-2/z}} - \hat{\omega}^2 + \sum_{i+j>2} \lambda_{i,j} \hat{\omega}^i \hat{\rho}^{i+j/z-2}. \tag{4.84}$$

The last term encodes an infinite set of higher derivative corrections to the equation of motion, where the (i, j) term corresponds to i temporal and j spatial derivatives. The size of the coefficients is expected to be set by a microscopic length scale ℓ, so that (after restoring units of L) $\lambda_{i,j} \sim (\ell/L)^{i+j-2}$. Since it is in general not possible to solve the corresponding Schrödinger equation for the potential (4.84) analytically, we will make use of the WKB approximation to obtain an approximate solution. This method can be used to calculate the imaginary part of the retarded Green's function, which is proportional to the spectral function. After switching to the $\hat{\rho}$ coordinates defined in (4.76), the spectral function can be approximated by[1] (4.30) with $b = 0$ (infalling boundary conditions):

$$K^{-1} \mathrm{Im}\, G_R(\omega, \vec{k}) \approx |\vec{k}|^{2\nu z} \lim_{\epsilon \to 0} \epsilon^{-2\nu} e^{-2S}. \tag{4.85}$$

Here K is a normalization constant and

$$S = \int_{\epsilon}^{\hat{\rho}_0} d\hat{\rho} \sqrt{\hat{U}(\hat{\rho}) + \frac{1}{4\hat{\rho}^2}}. \tag{4.86}$$

The additional $1/\hat{\rho}^2$ term is equivalent to an effective shift $\nu^2 \to \nu^2 + \frac{1}{4}$, which is necessary for consistency of the WKB approximation for $1/x^2$ potentials (see section 3.3). The integral is taken from a UV cutoff ϵ to the classical turning point $\hat{\rho}_0$. The WKB approximation for the imaginary part of the rescaled Green's function defined in (4.67) is given by

$$K^{-1} \mathrm{Im}\, \mathcal{G}(\hat{\omega}) \approx \lim_{\epsilon \to 0} \epsilon^{-2\nu} e^{-2S}. \tag{4.87}$$

[1] The additional prefactor of $|\vec{k}|^{2\nu z}$ arises from letting $\epsilon \to |\vec{k}|^{-z}\epsilon$, which is the proper UV cutoff needed to cancel the log-divergence of the integral.

This expression is valid for a potential with only one classical turning point, such that the wavefunction is oscillating near the horizon and tunnels towards the boundary. Close to the boundary, the $1/\hat{\rho}^2$ part of the potential leads to a power-law scaling of the wavefunction, which is stripped off by the factor of $\epsilon^{-2\nu}$ in (4.87). We can use (4.87) to determine the imprint of higher derivative corrections on the spectral function, provided that $\lambda_{i,j} < 0$. In this case, the potential goes to $-\infty$ at the horizon, but the wavefunction still remains oscillating and we can consistently impose infalling boundary conditions. Later we will argue that (4.87) can in fact be used to provide a formal expansion for corrections with arbitrary sign.

In order to perform a perturbative expansion of the WKB integral (4.86) in terms of $\lambda_{i,j}$, we need the higher derivative corrections to be subdominant compared to the other terms in $\hat{U}$, at least in the domain of integration. We therefore demand

$$\lambda_{i,j}\hat{\omega}^i\hat{\rho}^{i+j/z} \ll \nu^2, \qquad \lambda_{i,j}\hat{\omega}^i\hat{\rho}^{i+j/z} \ll \hat{\rho}^{2/z} \tag{4.88}$$

for all $0 < \hat{\rho} \leq \hat{\rho}_0$ (see also the discussion in section 4.3.2.2). We can already see that this imposes an $\hat{\omega}$-dependent condition on the coefficients $\lambda_{i,j}$, which we will make more explicit in what follows.

We can now determine the leading order correction to $\mathrm{Im}\,\mathcal{G}(\hat{\omega})$ by formally expanding the WKB integral in terms of the $\lambda_{i,j}$. At leading order, the higher derivative contributions are linear, so for our purposes it will be enough to drop the sum in (4.84) and only consider the effect of a single correction term with fixed (i,j). In a realistic model with a tower of higher derivative corrections, one may obtain a perturbative expansion for $\mathrm{Im}\,\mathcal{G}(\hat{\omega})$ by summing up the individual contributions, keeping in mind that if there are corrections at different order (e.g. α' and $(\alpha')^2$), one may have to go beyond linear order to study the effect of all correction terms.

A consistent expansion in $\lambda_{i,j}$ requires expanding both the integrand and the upper bound

$\hat{\rho}_0$, since the location of the turning point depends on the details of the correction terms. Writing $S = S^{(0)} + \delta S$, where $S^{(0)}$ is the two-derivative integral with $\lambda_{i,j} = 0$, we find (see appendix E for a rigorous derivation):

$$S^{(0)} = \int_\epsilon^{\hat{\rho}_0^{(0)}} d\hat{\rho} \sqrt{\frac{\nu^2}{\hat{\rho}^2} + \frac{1}{\hat{\rho}^{2-2/z}} - \hat{\omega}^2}, \tag{4.89}$$

$$\delta S \approx \int_\epsilon^{\hat{\rho}_0^{(0)}} d\hat{\rho} \frac{\lambda_{i,j} \hat{\omega}^i \hat{\rho}^{i+j/z-2}}{2\sqrt{\frac{\nu^2}{\hat{\rho}^2} + \frac{1}{\hat{\rho}^{2-2/z}} - \hat{\omega}^2}}, \tag{4.90}$$

where $\hat{\rho}_0^{(0)}$ is the turning point for the case $\lambda_{i,j} = 0$, i.e. the solution of

$$\frac{\nu^2}{\hat{\rho}_0^2} + \frac{1}{\hat{\rho}_0^{2-2/z}} - \hat{\omega}^2 = 0, \tag{4.91}$$

and we expanded up to linear order in $\lambda_{i,j}$. The large and small $\hat{\omega}$-behavior of the unperturbed integral $S^{(0)}$ was computed in sections 3.3.2 and 3.4:

$$S^{(0)}(\hat{\omega} \gg \nu^{1-z}) \approx -\nu - \nu \log\left(\frac{\epsilon}{2\nu}\right), \tag{4.92}$$

$$S^{(0)}(\hat{\omega} \ll \nu^{1-z}) \approx -z\nu + z\nu \log(2\nu) + \nu(z-1)\log z + \frac{\sqrt{\pi}\Gamma\left(\frac{1}{2(z-1)}\right)}{z\Gamma\left(\frac{z}{2(z-1)}\right)} \hat{\omega}^{-\frac{1}{z-1}}. \tag{4.93}$$

Let us now calculate the leading correction (4.90) in the same limits. For $\hat{\omega} \gg \nu^{1-z}$, the unperturbed turning point lies at $\hat{\rho}_0^{(0)} \approx \nu/\hat{\omega}$, which is well within the region where the $1/\hat{\rho}^2$ term dominates over $1/\hat{\rho}^{2-2/z}$. Hence we can approximate the integral as

$$\delta S \approx \int_\epsilon^{\nu/\hat{\omega}} d\hat{\rho} \frac{\lambda_{i,j} \hat{\omega}^i \hat{\rho}^{i+j/z-2}}{2\sqrt{\frac{\nu^2}{\hat{\rho}^2} - \hat{\omega}^2}}. \tag{4.94}$$

Letting $x \equiv \hat{\omega}\hat{\rho}/\nu$, we find

$$\delta S \approx \nu \lambda_{i,j} \nu^{i+j-2} \left(\frac{\nu^{1-z}}{\hat{\omega}}\right)^{\frac{j}{z}} \int_{\frac{\epsilon\hat{\omega}}{\nu}}^1 dx \frac{x^{i+\frac{j}{z}-2}}{2\sqrt{\frac{1}{x^2} - 1}}. \tag{4.95}$$

For $\hat{\omega} \gg \nu^{1-z}$, correction terms with $j \neq 0$ are highly suppressed. After taking the UV cutoff ϵ to zero, we therefore have

$$\delta S \approx \delta_{j,0} c_i \lambda_{i,0} \nu^{i-1} + O\left(\frac{\nu^{1/z-1}}{\hat{\omega}^{1/z}}\right), \tag{4.96}$$

where

$$c_i = \int_0^1 dx \frac{x^{i-1}}{2\sqrt{1-x^2}} = \frac{\sqrt{\pi}\Gamma\left(\frac{i}{2}\right)}{4\Gamma\left(\frac{i+1}{2}\right)}. \tag{4.97}$$

Using (4.96) and the unperturbed result (4.92), we arrive at the final answer

$$K^{-1}\mathrm{Im}\,\mathcal{G}(\hat{\omega} \gg \nu^{1-z}) \approx C\hat{\omega}^{2\nu}, \qquad C = (2\nu)^{-2\nu} \exp\left[2\nu\left(1 - \delta_{j,0} c_i \lambda_{i,0} \nu^{i-2} + \cdots\right)\right], \tag{4.98}$$

where the ellipsis indicates terms that are higher order in λ. The scaling of $\mathcal{G}$ with $\hat{\omega}^{2\nu}$ reflects the fact that at large frequencies, the Green's function $G_R(\omega, \vec{k}) = |\vec{k}|^{2\nu z}\mathcal{G}(\hat{\omega})$ becomes independent of $\vec{k}$ (see the discussion in section 4.3.1). The higher derivatives simply renormalize the numerical prefactor in a controlled way. The size of the higher derivative corrections at large $\hat{\omega}$ is controlled by

$$\lambda_{i,0}\nu^{i-2} \sim \left(\frac{\ell}{L}\nu\right)^{i-2} \sim (m\ell)^{i-2}, \tag{4.99}$$

where $i > 2$ is the number of temporal derivatives. Note that $\lambda_{i,0}\nu^{i-2} \ll 1$ is precisely what is required for the higher derivative corrections to be small up to the classical turning point $\hat{\rho}_0$, in the limit of large $\hat{\omega}$, as one can see by evaluating (4.88) at $\hat{\rho}_0$ in this limit, and noting that the unperturbed potential is monotonically decreasing.

We now turn to calculating the higher derivative corrections in the case of small frequencies ($\hat{\omega} \ll \nu^{1-z}$). In this case, the unperturbed classical turning point lies at $\hat{\rho}_0^{(0)} \approx \hat{\omega}^{-z/(z-1)}$. We can split up the integral (4.90) in the following way: Let $\hat{\rho}_* = \nu^z$ be the crossover scale, defined in the beginning of section 4.3.2.2, at which the two different terms in the potential (4.81), $\nu^2/\hat{\rho}^2$ and $1/\hat{\rho}^{2-2/z}$, become comparable. Since $\hat{\omega} \ll \nu^{1-z}$, we can then introduce a

regulator scale $\hat{\rho}_r$ such that $\hat{\rho}_* \ll \hat{\rho}_r \ll \hat{\rho}_0^{(0)}$, and split up the WKB integral in (4.90) as

$$\int_\epsilon^{\hat{\rho}_0^{(0)}} = \int_\epsilon^{\hat{\rho}_r} + \int_{\hat{\rho}_r}^{\hat{\rho}_0^{(0)}}. \tag{4.100}$$

The first of the integrals above is taken over $\epsilon \leq \hat{\rho} \leq \hat{\rho}_r \ll \hat{\rho}_0^{(0)}$, so we can approximate the potential in this region as

$$\hat{U} \approx \frac{\nu^2}{\hat{\rho}^2} + \frac{1}{\hat{\rho}^{2-2/z}} + \lambda_{i,j}\hat{\omega}^i\hat{\rho}^{i+j/z-2}. \tag{4.101}$$

On the other hand, the second integral is taken over $\hat{\rho}_r \leq \hat{\rho} \leq \hat{\rho}_0^{(0)}$, so in this region we can write

$$\hat{U} \approx \frac{1}{\hat{\rho}^{2-2/z}} - \hat{\omega}^2 + \lambda_{i,j}\hat{\omega}^i\hat{\rho}^{i+j/z-2}. \tag{4.102}$$

Using these approximations, we find

$$\begin{aligned} \delta S &= \delta S_1 + \delta S_2, \\ &\approx \int_\epsilon^{\hat{\rho}_r} d\hat{\rho} \frac{\lambda_{i,j}\hat{\omega}^i\hat{\rho}^{i+j/z-2}}{2\sqrt{\frac{\nu^2}{\hat{\rho}^2} + \frac{1}{\hat{\rho}^{2-2/z}}}} + \int_{\hat{\rho}_r}^{\hat{\rho}_0^{(0)}} d\hat{\rho} \frac{\lambda_{i,j}\hat{\omega}^i\hat{\rho}^{i+j/z-2}}{2\sqrt{\frac{1}{\hat{\rho}^{2-2/z}} - \hat{\omega}^2}}. \end{aligned} \tag{4.103}$$

Letting $u = \frac{1}{\nu^2}\hat{\rho}^{2/z}$, the first integral can be written as

$$\delta S_1 = \frac{z\nu}{4}\lambda_{i,j}\nu^{i+j-2}\left(\frac{\hat{\omega}}{\nu^{1-z}}\right)^i \int_{u_\epsilon}^{u_r} du \frac{u^{\frac{z}{2}i+\frac{j}{2}-1}}{\sqrt{1+u}}, \tag{4.104}$$

where the integration bounds are $u_\epsilon = \epsilon^{2/z}/\nu^2 \to 0$ and $u_r = (\hat{\rho}_r/\hat{\rho}_*)^{2/z} \gg 1$. In the small frequency limit $\hat{\omega} \ll \nu^{1-z}$, the correction term is highly suppressed unless $i = 0$. Hence we have

$$\delta S_1 \approx \delta_{i,0}\frac{z\nu}{4}\lambda_{0,j}\nu^{j-2}\int_{u_\epsilon}^{u_r} du \frac{u^{\frac{j}{2}-1}}{\sqrt{1+u}} + O\left(\frac{\hat{\omega}}{\nu^{1-z}}\right). \tag{4.105}$$

The remaining integral is divergent as $u_r \to \infty$. However, one can show that the contribution of the upper bound cancels with that from the lower bound of δS_2, since u_r is after all a

fictitious regulator scale. Hence the only contribution of (4.105) to δS is due to evaluating the integral at the lower bound $u_\epsilon \to 0$:

$$\delta S_1 \to -\delta_{i,0}\frac{z\nu}{4} d_j \lambda_{0,j} \nu^{j-2} + O\left(\frac{\hat{\omega}}{\nu^{1-z}}\right), \tag{4.106}$$

where

$$d_j = \int^{u=0} du \frac{u^{\frac{j}{2}-1}}{\sqrt{1+u}}. \tag{4.107}$$

This contribution is finite; in particular there are no $\log \epsilon$ terms, which would affect the boundary scaling. Similar to the large $\hat{\omega}$ case, higher derivative corrections are controlled by terms of order $\sim \lambda \nu^{n-2}$, where n counts the number of derivatives. This becomes qualitatively different when considering δS_2, which captures the contribution of higher derivative corrections deep in the bulk. Letting $x = \hat{\omega}^{z/(z-1)}\hat{\rho}$, we obtain

$$\delta S_2 = \frac{1}{2}\hat{\omega}^{-\frac{1}{z-1}} e_{i,j} \lambda_{i,j} \hat{\omega}^{-\frac{1}{z-1}(i+j-2)}, \tag{4.108}$$

where

$$e_{i,j} = \int_{\hat{\rho}_r/\hat{\rho}_0^{(0)}}^1 dx \frac{x^{i-1+\frac{j-1}{z}}}{\sqrt{1-x^{2-\frac{2}{z}}}}. \tag{4.109}$$

When expanding the lower bound in powers of $\hat{\rho}_r/\hat{\rho}_0^{(0)}$, each term is designed to cancel with the corresponding contribution from δS_1. Instead of carrying out this cancellation explicitly, we can therefore let

$$e_{i,j} \to \int_0^1 dx \frac{x^{i-1+\frac{j-1}{z}}}{\sqrt{1-x^{2-\frac{2}{z}}}} = \frac{\sqrt{\pi}\Gamma\left(\frac{iz+j-1}{2(z-1)}\right)}{(2-\frac{2}{z})\Gamma\left(\frac{(i+1)z+j-2}{2(z-1)}\right)}, \tag{4.110}$$

together with the prescription (4.106). Using (4.106), (4.108) and the zeroth order result (4.93), we arrive at the final answer

$$K^{-1}\mathrm{Im}\,\mathcal{G}(\hat{\omega} \ll \nu^{1-z}) \approx D \exp\left[-\hat{\omega}^{-\frac{1}{z-1}} E(\hat{\omega})\right], \tag{4.111}$$

where

$$D = (2\nu)^{-2z\nu} z^{2\nu(1-z)} \exp\left[2z\nu\big(1 + \delta_{i,0} d_j \lambda_{0,j} \nu^{j-2} + \cdots\big)\right],$$
$$E(\hat{\omega}) = \frac{\sqrt{\pi}\Gamma\left(\frac{1}{2(z-1)}\right)}{z\Gamma\left(\frac{z}{2(z-1)}\right)} + e_{i,j}\lambda_{i,j}\hat{\omega}^{-\frac{1}{z-1}(i+j-2)} + \cdots . \tag{4.112}$$

Here the ellipses indicate terms that are higher order in λ. We see that the higher derivative terms have two distinct effects: First, corrections with $i = 0$, which correspond to purely spatial derivatives, affect the overall normalization D of the spectral function. Second, and more importantly, higher derivative corrections with any i and j change the behavior of the spectral function as $\hat{\omega} \to 0$, encoded in $E(\hat{\omega})$. The $\hat{\omega}$-dependent correction terms become more and more important at small frequencies, and eventually the perturbative expansion breaks down. This was to be expected, since at small $\hat{\omega}$, the spectral function probes deep into the bulk, where higher derivatives dominate. However, recall that the coupling constants $\lambda_{i,j}$ are generically given by a ratio of a microscopic versus macroscopic length scale, $\lambda_{i,j} \sim (\ell/L)^{i+j-2}$. It is thus possible to keep the corrections in (4.111) small by demanding

$$\nu^{1-z} \gg \hat{\omega} \gg \left(\frac{\ell}{L}\right)^{z-1} . \tag{4.113}$$

This is precisely the bound we argued for in section 4.3.2.2. Since the condition (4.88), evaluated at large $\hat{\omega}$, also guarantees that $\ell\nu/L \ll 1$ (see the discussion around (4.99) and section 4.3.2.2), there is a wide range of frequencies that satisfy the inequality (4.113). For frequencies within this range, (4.111) is a universal result: The spectral function behaves as $\sim \exp\left(-\text{const.} \cdot \hat{\omega}^{-1/(z-1)}\right)$, and there are both constant and $\hat{\omega}$-dependent corrections that can be computed order by order in perturbation theory. The naive limit $\hat{\omega} \to 0$ is non-universal, since higher derivative corrections cannot be kept under control.

The procedure for calculating higher derivative corrections to the spectral function out-

lined here can in principle be applied to arbitrary corrections of the form (4.84). Note, however, that since we generally expect an infinite number of such corrections, going beyond leading order in ℓ/L may require expanding (4.86) to the appropriate order.

Finally, let us comment on the sign of $\lambda_{i,j}$. In the analysis above, we assumed that $\lambda_{i,j} < 0$, so that the wavefunction is always oscillating at the horizon, and no additional turning points are introduced. If $\lambda_{i,j}$ is positive, the wavefunction is tunneling in the deep IR, leading to another tunneling contribution $S_{\rm IR}$ to the spectral function (4.85). At large enough $\hat{\rho}$, the higher derivative corrections will always dominate the potential, so $S_{\rm IR}$ does not have a perturbative expansion in $\lambda_{i,j}$. This is simply a consequence of the fact that the potential in the IR is always sensitive to all of the (in principle infinitely many) coefficients that appear in the series of higher derivative corrections, and we cannot solve the equation of motion perturbatively in the IR. It therefore seems that one cannot trust our analysis in the case of generic corrections with arbitrary sign. However, one can circumvent this problem in the following way: For any given $\hat{\omega}$, we can define a regulator surface at $\hat{\rho} = \hat{\rho}_h(\hat{\omega}) \gg \hat{\rho}_0$, such that higher derivative corrections are still small at $\hat{\rho}_h$, i.e.

$$\lambda_{i,j}\hat{\omega}^i\hat{\rho}_h^{i+j/z} \ll \nu^2, \qquad \lambda_{i,j}\hat{\omega}^i\hat{\rho}_h^{i+j/z} \ll \hat{\rho}_h^{2/z}. \tag{4.114}$$

This guarantees that the wavefunction is still oscillating at $\hat{\rho}_h$, even though eventually higher derivatives may cause the potential to bend upwards again. Ignoring the (unknown) behavior of the wavefunction in the deep IR, we only impose infalling boundary conditions at $\hat{\rho}_h$, instead of $\hat{\rho} \to \infty$. The surface at $\hat{\rho}_h$ thus becomes an "effective horizon", where the wavefunction is infalling:

$$\psi(\hat{\rho} \to \hat{\rho}_h) \approx a e^{i\Phi(\hat{\rho})}. \tag{4.115}$$

Here Φ is an increasing function of $\hat{\rho}$. The retarded Green's function can then be computed using the usual formula (4.80), and the spectral function can be calculated approximately using the WKB-formula (4.85). On a practical level, this regularization prescription amounts

to simply taking (4.85) for granted, and formally expanding the WKB integral S in $\lambda_{i,j}$, without worrying about the dynamics close to the horizon.

4.3.4 Field Theory Models with $z = 2$

As we have demonstrated, a holographic computation of the spectral function yields the universal low-frequency behavior $\chi \sim \exp(-\text{const.} \cdot \hat{\omega}^{-1/(z-1)})$, provided $\hat{\omega}$ is in the range (4.113), where the higher derivative corrections are controlled. From a field theory point of view, such an exponential behavior is not expected to arise at any finite perturbative order, but can show up non-perturbatively. This, of course, fits the framework of non-relativistic holography, where the field theory dual is expected to involve strong correlations.

In this section, we explore a field theoretic model exhibiting $z = 2$ Lifshitz scaling, namely the quadratic band crossing model of [96]. Our strategy will be to identify phase-space regions with nonzero decay rates for bosonic quasi-particles, which, according to the optical theorem, will contribute to the imaginary part of the corresponding bosonic Green's function, and hence the spectral function. We confirm the presence of exponential suppression in the spectral function at small $\hat{\omega}$, in agreement with the holographic computation.

4.3.4.1 The Quadratic Band Crossing Model

To set up the quadratic band crossing model, let us start with a massless Dirac theory in $2+1$ dimensions, with action[2]

$$S = \int d\vec{x}dt \left[\bar{\Psi}\left(i\gamma_0\partial_0 - i\gamma_1\partial_x - i\gamma_2\partial_y\right)\Psi - g\psi_1^\dagger\psi_2^\dagger\psi_2\psi_1\right]. \tag{4.116}$$

[2]Note that we use signature $(+,-,-)$ for the field theory.

Here $\Psi = (\psi_1, \psi_2)^T$ is a two-component spinor and $\bar{\Psi} = \Psi^\dagger \gamma_0$. The $2+1$ dimensional Dirac matrices are given by

$$\gamma_0 = \begin{pmatrix} 0 & -i \\ i & 0 \end{pmatrix}, \quad \gamma_1 = \begin{pmatrix} 0 & i \\ i & 0 \end{pmatrix}, \quad \gamma_2 = \begin{pmatrix} -i & 0 \\ 0 & i \end{pmatrix}. \tag{4.117}$$

The interaction term in (4.116) is the only four-fermi term allowed for a two-component spinor. In the IR, this ψ^4 term is also the most relevant interaction term in the RG sense. At the Gaussian fixed point, this theory is conformally invariant with dynamical critical exponent $z = 1$. By setting the speed of light to unity, the theory contains only one control parameter, which is the interaction strength g.

The quadratic band crossing model generalizes the above to form a scaling invariant model with $z = 2$ [96]. It does so by replacing the derivatives in the Dirac theory (4.116) by the following operators:

$$\begin{aligned} i\partial_0 &\to i\partial_0 + t_0 \nabla^2, \\ i\partial_x &\to -t_1(\partial_x^2 - \partial_y^2), \\ i\partial_y &\to -2t_2 \partial_x \partial_y, \end{aligned} \tag{4.118}$$

where $\nabla^2 = \partial_x^2 + \partial_y^2$ and t_0, t_1 and t_2 are real parameters. After this substitution, we obtain a model with $z = 2$:

$$S = \int d\vec{x} dt \left\{ \bar{\Psi} \left[\gamma_0 \left(i\partial_0 + t_0 \nabla^2 \right) + \gamma_1 t_1 \left(\partial_x^2 - \partial_y^2 \right) + 2\gamma_2 t_2 \partial_x \partial_y \right] \Psi - g \psi_1^\dagger \psi_2^\dagger \psi_2 \psi_1 \right\}. \tag{4.119}$$

This action bears some resemblance with the original Dirac theory. However, in direct contrast to the Dirac theory, whose action only contains first-order derivatives, this model has a first order time derivative and second order spatial derivatives. As a result, space and time have different scaling dimensions, and it is straightforward to show that dimensionally $[t] =$

$2[\vec{x}]$, corresponding to $z = 2$ at the Gaussian fixed point. In condensed matter systems, this model describes band touching points with quadratic dispersions, which have been observed in bilayer graphene (see for example the review articles [104, 105, 106]); a realization has been proposed in optical lattice systems, using high angular momentum orbitals [107].

Generically, the action (4.119) contains four control parameters: t_0, t_1, t_2, and the interaction strength g. However, we can set one of the three t_i's to unity (say $t_2 = 1$) by rescaling. As shown in [96], if we require SO(2) spatial rotational symmetry, then t_1 and t_2 must coincide. Furthermore, if a fermion particle-hole symmetry (i.e. charge conjugation) is enforced, then t_0 must vanish. Here we will focus on the case with $t_0 = 0$ and $t_1 = t_2 = 1$, which preserves both the spatial rotational and charge-conjugation symmetries. In this case, the action reduces to

$$S = \int d\vec{x}dt \left\{ \bar{\Psi} \left[\gamma_0 i\partial_0 + \gamma_1 \left(\partial_x^2 - \partial_y^2 \right) + 2\gamma_2 \partial_x \partial_y \right] \Psi - g\psi_1^\dagger \psi_2^\dagger \psi_2 \psi_1 \right\}, \tag{4.120}$$

and the free dispersion relation for the two bands is given simply by

$$\epsilon_\pm(\vec{k}) = \pm k^2. \tag{4.121}$$

It is worth emphasizing that most of our conclusions remain valid as long as $|t_0| < |t_1|$ and $|t_0| < |t_2|$. These inequalities ensure that the model has both particles and holes in the weak coupling limit (small g).

4.3.4.2 Renormalization Group Analysis

At tree level, the ψ^4 term in the quadratic band crossing model is irrelevant (relevant) in the IR for systems above (below) 2+1 dimensions. In 2+1 dimensions, g is marginal at the tree level. A one-loop RG analysis indicates that a repulsive interaction ($g > 0$) is marginally relevant at IR, while an attractive interaction $g < 0$ is marginally irrelevant in the IR [96]. In the Dirac theory (4.116) on the other hand, the ψ^4 term is irrelevant (relevant) in the IR

for systems above (below) 1+1 dimensions. In 1+1 dimensions, due to the special properties of the 1+1 conformal group, the ψ^4 term remains exactly marginal, before the system hits a Kosterlitz-Thouless transition.

4.3.4.3 Boson Correlation Functions

Although the model discussed above describes fermionic fields, bosonic modes can be constructed from these fermionic degrees of freedom in the form of fermion bilinears. In the particle-hole channel, we can build four different fermion bilinears (boson modes)

$$b_i = \bar{\Psi}\gamma_i\Psi, \tag{4.122}$$

with $i = 0$, 1, 2, and 3, and the fourth gamma matrix is given by $\gamma_3 = i\gamma_0\gamma_1\gamma_2$. Here b_0 is the fermion density operator and the other three bosonic operators can be used as order parameters for various symmetry breaking phases (nematic or quantum anomalous Hall) [96]. At the Gaussian fixed point, these bosonic modes have $z = 2$, which is inherited from the fermions.

Additional bosonic modes can also be created in the particle-particle channel (e.g. $\psi_1^\dagger\psi_2^\dagger$), which are the order parameters for various superconducting states. In this section, we will only consider fermion bilinears in the particle-hole channel. These bosons can decay into particle-hole pairs and are thus expected to have a finite lifetime. Via the optical theorem, the existence of such decay channels is equivalent to a non-zero imaginary part of the two-point function (and thus the spectral function), generated by self-energy diagrams such as those shown in Fig. 28.

Although it is challenging to analytically compute these diagrams, it is straightforward to prove that for a boson with momentum $\vec{k}$, the imaginary part of each self-energy diagram can only arise when the energy ω of the boson is larger than a certain threshold. For each diagram, this threshold can be determined using energy-momentum conservation.

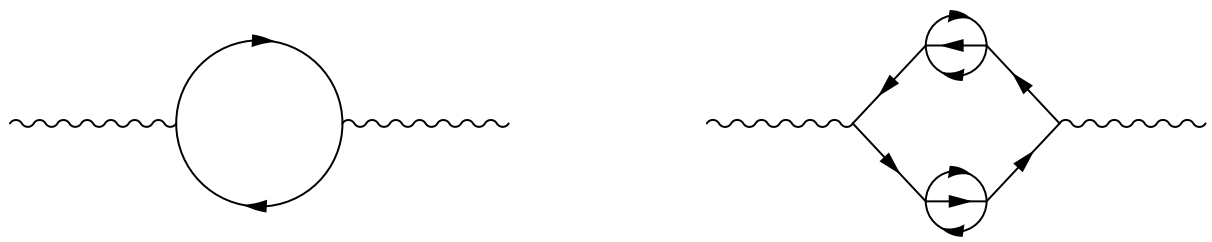

Figure 28: Self-energy corrections for the boson modes. Here, solid lines represent fermionic propagators and wiggly lines are boson propagators.

For example, the one loop diagram shown in Fig. 28 (the leading order correction) computes the scattering rate for a boson mode with energy ω and momentum $\vec{k}$ to decay into one particle with energy ω_p and momentum $\vec{k}_p$ and one hole with energy ω_h and momentum $\vec{k}_h$. Such a decay process can only take place when both the energy and momentum conservation laws are satisfied:

$$\begin{aligned} &\vec{k} = \vec{k}_p - \vec{k}_h, \\ &\omega = \omega_p - \omega_h = k_p^2 + k_h^2 \geq \frac{k^2}{2}. \end{aligned} \tag{4.123}$$

Here we used the quadratic dispersion relation (4.121). For fixed $\vec{k}$, the momentum conservation law enforces a relation between the momentum of the particle $\vec{k}_p$ and that of the hole $\vec{k}_h$, i.e. $\vec{k}_p = \vec{k} + \vec{k}_h$. With this constraint, the energy of the particle-hole excitation $k_p^2 + k_h^2$ has a lower bound of $k^2/2$ (which is reached when $\vec{k}_p = -\vec{k}_h = \vec{k}/2$). In other words, the energy conservation law can only be satisfied when $\omega \geq k^2/2$. As a result, for $\omega \geq k^2/2$, the boson can decay into a particle-hole pair, and thus have a finite lifetime, while for $\omega < k^2/2$, decay is kinematically forbidden. Thus, at the one-loop level, $O(g^0)$, the imaginary part of the bosonic correlation function only arises for $\omega \geq k^2/2$. This energy range is known as the particle-hole continuum.

When the ψ^4-interaction term is taken into consideration, the bosonic modes can decay through higher order processes (one example is shown in Fig. 28). For these higher order

diagrams, the same analysis can be utilized. At order $O(g^{2n})$, the energy and momentum conservation laws imply that

$$\begin{aligned}\vec{k} &= \sum_{i=1}^{n+1} \vec{k}_{p_i} - \sum_{i=1}^{n+1} \vec{k}_{h_i}, \\ \omega &= \sum_{i=1}^{n+1} \omega_{p_i} - \sum_{i=1}^{n+1} \omega_{h_i} = \sum_{i=1}^{n+1} (k_{p_i}^2 + k_{h_i}^2) \geq \frac{k^2}{2(n+1)}.\end{aligned} \tag{4.124}$$

Here we consider the decay of a bosonic mode into $n+1$ particles and $n+1$ holes (see Fig. 28 for an example with $n = 2$). For fixed $\vec{k}$, momentum conservation enforces a constraint on the momenta of the particles and holes. Given this constraint, the energy is minimized when the momenta are collinear, and the boson momentum $\vec{k}$ is equally distributed among the particles and holes. This results in a lower bound on the energy of $k^2/2(n+1)$. Thus the decay is kinematically forbidden unless $\omega \geq k^2/2(n+1)$.

This analysis demonstrates that, up to order of $O(g^{2n})$, the imaginary part of the boson correlation function only arises when the energy of the boson is above a threshold, $\omega \geq k^2/2(n+1)$. Furthermore, this threshold goes down to zero for higher order diagrams as $\sim 1/(n+1)$. Thus, if we sum the diagrammatic expansion to infinite order ($n \to \infty$), we expect that the boson correlation function can pick up a nonzero imaginary part for any $\omega > 0$.

Finally, we are ready to extract the asymptotic form of the imaginary part of the self-energy correction at small ω. For $\omega \ll k^2$, the imaginary part can only arise via processes of order $O(g^{2n})$, where $n \sim k^2/2\omega$. Therefore, we expect the imaginary part at energy ω and momentum $\vec{k}$ to scale as $\sim g^{2n} \sim g^{k^2/\omega}$. For sufficiently small g, this relation implies that the imaginary part of the self-energy correction decays to zero with the singular behavior $\sim e^{-\text{const.}/\hat{\omega}}$, where $\hat{\omega} = \omega/k^2$ is the dimensionless energy. This matches the $z = 2$ low frequency behavior (4.111) obtained holographically.

4.3.4.4 Dirac Theory Revisited and Systems with Higher z

We can repeat the kinematical analysis used above for similar models with arbitrary $z \geq 1$. In this case, for $O(g^{2n})$, the energy-momentum conservation law becomes

$$\begin{aligned} \vec{k} &= \sum_{i=1}^{n+1} \vec{k}_{p_i} - \sum_{i=1}^{n+1} \vec{k}_{h_i}, \\ \omega &= \sum_{i=1}^{n+1} \omega_{p_i} - \sum_{i=1}^{n+1} \omega_{h_i} = \sum_{i=1}^{n+1} (k_{p_i}^z + k_{h_i}^z) \geq \frac{k^z}{(2n+2)^{z-1}}. \end{aligned} \tag{4.125}$$

For any $z > 1$, the lower bound for having a nonzero imaginary part depends on n, and goes to zero as $n \to \infty$ (i.e. when considering higher and higher order diagrams). Similar to the discussion above, after summing over all the diagrams to infinite order, we find that at small ω, the imaginary part of the self-energy scales as

$$\operatorname{Im} \Pi \sim g^{(k^z/\omega)^{1/(z-1)}}. \tag{4.126}$$

For small g, this indicates that $\operatorname{Im} \Pi$ decays to zero as $e^{-\text{const.}\cdot \hat{\omega}^{-1/(z-1)}}$, where now $\hat{\omega} = \omega/k^z$, in agreement with the holographic result (4.111). This suggests that the exponential suppression of the spectral function is a generic property of Lifshitz models at $\omega \ll k^z$.

Note that for $z = 1$, the Dirac theory is recovered, and the fate of the system is fundamentally different. As can be seen by substituting $z = 1$ into (4.125), the energy threshold becomes independent of n. For any diagram, regardless of its order, the imaginary part arises only for $\omega \geq k$. After summing over all diagrams (to infinite order), the same lower bound of energy remains ($\omega \geq k$). As a result, for $z = 1$ the imaginary part of the correlation function vanishes identically in a finite region $\omega \leq k$, which is in sharp contrast to the $z > 1$ case. This conclusion is consistent with a symmetry analysis, which tells us that at $z = 1$, the Lorentz and conformal symmetries require the bosonic correlation function to be proportional to $(-\omega + |\vec{k}|)^\alpha$, where α is some scaling exponent. For non-integer α, $(-\omega + |\vec{k}|)^\alpha$ is real for $\omega < |\vec{k}|$, while the imaginary part arises for $\omega > |\vec{k}|$. For $z > 1$, however, the absence

of the Lorentz and conformal symmetries allows for very different types of behavior.

In summary, we find that models with $z > 1$ and $z = 1$ belong to fundamentally different universality classes. The case with $z = 1$ (i.e. Dirac) has been well understood with the help of conformal symmetry, which almost fully fixes the functional form of the correlation functions. However, for $z > 1$, the absence of conformal symmetry allows for richer structure in the correlation function. For arbitrary $z > 1$, we have presented an argument suggesting a characteristic exponential behavior $e^{-\text{const.}/\hat{\omega}^{1/(z-1)}}$ for the imaginary part of the self-energy correction at low energy.

4.3.4.5 Limitations of the Analysis

An exponential fall-off $\sim e^{-\text{const.}/\hat{\omega}^{1/(z-1)}}$ of the spectral function all the way down to $\omega \to 0$ would correspond to an essential singularity of the two-point function at the origin. However, it is worth noting that there are two limitations of the analysis presented above. First, because we only considered the decay of bosonic modes into $n+1$ particle-hole pairs without taking into account the renormalization of the vertex function (i.e. the renormalization of the coupling constant g), the above analysis is not expected to give quantitatively accurate results in the extremely low (or high) energy limit. This is because, as discussed above, in 2+1 dimensions, the coupling constant g is marginally relevant or irrelevant (depending on the sign of g). For the IR or UV limit, the flow of g cannot be ignored. However, because g is only marginally relevant or irrelevant, the flow of g is expected to be slow (i.e. logarithmic). Hence there may exist a range for ω (i.e. ω is small, but not too small) in which the RG flow of g may be weak enough to be ignored, so that the analysis above can produce a reasonable estimate for the scaling behavior of $\operatorname{Im}\Pi$.

Second, in the context of QFT, the perturbation series in terms of Feynman diagrams is typically expected to be an asymptotic series. This means that our kinematical argument using loop diagrams only captures the behavior of the imaginary part of the self-energy correctly up to some finite order $O(g^{2N})$, where N is large but finite. In particular, this

implies that the scaling $\mathrm{Im}\,\Pi \sim g^{2n} \sim g^{1/\hat{\omega}^{1/(z-1)}}$ is only valid for $n \leq N$ and thus for $\hat{\omega}$ above some cutoff $\hat{\omega}_\star(N)$.

Both of these points suggest that while the exponential suppression of the spectral function is a generic feature in a finite region where $\hat{\omega}$ is small, the behavior in the strict limit $\hat{\omega} \to 0$ is model-dependent. This is consistent with the observation in the gravity theory, where the would-be singular behavior of the two-point function may receive significant corrections at very small $\hat{\omega}$ from model-dependent higher derivative terms.

4.4 Summary and Discussion

In this chapter, we demonstrated that the spectral function for a minimally coupled scalar in a Lifshitz background is nonzero, but exponentially small, in the low-frequency regime $\omega \ll k^z$. We then showed that this behavior is a robust holographic prediction for field theories with Lifshitz symmetry, in the absence of further constraining symmetries. For the classes of higher derivative theories we study holographically, we generically find that the spectral function is suppressed in the low frequency region as $\chi \sim \exp(-\text{const.} \cdot \hat{\omega}^{-1/(z-1)})$, so long as $\hat{\omega} \gg (\ell/L)^{z-1}$, where ℓ is the length scale at which higher derivatives become important.

On the field theory side, the Lifshitz scaling symmetry is a priori not expected to lead to a universal 2-point function, and perturbative calculations do not reveal any similarities either between different field theories with Lifshitz symmetry, or with the holographic theory. However, in the example of the quadratic band crossing model we presented a simple kinematical argument involving energy-momentum conservation and a resummation of loop diagrams that reveals a similar exponential suppression as predicted by holography. Furthermore, this exponential suppression is expected for any field theory containing the following three key features: The existence of particles and holes, an interaction that allows for decay channels, and a dispersion relation with $z > 1$ scaling symmetry. Therefore, we expect our

conclusion to be generic and applicable to a wide range of systems (with $z > 1$) regardless of microscopic details, in agreement with the holographic prediction. In particular, we have checked that it applies to the quadratic band crossing model (1.3) (see [31] for more details).

Although in both the holographic and the field theory calculation, the exponential suppression is a robust feature of the spectral function for small $\hat{\omega}$, the strict limit $\hat{\omega} \to 0$ is non-universal in both cases. In the holographic calculation, the model-dependence enters through higher derivative terms, which introduce corrections whose size can be quantified precisely (see equation (4.113)). However, the precise regime of validity of the field theory calculations is less clear. In the quadratic band crossing theory considered here, the flow of the coupling constant g can no longer be neglected when taking the exact limit $\hat{\omega} \to 0$. Instead of just being a simple exponential, the exact (nonperturbative) spectral function will therefore have a more complicated dependence on $\hat{\omega}$. Naively, one may expect a dependence of the form

$$\operatorname{Im} \mathcal{G} \sim g(\hat{\omega})^{\hat{\omega}^{-1/(z-1)}}. \tag{4.127}$$

In 2+1 dimensions, the coupling g is marginal, and we expect g to depend only weakly on $\hat{\omega}$, so that the spectral function still shows an approximately exponential behavior. It would be interesting to further study the renormalization group flow of g to make a precise statement about the range of $\hat{\omega}$ for which this is the case. Along the same lines, in order to put a precise lower bound on $\hat{\omega}$, it would be important to account for the fact that the perturbative expansion is in fact only an asymptotic series (see the discussion in section 4.3.4.5).

In our field theory calculation, we found that $\operatorname{Im} \mathcal{G} \sim g^{1/\hat{\omega}^{1/(z-1)}}$, so that exponential suppression in fact only arises for $g \ll 1$. It is important to note that this is not in contradiction to AdS/CFT being a weak-strong coupling duality. The strong coupling nature of the field theory does not necessarily mean that the parameter g has to be chosen large, but rather that strong correlations (for example seen as long-range interactions) may emerge dynamically. This feature is familiar from the standard case of relativistic AdS/CFT, where

it is not $g_{\rm YM}$ itself that is taken large, but rather the 't Hooft coupling $g_{\rm YM}^2 N \gg 1$. In order to better understand the relation between strong/weak coupling on the field theory/gravity side in non-relativistic AdS/CFT, it would be desirable to develop a more precise version of the holographic dictionary for this case.

Although we have chosen not to consider higher derivatives in the radial direction ρ beyond second order, this is in fact not a true limitation of the perturbative analysis. Assuming we are only interested in solutions to the higher derivative equation that are perturbatively connected to the lowest order (*i.e.* the two-derivative) equation, we may always eliminate higher derivatives by substituting in the lower order equations. Consider, for example, the addition of a fourth order term to the Schrödinger-like equation (4.77)

$$-\psi''(\hat{\rho}) + \hat{U}(\hat{\rho})\psi(\hat{\rho}) = \lambda\psi^{(4)}(\hat{\rho}). \tag{4.128}$$

We now rewrite this as $\psi'' = U\psi - \lambda\psi^{(4)}$ and take two derivatives to obtain $\psi^{(4)} = (U\psi)'' - \lambda\psi^{(6)}$. Substituting this in the right-hand side of (4.128) and working only to linear order in λ then reduces the equation to second order

$$-\psi''(\hat{\rho}) + \hat{U}(\hat{\rho})\psi(\hat{\rho}) - \lambda(\hat{U}(\hat{\rho})\psi(\hat{\rho}))'' = \mathcal{O}(\lambda^2). \tag{4.129}$$

While this equation is no longer in manifest Schrödinger form, it can be so transformed if desired. Thus our analysis is in fact applicable to this more general case as well.

As we discussed at the end of section 4.3.3, the perturbative expansion of the spectral function in terms of higher derivative coefficients $\lambda_{i,j}$ strictly speaking only makes sense if these coefficients are chosen such that no additional turning points are introduced deep in the bulk. However, we argued that our formal perturbation series can still be used even in the case of higher derivatives with "wrong" sign, i.e. for the case where the effective potential bends upwards at large ρ. It would be interesting to determine if in a realistic theory, there are constraints on the signs of the coefficients $\lambda_{i,j}$, for example due to bulk

causality or unitarity. It would also be interesting to study string theory embeddings of Lifshitz spacetimes, where the coefficients of higher derivative corrections can be determined exactly, and calculate the corrections to holographic correlation functions.

Appendix A

Metric and Curvature of Planar Spacetimes

Here we provide the curvature components used in the derivation of the Lifshitz solution in section 2.1. Although not needed for the Lifshitz case, we consider slightly more general metrics of the form

$$ds^2 = -e^{2b_0(r)}dt^2 + dr^2 + \sum_{i=1}^{d} e^{2b_i(r)} \left(dx^i\right)^2 . \tag{A.1}$$

The nonvanishing curvature terms are

$$\begin{aligned}
R^{\rho}{}_{\sigma\mu\nu} &= \delta^{\rho}_{\nu}\eta_{\mu\sigma}b'_{\nu}b'_{\sigma}e^{2b_\sigma} - (\mu \leftrightarrow \nu), && \text{(A.2)}\\
R^{r}{}_{\mu r\nu} &= -\eta_{\mu\nu}e^{2b_\nu}\left(b''_{\nu} + (b'_{\nu})^2\right) && \text{(A.3)}\\
R_{rr} &= -\sum_{\lambda}(b''_{\lambda} + (b'_{\lambda})^2), && \text{(A.4)}\\
R_{\mu\nu} &= -\eta_{\mu\nu}e^{2b_\nu}\left(b''_{\nu} + b'_{\nu}\sum_{\lambda} b'_{\lambda}\right), && \text{(A.5)}\\
R &= -\sum_{\lambda}\left(2b''_{\lambda} + (b'_{\lambda})^2\right) - \left(\sum_{\lambda} b'_{\lambda}\right)^2, && \text{(A.6)}
\end{aligned}$$

where $\mu, \nu = 0, \ldots, d$, and repeated indices are not summed over unless explicitly stated. The Lifshitz solution is given by

$$b_0(r) = zr\ , \qquad b_i(r) = r\ , \qquad z > 1, \tag{A.7}$$

and the case $z = 1$ corresponds to AdS_{d+2}. For this class of solutions, we have

$$\begin{aligned}
R^r{}_{0r0} &= z^2 e^{2zr}, \\
R^r{}_{irj} &= -\delta_{ij} e^{2r}, \\
R^0{}_{i0j} &= -\delta_{ij} z e^{2r}, \\
R^i{}_{jkl} &= (\delta^i_l \delta_{jk} - \delta^i_k \delta_{jl}) e^{2r}, \\
R_{00} &= z(z+d) e^{2zr}, \\
R_{rr} &= -(z^2 + d), \\
R_{ij} &= -\delta_{ij}(z+d) e^{2r}, \\
R &= -(z^2 + d + (z+d)^2).
\end{aligned} \tag{A.8}$$

Appendix B

Higher Derivative Solutions in Alternative Gauge

In our numerical analysis in section 2.3.2, we chose the parametrization (2.33) for the metric, which is different from (A.1). In this gauge, the Lifshitz metric of section 2.1 takes the form:

$$ds^2 = \frac{1}{r^2}\left(-dt^2+dr^2+r^{2\tilde{z}}\left(dx^2+dy^2\right)\right). \tag{B.1}$$

The scaling parameters are related via $z=(1-\tilde{z})^{-1}$. Furthermore,

$$\phi = \frac{4\left(1-\tilde{z}\right)}{\lambda_1}\log r + C, \tag{B.2}$$

$$Q^2 e^{-\lambda_1 C} = \left(\frac{3}{2}-\tilde{z}\right)\tilde{z}\left(1-4\alpha\left(\tilde{z}-\frac{3}{4}\right)\right), \tag{B.3}$$

$$\Lambda = 2\left(\frac{3}{2}-\tilde{z}\right)\left(2-\tilde{z}\right)+4\alpha\tilde{z}\left(1-\tilde{z}\right)\left(\frac{3}{4}-\tilde{z}\right), \tag{B.4}$$

$$\lambda_1^2 = \frac{4\left(\frac{3}{2}-\tilde{z}\right)\left(1-\tilde{z}\right)}{Q^2 e^{-\lambda_1 C}} = \frac{1-\tilde{z}}{\tilde{z}\left(\frac{1}{4}-\alpha\left(\tilde{z}-\frac{3}{4}\right)\right)}. \tag{B.5}$$

It is straightforward to show that $\lambda_1^2(\tilde{z})$ has a local minimum at

$$\tilde{z}_{\pm} = 1 \pm \frac{1}{2}\sqrt{1-\frac{1}{\alpha}}\,, \tag{B.6}$$

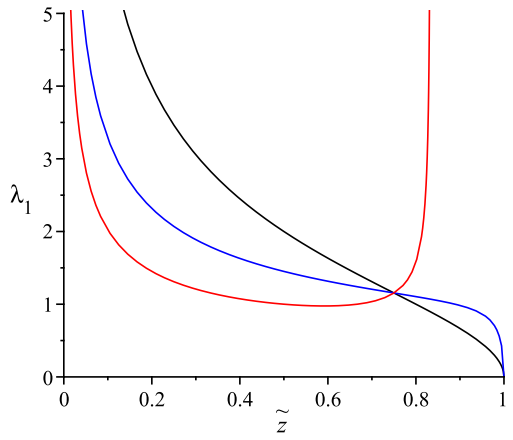

Figure 29: Plot of $\lambda_1(\tilde{z})$ for $\alpha = 0$ (black), $\alpha = 0.9$ (blue) and $\alpha = 3$ (red).

provided that $\alpha \geq 1$. In this case there are two different scaling parameters $\tilde{z}_1 < \tilde{z}_2$ for any given λ_1^2 (away from the minimum) (see Figure 29). Notice also that λ_1^2 blows up for $\tilde{z}_\star = 3/4 + 1/(4\alpha)$, which is within the range of physical solutions for $\alpha \geq 1$ only. To summarize, the possible ranges for the parameters are:

$$\begin{aligned} \alpha < 1: &\qquad 0 \leq \lambda_1 < \infty\,, &&\qquad 0 < \tilde{z} \leq 1, \\ \alpha \geq 1: &\qquad \lambda_{\min} \leq \lambda_1 < \infty\,, &&\qquad 0 < \tilde{z} < \tilde{z}_\star, \end{aligned} \tag{B.7}$$

where $\lambda_{\min} \equiv \lambda_1(\tilde{z}_-)$.

Appendix C

Irrelevant Perturbations around Higher Derivative Solutions

There are two ways in which the exponent of the dilaton perturbations, ν may become complex:

1. The smaller square-root in (2.64) becomes imaginary. This happens when

$$\lambda_2 = \frac{1}{\alpha\lambda_1}\left(-\left(\lambda_1 - \frac{2}{\sqrt{3}}\right)^2 + \frac{2}{3}\right). \tag{C.1}$$

2. Even if the small root is real-valued, $\widetilde{\nu}^2$ may still cross zero, which happens at

$$\begin{aligned}\lambda_2 = \frac{1}{\lambda_1\left(11\alpha^2 - 19\alpha + 8\right)}\Bigg\{&\frac{4}{3}\left(1-\alpha\right)\lambda_1^2 + \frac{11}{8}\alpha - 1 \\ &\pm \frac{3}{2}\Bigg[\left(\alpha-1\right)^2\lambda_1^4 - \frac{1}{2}\left(11\alpha^2 - 19\alpha + 8\right)\lambda_1^2 + \left(\frac{11}{12}\alpha - \frac{2}{3}\right)^2\Bigg]\Bigg\}\end{aligned} \tag{C.2}$$

To find out when the dilaton perturbations are irrelevant, i.e. $\widetilde{\nu}^2 = 1/4$, notice that $\widetilde{\nu}^2 - 1/4$ can only change its sign as we go from case 1) to case 2) in (2.65). As a consequence, irrelevant perturbations will stay irrelevant as long as $\alpha\lambda_2/\lambda_1 \gtrless 1$. In practice, it is therefore easiest to plot the curves (C.1)/(C.2) and determine the number of irrelevant perturbations

numerically, making use of continuity arguments (see Figures 1 and 2).

Appendix D

WKB Approximation for Spectral Functions

Here we give a brief discussion of the accuracy of the WKB approximation in the context of calculating holographic spectral functions. The wavefunction (4.22) is only the leading order approximation to the exact result. We can parametrize a finite error in our approximation by writing

$$\phi_{3/4} = \sqrt{\nu}\left(U-\omega^2\right)^{-\frac{1}{4}}(1+\delta)\, e^{\pm S(\rho,\rho_0)}, \qquad \delta \ll 1. \tag{D.1}$$

This error propagates to the matching coefficients in $\mathcal{M}'$ in the following way:

$$\mathcal{M}' = \begin{pmatrix} (1+\mathcal{O}(\delta))\,\epsilon^{\nu} e^{S(\epsilon,\rho_0)} & \mathcal{O}(\delta)\,\epsilon^{\nu} e^{-S(\epsilon,\rho_0)} \\ \mathcal{O}(\delta)\,\epsilon^{-\nu} e^{S(\epsilon,\rho_0)} & (1+\mathcal{O}(\delta))\,\epsilon^{-\nu} e^{-S(\epsilon,\rho_0)} \end{pmatrix}. \tag{D.2}$$

While $\mathcal{M}'_{AD} \to 0$ for $\epsilon \to 0$, $\mathcal{M}'_{BC}$ actually blows up in this limit. This means that we have no theoretical control over this coefficient, and results containing $\mathcal{M}'_{BC}$ cannot be trusted. There is a simple explanation for this problem: We perform the matching at $\epsilon \to 0$, where the A-mode generically blows up, but the B-mode goes to zero. For a generic solution with $A, B \neq 0$, we can then take an arbitrary finite amount of B and "hide" it under the non-normalizable mode A by taking $B \to B - \delta B$ and $A \to A + \delta B$. The relative error we make

by doing so will always be shrunk to zero near the boundary. This means that generically, we cannot trust the WKB-calculation of B. However, any result that does not contain the "mixing"-term $\mathcal{M}'_{BC}$ can still be calculated accurately. For example, we can calculate B for a normalizable wavefunction, where $A = 0$. In this case, we need to choose $a = -ib$ and we obtain

$$\begin{pmatrix} A \\ B \end{pmatrix} = \begin{pmatrix} 0 \\ \mathcal{M}'_{BD} e^{-i\frac{\pi}{4}} b \end{pmatrix}. \tag{D.3}$$

Since $\mathcal{M}'_{BC}$ automatically shows up in the expression for the Green's function (4.17), one might expect that we cannot trust this result. However, once we plug in (D.2), we see that

$$G_{\mathrm{WKB}}(\omega, \vec{k}) = K \left(\frac{\mathcal{M}'_{BC}}{\mathcal{M}'_{AC}} + \frac{i}{2} \frac{\mathcal{M}'_{BD}}{\mathcal{M}'_{AC}} \frac{1 - i\frac{b}{a}}{1 + i\frac{b}{a}} \right), \tag{D.4}$$

so the problematic term only appears in the real part of the Green's function. This means that while we cannot trust WKB for $\mathrm{Re}\, G(\omega, \vec{k})$, we can still get accurate results for the imaginary part, up to an $O(\delta)$-error. In particular, one can check that $\mathcal{M}'_{BC} \sim \epsilon^{-2\nu}$ and $\mathcal{M}'_{AD} \sim \epsilon^{2\nu}$ do not conspire with each other to make this error divergent.

Appendix E

Perturbative Expansion of the WKB Integral for Spectral Functions

We would like to obtain an approximate expression for the WKB integral (4.86) for a potential of the form

$$\hat{U}(\hat{\rho}) = \hat{U}_0(\hat{\rho}) + \delta\hat{U}(\hat{\rho}), \tag{E.1}$$

where

$$\hat{U}_0 = \frac{\nu^2}{\hat{\rho}^2} + \frac{1}{\hat{\rho}^{2-2/z}} - \hat{\omega}^2, \tag{E.2}$$

and $\delta\hat{U}$ represents a small correction to the potential. To be precise, we assume that $\delta\hat{U}$ is subdominant compared to the other terms in the potential for all $\hat{\rho}$ between the boundary and the classical turning point. To guarantee this, it is sufficient to demand that

$$\delta\hat{U}(\hat{\rho}) \ll \hat{\omega}^2 \quad \text{for} \quad 0 \leq \hat{\rho} \leq \hat{\rho}_0. \tag{E.3}$$

We can then expand the turning point as follows:

$$\hat{\rho}_0(t) = \hat{\rho}_0^{(0)}\left(1 + t + \cdots\right), \tag{E.4}$$

where

$$t \sim \frac{\delta\hat{U}(\hat{\rho}_0^{(0)})}{\hat{\omega}^2} \ll 1, \tag{E.5}$$

and $\hat{\rho}_0^{(0)}$ is the turning point of the unperturbed potential, i.e. $\hat{U}_0(\hat{\rho}_0^{(0)}) = 0$. The relative size of $\delta\hat{U}$ at the unperturbed turning point is what controls the higher derivative expansion. The WKB integral (4.86) can be written as $S = S^{(0)} + \delta S$, where

$$\delta S = S - S^{(0)} = \int_\epsilon^{\hat{\rho}_0(t)} d\hat{\rho}\sqrt{\hat{U}_0(\hat{\rho}) + \delta\hat{U}(\hat{\rho})} - \int_\epsilon^{\hat{\rho}_0^{(0)}} d\hat{\rho}\sqrt{\hat{U}_0(\hat{\rho})}. \tag{E.6}$$

One could attempt to simply expand the above expression formally in t and $\delta\hat{U}$, and it turns out that this does indeed give the correct result (4.90). However, this approach is problematic, since $\hat{U}_0$ goes to zero at $\hat{\rho}_0^{(0)}$, and thus the formal expansion parameter $\delta\hat{U}/\hat{U}_0$ blows up at this location. The solution is to split up the integrals in (E.6) in a way that the integrand always has a well-defined expansion in terms of $\delta\hat{U}$. To do this, we shift the first integral by rescaling $x \equiv \hat{\rho}\hat{\rho}_0^{(0)}/\hat{\rho}_0(t)$, so that the upper bounds of both integrals are identical. We can then combine both terms to obtain

$$\delta S \approx \int_{\frac{\epsilon}{1+t}}^{\epsilon} dx\sqrt{\frac{\nu^2}{x^2} + \frac{1+\frac{2}{z}t}{x^{2-2/z}} - (1+2t) + \delta\hat{U}\,(x)} + \int_\epsilon^{\hat{\rho}_0^{(0)}} dx\sqrt{\hat{U}_0(x)}\left[\sqrt{1+V(x)} - 1\right], \tag{E.7}$$

where

$$V(x) = \frac{\delta\hat{U}(x) + \frac{2}{z\hat{\rho}^{2-2/z}}t - 2t}{\hat{U}_0(x)}, \tag{E.8}$$

and we expanded to linear order in t. The first term in (E.7) is due to the shift of the lower bound of the first integral in (E.6). Assuming that $\lim_{x\to 0} x^2\delta\hat{U}(x) = 0$, this term evaluates to νt after we send $\epsilon \to 0$. To compute the second integral, notice that although $\hat{U}_0(x)$ itself blows up at the upper bound, the ratio $V(x)$ remains finite everywhere. Moreover, it is small by assumption, so we can expand (E.7) in terms of $V(x)$: s

$$\delta S \approx \nu t + \int_\epsilon^{\hat{\rho}_0^{(0)}} dx\frac{\delta\hat{U}(x) + \frac{2}{z\hat{\rho}^{2-2/z}}t - 2t}{2\sqrt{\hat{U}_0}}. \tag{E.9}$$

The integral over the terms linear in t exactly cancels the νt term, and we arrive at the final result:

$$\delta S \approx \int_{\epsilon}^{\hat{\rho}_0^{(0)}} dx \frac{\delta \hat{U}(x)}{2\sqrt{\hat{U}_0}}. \tag{E.10}$$

This is the first order correction to the WKB integral in the presence of a perturbation $\delta \hat{U}$.

Bibliography

[1] J. M. Maldacena, *The Large N limit of superconformal field theories and supergravity*, *Adv.Theor.Math.Phys.* **2** (1998) 231–252, [hep-th/9711200].

[2] E. Witten, *Anti-de Sitter space and holography*, *Adv.Theor.Math.Phys.* **2** (1998) 253–291, [hep-th/9802150].

[3] S. Gubser, I. R. Klebanov, and A. M. Polyakov, *Gauge theory correlators from noncritical string theory*, *Phys.Lett.* **B428** (1998) 105–114, [hep-th/9802109].

[4] O. Aharony, S. S. Gubser, J. M. Maldacena, H. Ooguri, and Y. Oz, *Large N field theories, string theory and gravity*, *Phys. Rept.* **323** (2000) 183–386, [hep-th/9905111].

[5] E. D'Hoker and D. Z. Freedman, *Supersymmetric gauge theories and the AdS / CFT correspondence*, in *Strings, Branes and Extra Dimensions: TASI 2001: Proceedings*, pp. 3–158, 2002. hep-th/0201253.

[6] G. 't Hooft, *A Planar Diagram Theory for Strong Interactions*, *Nucl. Phys.* **B72** (1974) 461.

[7] D. J. Gross and E. Witten, *Superstring Modifications of Einstein's Equations*, *Nucl. Phys.* **B277** (1986) 1.

[8] M. T. Grisaru and D. Zanon, *σ Model Superstring Corrections to the Einstein-hilbert Action*, *Phys. Lett.* **B177** (1986) 347.

[9] M. D. Freeman, C. N. Pope, M. F. Sohnius, and K. S. Stelle, *Higher Order σ Model Counterterms and the Effective Action for Superstrings*, *Phys. Lett.* **B178** (1986) 199.

[10] P. Kovtun, D. T. Son, and A. O. Starinets, *Viscosity in strongly interacting quantum field theories from black hole physics*, *Phys.Rev.Lett.* **94** (2005) 111601, [hep-th/0405231].

[11] S. A. Hartnoll, *Lectures on holographic methods for condensed matter physics*, *Class.Quant.Grav.* **26** (2009) 224002, [arXiv:0903.3246].

[12] P. Koroteev and M. Libanov, *On Existence of Self-Tuning Solutions in Static Braneworlds without Singularities*, *JHEP* **02** (2008) 104, [arXiv:0712.1136].

[13] L. Mazzucato, Y. Oz, and S. Theisen, *Non-relativistic Branes*, *JHEP* **04** (2009) 073, [arXiv:0810.3673].

[14] A. Donos and J. P. Gauntlett, *Supersymmetric solutions for non-relativistic holography*, *JHEP* **03** (2009) 138, [arXiv:0901.0818].

[15] Y. Nakayama, M. Sakaguchi, and K. Yoshida, *Non-Relativistic M2-brane Gauge Theory and New Superconformal Algebra*, *JHEP* **04** (2009) 096, [arXiv:0902.2204].

[16] G. Bertoldi, B. A. Burrington, and A. W. Peet, *Thermodynamics of black branes in asymptotically Lifshitz spacetimes*, *Phys. Rev.* **D80** (2009) 126004, [arXiv:0907.4755].

[17] A. Donos, J. P. Gauntlett, N. Kim, and O. Varela, *Wrapped M5-branes, consistent truncations and AdS/CMT*, *JHEP* **12** (2010) 003, [arXiv:1009.3805].

[18] W. Chemissany and J. Hartong, *From D3-Branes to Lifshitz Space-Times*, *Class. Quant. Grav.* **28** (2011) 195011, [arXiv:1105.0612].

[19] P. Dey and S. Roy, *Intersecting D-branes and Lifshitz-like space-time*, *Phys. Rev.* **D86** (2012) 066009, [arXiv:1204.4858].

[20] S. Kachru, X. Liu, and M. Mulligan, *Gravity Duals of Lifshitz-like Fixed Points*, *Phys.Rev.* **D78** (2008) 106005, [arXiv:0808.1725].

[21] D. Son, *Toward an AdS/cold atoms correspondence: A Geometric realization of the Schrodinger symmetry*, *Phys.Rev.* **D78** (2008) 046003, [arXiv:0804.3972].

[22] K. Balasubramanian and J. McGreevy, *Gravity duals for non-relativistic CFTs*, *Phys.Rev.Lett.* **101** (2008) 061601, [arXiv:0804.4053].

[23] E. Ardonne, P. Fendley, and E. Fradkin, *Topological order and conformal quantum critical points*, *Annals Phys.* **310** (2004) 493–551, [cond-mat/0311466].

[24] R. M. Hornreich, M. Luban, and S. Shtrikman, *Critical behavior at the onset of $\vec{k}$-space instability on the λ line*, *Phys. Rev. Lett.* **35** (Dec, 1975) 1678–1681.

[25] D. T. Son and A. O. Starinets, *Minkowski space correlators in AdS / CFT correspondence: Recipe and applications*, *JHEP* **0209** (2002) 042, [hep-th/0205051].

[26] G. L. Cardoso, M. Haack, and S. Nampuri, *Nernst branes with Lifshitz asymptotics in N=2 gauged supergravity*, arXiv:1511.0767.

[27] A. Adams, K. Balasubramanian, and J. McGreevy, *Hot Spacetimes for Cold Atoms*, *JHEP* **0811** (2008) 059, [arXiv:0807.1111].

[28] G. Knodel and J. T. Liu, *Higher derivative corrections to Lifshitz backgrounds*, *JHEP* **1310** (2013) 002, [arXiv:1305.3279].

[29] C. Keeler, G. Knodel, and J. T. Liu, *What do non-relativistic CFTs tell us about Lifshitz spacetimes?*, *JHEP* **1401** (2014) 062, [arXiv:1308.5689].

[30] C. Keeler, G. Knodel, and J. T. Liu, *Hidden horizons in non-relativistic AdS/CFT*, *JHEP* **1408** (2014) 024, [arXiv:1404.4877].

[31] C. Keeler, G. Knodel, J. T. Liu, and K. Sun, *Universal features of Lifshitz Green's functions from holography*, *JHEP* **08** (2015) 057, [arXiv:1505.0783].

[32] M. Taylor, *Non-relativistic holography*, arXiv:0812.0530.

[33] K. Goldstein, S. Kachru, S. Prakash, and S. P. Trivedi, *Holography of Charged Dilaton Black Holes*, *JHEP* **1008** (2010) 078, [arXiv:0911.3586].

[34] M. Cadoni, G. D'Appollonio, and P. Pani, *Phase transitions between Reissner-Nordstrom and dilatonic black holes in 4D AdS spacetime*, *JHEP* **03** (2010) 100, [arXiv:0912.3520].

[35] C.-M. Chen and D.-W. Pang, *Holography of Charged Dilaton Black Holes in General Dimensions*, *JHEP* **06** (2010) 093, [arXiv:1003.5064].

[36] C. Charmousis, B. Gouteraux, B. S. Kim, E. Kiritsis, and R. Meyer, *Effective Holographic Theories for low-temperature condensed matter systems*, *JHEP* **1011** (2010) 151, [arXiv:1005.4690].

[37] E. Perlmutter, *Domain Wall Holography for Finite Temperature Scaling Solutions*, *JHEP* **02** (2011) 013, [arXiv:1006.2124].

[38] K. Goldstein, N. Iizuka, S. Kachru, S. Prakash, S. P. Trivedi, and A. Westphal, *Holography of Dyonic Dilaton Black Branes*, *JHEP* **10** (2010) 027, [arXiv:1007.2490].

[39] S. Harrison, S. Kachru, and H. Wang, *Resolving Lifshitz Horizons*, arXiv:1202.6635.

[40] J. Tarrio and S. Vandoren, *Black holes and black branes in Lifshitz spacetimes*, *JHEP* **09** (2011) 017, [arXiv:1105.6335].

[41] M. R. Mohammadi Mozaffar and A. Mollabashi, *Holographic quantum critical points in Lifshitz space-time*, *JHEP* **04** (2013) 081, [arXiv:1212.6635].

[42] K. Copsey and R. Mann, *Pathologies in Asymptotically Lifshitz Spacetimes*, *JHEP* **1103** (2011) 039, [arXiv:1011.3502].

[43] G. T. Horowitz and B. Way, *Lifshitz Singularities*, *Phys.Rev.* **D85** (2012) 046008, [arXiv:1111.1243].

[44] A. Adams, A. Maloney, A. Sinha, and S. E. Vazquez, *1/N Effects in Non-Relativistic Gauge-Gravity Duality*, *JHEP* **03** (2009) 097, [arXiv:0812.0166].

[45] E. Ayon-Beato, A. Garbarz, G. Giribet, and M. Hassaine, *Lifshitz Black Hole in Three Dimensions*, *Phys. Rev.* **D80** (2009) 104029, [arXiv:0909.1347].

[46] R.-G. Cai, Y. Liu, and Y.-W. Sun, *A Lifshitz Black Hole in Four Dimensional R**2 Gravity*, *JHEP* **10** (2009) 080, [arXiv:0909.2807].

[47] D.-W. Pang, *On Charged Lifshitz Black Holes*, *JHEP* **01** (2010) 116, [arXiv:0911.2777].

[48] E. Ayon-Beato, A. Garbarz, G. Giribet, and M. Hassaine, *Analytic Lifshitz black holes in higher dimensions*, *JHEP* **04** (2010) 030, [arXiv:1001.2361].

[49] M. H. Dehghani and R. B. Mann, *Lovelock-Lifshitz Black Holes*, *JHEP* **07** (2010) 019, [arXiv:1004.4397].

[50] M. H. Dehghani and R. B. Mann, *Thermodynamics of Lovelock-Lifshitz Black Branes*, *Phys. Rev.* **D82** (2010) 064019, [arXiv:1006.3510].

[51] W. G. Brenna, M. H. Dehghani, and R. B. Mann, *Quasi-Topological Lifshitz Black Holes*, *Phys. Rev.* **D84** (2011) 024012, [arXiv:1101.3476].

[52] H. Lu, Y. Pang, C. N. Pope, and J. F. Vazquez-Poritz, *AdS and Lifshitz Black Holes in Conformal and Einstein-Weyl Gravities*, *Phys. Rev.* **D86** (2012) 044011, [arXiv:1204.1062].

[53] J. Bhattacharya, S. Cremonini, and A. Sinkovics, *On the IR completion of geometries with hyperscaling violation*, *JHEP* **1302** (2013) 147, [arXiv:1208.1752].

[54] N. Bao, X. Dong, S. Harrison, and E. Silverstein, *The Benefits of Stress: Resolution of the Lifshitz Singularity*, *Phys.Rev.* **D86** (2012) 106008, [arXiv:1207.0171].

[55] H. Braviner, R. Gregory, and S. F. Ross, *Flows involving Lifshitz solutions*, *Class.Quant.Grav.* **28** (2011) 225028, [arXiv:1108.3067].

[56] J. T. Liu and Z. Zhao, *Holographic Lifshitz flows and the null energy condition*, arXiv:1206.1047.

[57] E. Alvarez and C. Gomez, *Geometric holography, the renormalization group and the c theorem*, *Nucl. Phys.* **B541** (1999) 441–460, [hep-th/9807226].

[58] L. Girardello, M. Petrini, M. Porrati, and A. Zaffaroni, *Novel local CFT and exact results on perturbations of N=4 superYang Mills from AdS dynamics*, *JHEP* **12** (1998) 022, [hep-th/9810126].

[59] D. Z. Freedman, S. S. Gubser, K. Pilch, and N. P. Warner, *Renormalization group flows from holography supersymmetry and a c theorem*, *Adv. Theor. Math. Phys.* **3** (1999) 363–417, [hep-th/9904017].

[60] V. Balasubramanian, P. Kraus, and A. E. Lawrence, *Bulk versus boundary dynamics in anti-de Sitter space-time*, *Phys.Rev.* **D59** (1999) 046003, [hep-th/9805171].

[61] V. Balasubramanian, P. Kraus, A. E. Lawrence, and S. P. Trivedi, *Holographic probes of anti-de Sitter space-times*, *Phys.Rev.* **D59** (1999) 104021, [hep-th/9808017].

[62] I. Bena, *On the construction of local fields in the bulk of AdS(5) and other spaces*, *Phys.Rev.* **D62** (2000) 066007, [hep-th/9905186].

[63] A. Hamilton, D. N. Kabat, G. Lifschytz, and D. A. Lowe, *Local bulk operators in AdS/CFT: A Boundary view of horizons and locality*, *Phys.Rev.* **D73** (2006) 086003, [hep-th/0506118].

[64] A. Hamilton, D. N. Kabat, G. Lifschytz, and D. A. Lowe, *Holographic representation of local bulk operators*, *Phys.Rev.* **D74** (2006) 066009, [hep-th/0606141].

[65] V. Balasubramanian, S. B. Giddings, and A. E. Lawrence, *What do CFTs tell us about Anti-de Sitter space-times?*, *JHEP* **9903** (1999) 001, [hep-th/9902052].

[66] T. Banks, M. R. Douglas, G. T. Horowitz, and E. J. Martinec, *AdS dynamics from conformal field theory*, hep-th/9808016.

[67] A. L. Fitzpatrick and J. Kaplan, *Scattering States in AdS/CFT*, arXiv:1104.2597.

[68] R. Bousso, B. Freivogel, S. Leichenauer, V. Rosenhaus, and C. Zukowski, *Null Geodesics, Local CFT Operators and AdS/CFT for Subregions*, *Phys.Rev.* **D88** (2013) 064057, [arXiv:1209.4641].

[69] S. Leichenauer and V. Rosenhaus, *AdS black holes, the bulk-boundary dictionary, and smearing functions*, *Phys.Rev.* **D88** (2013) 026003, [arXiv:1304.6821].

[70] C. Hoyos and P. Koroteev, *On the Null Energy Condition and Causality in Lifshitz Holography*, *Phys.Rev.* **D82** (2010) 084002, [arXiv:1007.1428].

[71] P. Breitenlohner and D. Z. Freedman, *Stability in Gauged Extended Supergravity*, *Annals Phys.* **144** (1982) 249.

[72] H. Singh, *Holographic flows to IR Lifshitz spacetimes*, *JHEP* **1104** (2011) 118, [arXiv:1011.6221].

[73] H. Singh, *Lifshitz to AdS flow with interpolating p-brane solutions*, *JHEP* **1308** (2013) 097, [arXiv:1305.3784].

[74] F. Brau and F. Calogero, *Upper and lower limits for the number of S-wave bound states in an attractive potential*, *J. Math. Phys* **44** (2003) 1554.

[75] L. Susskind and N. Toumbas, *Wilson loops as precursors*, *Phys.Rev.* **D61** (2000) 044001, [hep-th/9909013].

[76] S. A. Hartnoll, D. M. Hofman, and D. Vegh, *Stellar spectroscopy: Fermions and holographic Lifshitz criticality*, *JHEP* **1108** (2011) 096, [arXiv:1105.3197].

[77] S. A. Hartnoll and E. Shaghoulian, *Spectral weight in holographic scaling geometries*, *JHEP* **1207** (2012) 078, [arXiv:1203.4236].

[78] M. Alishahiha, M. R. Mohammadi Mozaffar, and A. Mollabashi, *Fermions on Lifshitz Background*, *Phys. Rev.* **D86** (2012) 026002, [arXiv:1201.1764].

[79] U. Gursoy, V. Jacobs, E. Plauschinn, H. Stoof, and S. Vandoren, *Holographic models for undoped Weyl semimetals*, *JHEP* **1304** (2013) 127, [arXiv:1209.2593].

[80] S.-S. Lee, *A Non-Fermi Liquid from a Charged Black Hole: A Critical Fermi Ball*, *Phys.Rev.* **D79** (2009) 086006, [arXiv:0809.3402].

[81] A. Chamblin, R. Emparan, C. V. Johnson, and R. C. Myers, *Charged AdS black holes and catastrophic holography*, *Phys.Rev.* **D60** (1999) 064018, [hep-th/9902170].

[82] P. Basu, J. He, A. Mukherjee, and H.-H. Shieh, *Holographic Non-Fermi Liquid in a Background Magnetic Field*, *Phys.Rev.* **D82** (2010) 044036, [arXiv:0908.1436].

[83] T. Faulkner, H. Liu, J. McGreevy, and D. Vegh, *Emergent quantum criticality, Fermi surfaces, and AdS(2)*, *Phys.Rev.* **D83** (2011) 125002, [arXiv:0907.2694].

[84] T. Faulkner, N. Iqbal, H. Liu, J. McGreevy, and D. Vegh, *Holographic non-Fermi liquid fixed points*, *Phil. Trans. Roy. Soc.* **A 369** (2011) 1640, [arXiv:1101.0597].

[85] A. Donos and J. P. Gauntlett, *Holographic striped phases*, *JHEP* **1108** (2011) 140, [arXiv:1106.2004].

[86] A. Donos, J. P. Gauntlett, and C. Pantelidou, *Spatially modulated instabilities of magnetic black branes*, *JHEP* **1201** (2012) 061, [arXiv:1109.0471].

[87] S. Cremonini and A. Sinkovics, *Spatially Modulated Instabilities of Geometries with Hyperscaling Violation*, *JHEP* **1401** (2014) 099, [arXiv:1212.4172].

[88] S. Cremonini, *Spatially Modulated Instabilities for Scaling Solutions at Finite Charge Density*, arXiv:1310.3279.

[89] S. A. Hartnoll and J. E. Santos, *Cold planar horizons are floppy*, arXiv:1403.4612.

[90] N. Bao, S. Harrison, S. Kachru, and S. Sachdev, *Vortex Lattices and Crystalline Geometries*, *Phys.Rev.* **D88** (2013), no. 2 026002, [arXiv:1303.4390].

[91] N. Iizuka, S. Kachru, N. Kundu, P. Narayan, N. Sircar, *et. al.*, *Bianchi Attractors: A Classification of Extremal Black Brane Geometries*, *JHEP* **1207** (2012) 193, [arXiv:1201.4861].

[92] S. Kachru, N. Kundu, A. Saha, R. Samanta, and S. P. Trivedi, *Interpolating from Bianchi Attractors to Lifshitz and AdS Spacetimes*, *JHEP* **1403** (2014) 074, [arXiv:1310.5740].

[93] G. T. Horowitz and M. M. Roberts, *Zero Temperature Limit of Holographic Superconductors*, *JHEP* **0911** (2009) 015, [arXiv:0908.3677].

[94] P. Basu, *Energy scales in a holographic black hole and conductivity at finite momentum*, *Can.J.Phys.* **89** (2011) 271–276, [arXiv:0911.5082].

[95] S.-J. Rey and V. Rosenhaus, *Scanning Tunneling Macroscopy, Black Holes, and AdS/CFT Bulk Locality*, arXiv:1403.3943.

[96] K. Sun, H. Yao, E. Fradkin, and S. Kivelson, *Topological insulators and nematic phases from spontaneous symmetry breaking in 2d fermi systems with a quadratic band crossing*, *Phys. Rev. Lett.* **103** (Jul, 2009) 046811, [arXiv:0905.0907].

[97] G. Policastro, D. T. Son, and A. O. Starinets, *The Shear viscosity of strongly coupled N=4 supersymmetric Yang-Mills plasma*, *Phys.Rev.Lett.* **87** (2001) 081601, [hep-th/0104066].

[98] G. Policastro, D. T. Son, and A. O. Starinets, *From AdS / CFT correspondence to hydrodynamics*, *JHEP* **0209** (2002) 043, [hep-th/0205052].

[99] G. Policastro, D. T. Son, and A. O. Starinets, *From AdS / CFT correspondence to hydrodynamics. 2. Sound waves*, *JHEP* **0212** (2002) 054, [hep-th/0210220].

[100] C. P. Herzog, *The Hydrodynamics of M theory*, *JHEP* **0212** (2002) 026, [hep-th/0210126].

[101] C. P. Herzog, *The Sound of M theory*, *Phys.Rev.* **D68** (2003) 024013, [hep-th/0302086].

[102] A. Buchel, J. T. Liu, and A. O. Starinets, *Coupling constant dependence of the shear viscosity in N=4 supersymmetric Yang-Mills theory*, *Nucl.Phys.* **B707** (2005) 56–68, [hep-th/0406264].

[103] D. T. Son and A. O. Starinets, *Viscosity, Black Holes, and Quantum Field Theory*, *Ann.Rev.Nucl.Part.Sci.* **57** (2007) 95–118, [arXiv:0704.0240].

[104] J. Nilsson, A. H. Castro Neto, F. Guinea, and N. M. R. Peres, *Electronic properties of bilayer and multilayer graphene*, *Phys. Rev. B* **78** (2008), no. 4 045405, [arXiv:0712.3259].

[105] A. H. Castro Neto, F. Guinea, N. M. R. Peres, K. S. Novoselov, and A. K. Geim, *The electronic properties of graphene*, *Rev. Mod. Phys.* **81** (2009), no. 1 109, [arXiv:0709.1163].

[106] V. Kotov, B. Uchoa, V. Pereira, F. Guinea, and A. Castro Neto, *Electron-electron interactions in graphene: Current status and perspectives*, *Rev. Mod. Phys.* **84** (Jul, 2012) 1067–1125, [arXiv:1012.3484].

[107] K. Sun, W. V. Liu, A. Hemmerich, and S. D. Sarma, *Topological semimetal in a fermionic optical lattice*, *Nature Physics* **8** (2012) 67–70, [arXiv:1011.4301].